UPSTREAM HISTORY
AND
APPARENT STRESS
IN
TURBULENT BOUNDARY LAYERS

PERRY GOLDBERG

MAY 1966

GAS TURBINE LABORATORY
MASSACHUSETTS INSTITUTE OF TECHNOLOGY
CAMBRIDGE · 39 · MASSACHUSETTS

UPSTREAM HISTORY AND APPARENT STRESS

IN TURBULENT BOUNDARY LAYERS

by

PERRY GOLDBERG

GAS TURBINE LABORATORY

REPORT No. 85

May 1966

MASSACHUSETTS INSTITUTE OF TECHNOLOGY

Cambridge, Massachusetts

ABSTRACT

A comprehensive experimental and analytical study specifically designed to investigate upstream history and apparent stresses in incompressible, two-dimensional, turbulent boundary layers has been conducted. Hot-wire measurements of turbulent shear stress and longitudinal turbulence intensity, as well as velocity profiles and wall shear stress measurements, were made for six different pressure distributions.

It was found that the turbulent shear stress is dependent upon the upstream history of the flow and not a unique function of the local velocity profile. A simple equation for the dissipation integral,

$$\theta \, \frac{dC_D}{dx} = K(C_{D_{equi}} - C_D)$$

with a constant K was found to represent the data well. This expression was used with the mean-flow energy integral equaiton to obtain a practical method for predicting turbulent boundary layer behavior which accounts for upstream history. The predictions made with this method for the six pressure distributions of this study and for others extracted from the literature agreed well with the experimental data.

ACKNOWLEDGEMENTS

TABLE OF CONTENTS

LIST OF FIGURES

NOMENCLATURE

B	Constant in "law of the wall" velocity profile.
C	Constant in "law of the wall" velocity profile.
C_D	Dissipation integral in Eq. (17).
$C_{D_{equi}}$	Equilibrium value of C_D.
$C_{D_{F.P.}}$	Flate plate (equilibrium zero pressure gradient) value of C_D.
C_{fw}	Wall friction coefficient $2\tau/\rho U_\infty^2$.
e	Hot-wire voltage.
E	Normalized longitudinal turbulence intensity energy spectrum function.
H	Shape factor δ^*/θ
$\overline{H}$	Energy factor δ^{**}/θ
k	Wave number $2\pi n/u$.
K	Constant in Eq. (25).
K_e	Proportionality constant for not-wires.
ℓ	Mixing length $[\tau/\rho \ (\frac{\partial u}{\partial y})^2]^{1/2}$.
n	Frequency
N.S.C.	Normal stress correction to von Karman momentum integral equation.
R	Radius.
R_θ	Reynolds number based upon momentum thickness $\theta U_\infty/\nu$
u	Component of mean velocity parallel to wall.
u'	Fluctuating component of u.
ν_τ	Friction velocity $\sqrt{\tau_w/\rho}$
U_∞	Free stream velocity.
$U_{o\infty}$	Free stream velocity at start of test section.

v   Component of mean velocity normal to wall.

v'   Fluctuating component of v.

x   Coordinate parallel to wall.

y   Coordinate perpendicular to wall.

α Angle.

δ Boundary layer thickness.

δ^* Displacement thickness $\int_0^\infty (1 - \frac{u}{U_\infty}) (1 + \frac{y}{R}) dy$.

δ^{**} Energy thickness $\int_0^\infty \frac{u}{U_\infty} (1 - \frac{u^2}{U_\infty^2}) (1 + \frac{y}{R}) dy$.

ΔP Pressure drop.

ϵ Eddy viscosity $- \overline{u'v'} / \frac{\partial u}{\partial y}$.

θ Momentum thickness $\int_0^\infty \frac{u}{U_\infty} (1 - \frac{u}{U_\infty}) (1 + \frac{y}{R}) dy$.

ν Kinematic viscosity.

ρ Density.

τ Shear stress.

τ_w Wall shear stress.

UPSTREAM HISTORY AND APPARENT STRESS

IN TURBULENT BOUNDARY LAYERS

Perry Goldberg

I. INTRODUCTION

A. General Review

The fundamental difficulty in the analysis of any turbulent shear flow is relating the turbulent exchange of momentum (apparent or turbulent shear stress) to the mean-flow. Due to limited understanding of the turbulent process, and also because of limited analytical and experimental methods, this difficulty cannot be completely avoided at the present time.

Most previous attempts at solving the turbulent boundary layer problem were based on knowledge concerning the behavior of laminar boundary layers where the shear stress is proportional to the derivative of velocity profile. These attempts centered around the assumption that the turbulent fluctuations were only a function of the local velocity profile. Based upon this assumption and experimental data the turbulent shear stress was expressed by means of an eddy viscosity or mixing length which was correlated in terms of local properties. These empirical correlations along with integral methods allowed prediction of turbulent boundary layer behavior.

Recently, as more experimental turbulent boundary layer data has become available, more people have begun to question the hypothesis that the turbulent shear stress is uniquely defined by the local velocity profile. From hot-wire measurements, it appears as though the upstream development of the flow (history), as well as mean velocity profile, plays a role in determining the turbulent shear stress.

In 1960 Stewart[1] published the results of a study of six turbulent boundary layer prediction methods, all of which used the local property hypothesis. He found that the methods worked moderately well when applied to

conditions that were similar to those from which the methods themselves ev-
olved. But, when these conditions were somewhat different, the methods failed
rather badly.

Rotta[2] presented an excellent review of turbulent boundary layers in
1962. He concluded that the problem is far from being solved and that the
central problem is that of relating the shear stress distributions to the mean
flow and other characterizing parameters. In regard to this problem he states,
"Actually the shear stress distribution is also affected by the previous his-
tory. No proposals for the shape parameter equation which make proper allow-
ance for this circumstance have yet been made. But, at least one knows now
for certain that the insufficiency of the present calculation methods, . . .
originate here, and any attempts at a positive improvement must start at
this point."

In January of 1964, Moses[3] reported on a study of the behavior of tur-
bulent boundary layers in adverse pressure gradients. After a review of the
pertinent literature and an extensive experimental program he concludes that
the turbulent shear stress within the boundary layer is the most critical
part of any prediction method and that "A more reliable correlation and per-
haps a better understanding of the turbulent shear stress is definitely
needed."

The most recent review of existing turbulent boundary layer methods was
published by Thompson[4] in August of 1964. Thompson concludes, after a crit-
ical review of existing methods, that there is need for some precise, two-
dimensional, turbulent boundary layer measurements and also that the exist-
ing methods give widely differing and often inaccurate results.

The four reviewers mentioned above, as well as most other workers in the
field, including Clauser[5], Tetervin and Lin[6], Schubauer and Tchen[7],
etc., agree that much more work needs to be done before an adequate method

for predicting turbulent boundary layer behavior can be obtained. In general, the problem is one of understanding and describing quantitatively the turbulent processes that occur in turbulent shear flow.

The purpose of the present report is to present the results of an experimental and analytical study of the effects of upstream history on two-dimensional, incompressible, turbulent boundary layers.

B. The Problem of Upstream History

The fact that the existing calculation methods which are based upon the local property hypothesis do not work well in general could mean one of three things:

i) It could simply mean that we do not understand the processes well enough to be able to specify the correct dependence of shear stress upon local conditions.

ii) It could mean that other approximations and empirical correlations such as velocity profiles and wall shear stress required for a solution are not well enough known. For example, when using integral methods the velocity profiles which may actually form a two or three parameter family are generally assumed to form a one parameter family.

iii) Or perhaps it means that the failure of the existing methods is due to the lack of proper accounting for the upstream history of the flow. Intuitively, the turbulent fluctuations and hence turbulent shear stress must lag behind the local velocity profile changes since these fluctuations have inertia associated with them and are produced by the mean flow.

Due to the uncertainties involved in the turbulent shear stress few attempts have been made to solve the boundary layer equations exactly. Rather, the integral approach is taken, whereby the relationships of continuity and momentum are satisfied on the average and not necessarily at every point within the boundary layer. The integral approach allows one to calculate

parameters such as displacement thickness, momentum thickness, shape factor, and wall shear stress which in turn can be used to predict airfoil drag, diffuser performance, heat and mass transfer rates, etc.

The usual approach to the integral method is to assume a one, or at most a two, parameter family for the velocity profile.

$$\frac{u}{U_\infty} = f(H, \frac{y}{\delta}) \text{ or } f(H, R_\theta, \frac{y}{\delta}) \tag{1}$$

where H is a shape factor which defines the velocity profile, not necessarily δ^*/θ (although this is the most frequent definition of H). The momentum equation integrated across the boundary layer

$$\frac{d\theta}{dx} = \frac{C_{fw}}{2} - (H + 2) \frac{\theta}{U_\infty} \frac{dU_\infty}{dx} \quad \text{(Ref. 8)} \tag{2}$$

is then solved simultaneously with one auxiliary shape factor equation. The normal stress corrections to the momentum integral equation are not shown in Eq. (2) because they are generally neglected.

Auxiliary equations have generally been obtained in one of four ways:

    i)   By pure empiricism,

    ii) By integrating the momentum equation across a part of the boundary layer,

    iii) By making use of the moment of momentum equation,

    iv) By making use of the energy equation.

Any auxiliary equation must imply something concerning the turbulent shear stress. Therefore, methods (ii) to (iv), as well as (i) above, require empirical correlations. Method (ii) requires the value of τ at some point in the boundary layer, method (iii) requires the value of $\int \tau dy$, and method (iv) requires the value of $\int \tau \frac{\partial u}{\partial y} dy$.

Most auxiliary equations based only on local velocity profile parameters can be written in the following general way:

$$\theta \, \frac{dH}{dx} = f_1 (H, \, R_\theta) \, \frac{\theta}{U_\infty} \, \frac{dU_\infty}{dx} + f_2 (H, \, R_\theta) \quad \text{(Reference 2)} \tag{3}$$

We can now see that mean flow history is accounted for in the boundary layer calculations through the initial values of θ and H. However, we also see that the auxiliary equation, Equation (3), implies that the turbulent shear stress which is usually incorporated in the function f_2 is a function of local properties only and hence is not dependent upon history directly.

Some significant experimental evidence that this situation cannot be true is available in Reference (3). Figure 1 shows the variation of free stream pressure, θ, and H for three different pressure distributions reproduced from Reference (3) (distribution 1 was not included in the original report). Each of these pressure distributions is characterized by an initial adverse gradient section followed by a zero gradient section. In the zero gradient section $\theta \, \frac{dH}{dx}$ varies with H as shown in Figure 2. Based upon Equation (3) and the results shown in Figures 1 and 2, one must conclude that either f_2 is a strong function of R_θ or that something is missing in Equation (3). The former is not likely to be true since many studies of flat plate (zero $\frac{dU_\infty}{dx}$) boundary layers indicate that f_2 is a very weak function of R_θ. Therefore, it appears that something is missing. A plausible argument which can explain the behavior illustrated in Figures 1 and 2 is that in the adverse gradient sections the turbulent levels, and hence turbulent shear stresses grow; when the pressure gradient is removed the turbulence decays toward equilibrium at a rate which is slower than the rate of decay of the mean velocity profile; since the turbulence would be expected to grow faster in the steeper pressure gradients, the shear stress at the location at which the pressure gradient is removed would be larger for pressure distribution #3 than for #2. Hence, the initial rate of decay of H would be expected to be greater for #3 than for #2, as indeed it is.

The boundary layer behavior after a sudden removel of the pressure grad-
ient has been studied by Bradshaw and Ferriss[9]. In their report they
concluded that the shear stress profile cannot be a unique function of velocity
profile. They also made some observations which tend to support the argument
used above to explain the data from Reference (3), "The response of a boundary
layer to a change in pressure gradient is slow:....the earlier stages of the
response to a sudden perturbation are much nearer that which would occur if
the turbulence was unaffected by the perturbation than the response calculated
by assuming any sort of local equilibrium or a universal eddy viscosity."

Two methods for calculating turbulent boundary layers which attempt to
include the effect of the upstream history on the shear stress have appeared
in the literature after the present study had started. The first of these by
McDonald and Stoddart[10] makes use of the moment-or-momentum equation and
Coles[11] universal velocity profiles. The authors were able to get reason-
able agreement with data by a trial and error selection of one initial cond-
ition. The method appears to have some limitations, since it prevents the
boundary layer from ever reaching equilibrium. The second of these methods,
by Bradshaw, et al[12] makes use of the energy equation for the turbulent
fluctuations. This method is in the early stages of its development and
requires specifying three empirical relationships between the turbulent int-
ensities and the turbulent shear stress.

The present study was initiated with the following objectives in mind:

    i) To establish whether more upstream history than simply the
initial values of θ and H was ever required to predict turbulent boundary
layer behavior accurately,

    ii) To determine when this additional information is important,

    iii) To develop a practical and simple calculation method which
will correctly account for the additional upstream history required.

In the main, these objectives have been achieved. In addition, based upon the particular data generated in this study, it was possible to confirm the conclusions that (a) Reynolds normal stresses sometimes contribute significantly to the two-dimensional, momentum, integral equation, and (b) that in a limited Reynolds number range the velocity profiles form a one parameter family.

II. EXPERIMENTAL PROGRAM

The experimental investigation carried out during this study was designed to obtain precise measurements of turbulence quantities as well as mean flow quantities in two-dimensional, incompressible, turbulent, boundary layers for a number of different pressure distributions. The test section used was similar to that used by Moses[3]. With this test section, boundary layers free of three-dimensional effects could be generated for various pressure distributions with relative ease. The working fluid used was air. A relatively simple and efficient air supply system was constructed for these experiments.

A. Apparatus

Figure 3 presents a schematic of the test apparatus. An axial flow fan, rated at 16,000 cfm at 3 inches of water static, fitted with a radial inlet, supplies air to the system. Downstream of the fan are flow straightening vanes, a screen, motor fairing, and diffuser all of which serve the purpose of reducing losses and steadying the flow. The air which leaves the diffuser enters an aluminum settling chamber 6 feet in diameter and 10 feet long. The settling chamber contains a honeycomb flow straightener, a center tube which is held in place by a vertically mounted airfoil strut, and an 86 mesh silk screen with approximately 46% free flow area for reducing turbulence. The center tube provides support for the upstream end of the test section, as well as for the honeycomb. To prevent blower vibrations from reaching the settling chamber a flexible coupling, actually a piece of heavy fabric, is used to seal the gap between blower and diffuser (the diffuser being rigidly attached to the settling chamber). The flow leaving the settling chamber is accelerated to approximately 85 ft/sec by a 9 to 1 area contraction which further reduces the turbulence levels and also reduces any longitudinal velocity variations which might be present. The free stream turbulence intensity measured at the exit of the contraction is approximately 0.2%.

The test boundary layer was grown on a central, 10 inch diameter, Plexiglas cylinder 6 feet in length. This cylinder is concentric with a 4 foot long, 24 inch diameter outer porous metal cylinder. An adjustable end plate causes the annulus pressure to be greater than ambient. Thus, flow diffuses out through the porous metal and creates an adverse pressure gradient. The end plate can be removed for generating zero pressure gradient. The pressure distribution was adjusted as desired by controlling the flow diffusing through the porous cylinder. This was accomplished with cloth bands which were wrapped around the outer cylinder. The outer cylinder had been provided with a longitudinal slot and guides for making boundary layer traverses.

Figure 4 presents a number of photographs of the test apparatus: Figure 4a shows the fan with its radial inlet, exit cone and exit screen; Figure 4b, the settling chamber with its diffuser and contraction section; Figure 4c, the center tube, airfoil strut and honeycomb flow straightener; Figure 4d, the test section - inner Plexiglas cylinder fitted with contoured nose piece, outer porous metal cylinder with traversing slot and guides, center support tube, and adjustable back-up plate.

B. Instrumentation

Static pressure and wall shear stress measurements made with a Preston tube and sub-layer fences were recorded by hand. All measurements of quantities distributed across the boundary layer were recorded on a Moseley Autograph X-Y Plotter. The y-axis of the plotter was driven by a signal proportional to distance from the wall and the x-axis by the particular quantity being measured.

B.1 Traversing Mechanism

A micrometer with 2 inch maximum travel was used to traverse probes across the boundary layer. The micrometer barrel was connected to a ten turn

Micro-pot by means of a friction reduction drive. The Micro-pot was supplied with a fixed DC exicitation of 6 volts, thus giving as output a DC voltage proportional to probe displacement, which was then used to drive the y-axis of the X-Y recorder.

B.2 Pressure Measurements

Static pressure distribution: the inner Plexiglas cylinder was fitted with static pressure taps spaced 2 inches apart along a line parallel to the cylinder center line. Also, at 12 inch intervals, 3 additional taps were installed symmetrically around the cylinder to allow a quick check of the lateral static pressure variation. The inner cylinder could also be rotated to more precisely check the transverse pressure variation. The static taps were .025 inches in diameter, and were machined from 1/8 inch brass plugs which were pressed into the Plexiglas cylinder then ground flush to the surface.

The static pressures were read on a 26 tube manometer board inclined at approximately 8.5° to the horizontal. This manometer board allowed the pressure distribution to be observed directly, thus facilitating the establishment of desired test conditions.

Wall shear stress: wall shear stress was measured with a Preston tube and with sub-layer fences. The Preston tube used was .050 inches in diameter.

Seventeen sub-layer fences were located on the test cylinder along a line parallel to the row of static pressure taps. The sub-layer fences were offset laterally about 2 inches from the static pressure taps. Each of the sub-layer fences shown in the following sketch was machined
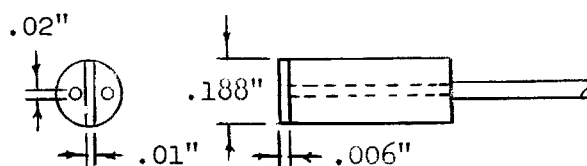
out of a brass plug 3/16 of an inch in diameter, which was pressed into the

Plexiglas cylinder and then ground flush with the surface on either side of the fence. The fences are approximately .010 inches thick and .006 inches high. Two .020 inch diameter static pressure holes are placed in each plug on either side of the fence.

The Preston tube and sub-layer fence pressures were read on inclined manometer boards. The fence pressures were displayed on a board similar to the one used for the static pressure distribution. Thus, the wall shear stress distribution could also be observed directly.

Velocity profiles: the mean velocity measurements were made with a flattened total head tube having an outside height of .014 inches. A Statham ΔP pressure transducer with a maximum range of $\pm$ .05 psi was used to transduce the velocity pressure to a DC voltage which then was used to drive the x-axis of the X-Y recorder.

B.3 Hot-Wire Measurements

The constant temperature system for hot-wire measurements was used in this study. Power was supplied to a transistorized, constant temperature amplifier and linearizer, manufactured by Leslie T. Miller of Baltimore, Maryland, by two 6 volt wet-cell batteries. The DC component of the linearizer output was monitored on a Heathkit VTVM and the AC or fluctuating component on a Hewlett-Packared Model #3400A RMS Meter. The linearizer output was also displayed on a Tektronik Type 535 Oscilloscope and recorded on the X-Y recorder. The output of the RMS meter was also recorded on the X-Y plotter. A General Radio Sound and Vibration Meter was used to obtain the energy spectrum measurements.

The hot-wires used were tungsten, .00015 inches in diameter, copper plated on each end of a bare section, and soft soldered to two supporting needles. The mounted wire resistance was normally between 8 and 12 ohms.

Turbulent shear stress Distributions: these measure-

ments were made with the single wire probe sketched below and shown in Figure 5 along with the micrometer traversing mechanism.
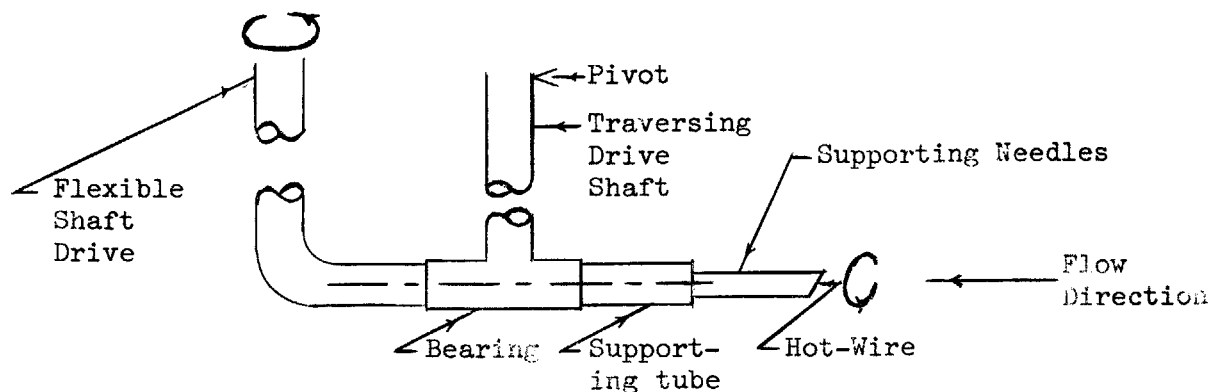
The single wire was aligned at approximately 45° to the center line of the supporting tube which was free to rotate 180° in a bearing fixed to the traversing drive shaft. A flexible shaft drive allowed the wire to be rotated from above. The axis of rotation of the probe could be aligned with the flow direction by tilting the whole probe about the pivot provided by the micrometer traversing unit.

Figure 6 shows the various probes used in this study, and Figure 7 the major instrumentation.

C. Experimental Procedure

Before making any quantitative measurements the boundary layer flow was checked for axi-symmetry as follows: First, the lateral static pressure variations were checked; second, the lateral variation of the wall shear stress, as indicated by the sub-layer fences, was checked; finally, the movement of the separation line, as indicated by tufts and sub-layer fences as the cylinder was rotated, was checked. No evidence of any three-dimensional flow was found.

After it was established that there was no three-dimensional flow present, a zero pressure gradient case was set-up to verify that the instrumentation and measurement schemes were working properly and also, to obtain calibration curves for the sub-layer fences. A complete set of pressure and hot-wire

measurements was then taken. This data, when reduced, agreed with the measurements presented by Klebanoff[13]. In addition, the wall shear stresses, 1) measured with a Preston tube, 2) calculated from the momentum integral equation and velocity profile data, 3) obtained by extrapolating the measured shear stress distributions to the wall, and 4) estimated by the two Ludwig-Tillmann[14] correlations

$$\text{L.-T. 1} \qquad \frac{C_{fw}}{2} = \frac{.0167}{(\log_{10} R_\theta)^{1.838}} \qquad (4)$$

$$\text{L.-T. 2} \qquad C_{fw} = \frac{.246}{R_\theta^{.268} \, 10^{.678H}} \qquad (5)$$

showed very good agreement as seen in Figure 8.

The sub-layer fence Δp's were calibrated against a Preston tube Δp in zero pressure gradient. Four experimental points, in addition to the origin, were used to generate calibration curves. These points were obtained by varying the test section flow. Figure 9 shows 3 typical calibration curves. A separate curve was required for each fence, due to variations in dimensions, as well as variations in orientation (with respect to the flow direction) of the installed fences.

Five additional pressure distributions were then established and studied. The experimental data for each pressure distribution was obtained in the following sequence: 1) wall static pressure, 2) sub-layer fence Δp, 3) Preston tube Δp, 4) total head tube velocity profiles, 5) mean velocity from hot-wire, 6) longitudinal turbulence intensity, 7) longitudinal turbulence energy spectrum, 8) mean readings of the shear stress wire in both the $0°$ and the $180°$ positions, 9) RMS readings of the shear stress wire in both positions.

D. Data Reduction

Some typical raw data is shown in Figure 10. The X-Y recorder traces of velocity pressure, longitudinal turbulence intensity, and shear stress are

shown in Figure 10a, b, and c, respectively.

In reducing the recorder data a mean line was first drawn through each trace. Then, values taken from the mean line were tabulated at appropriate intervals. The tabulated data was punched on IBM cards and a 7094 IBM Digital Computer was used to reduce the data further.

Three computer programs were utilized in reducing the data. The first of these evaluated mean flow parameters from the pressure measurement. The values of displacement thickness, momentum thickness, energy thickness, shape factor, and energy shape factor were calculated for both their two-dimensional and axi-symmetric definitions:

	Two-Dimensional	Axi-Symmetric
Displacement Thickness δ^*	$\int_0^\infty (1 - \dfrac{u}{U_\infty})\,dy$	$\int_0^\infty (1 - \dfrac{u}{U_\infty})(1 + \dfrac{y}{R})\,dy$
Momentum Thickness θ	$\int_0^\infty \dfrac{u}{U_\infty}(1 - \dfrac{u}{U_\infty})\,dy$	$\int_0^\infty \dfrac{u}{U_\infty}(1 - \dfrac{u}{U_\infty})(1 + \dfrac{y}{R})\,dy$
Energy Thickness δ^{**}	$\int_0^\infty \dfrac{u}{U_\infty}(1 - \dfrac{u^2}{U_\infty^2})\,dy$	$\int_0^\infty \dfrac{u}{U_\infty}(1 - \dfrac{u^2}{U_\infty^2})(1 + \dfrac{y}{R})\,dy$
Shape Factor H	$\dfrac{\delta^*}{\theta}$	$\dfrac{\delta^*}{\theta}$
Energy Shape Factor $\overline{H}$	$\dfrac{\delta^{**}}{\theta}$	$\dfrac{\delta^{**}}{\theta}$

The maximum difference between the axi-symmetric and two-dimensional values of δ^*, θ, and δ^{**} was found to be about 10%, whereas the maximum difference for H and $\overline{H}$ was found to be only about 2%. Throughout the remainder of this report the axi-symmetric definitions will be implied unless specifically mentioned otherwise. With these values the momentum integral equation, as presented in Equation (2), need not be changed. Had the two-dimensional

definitions been used this equation would have had to be corrected for transverse curvature.

The second program was used to compute the values of $\overline{u'^2}/u_\infty$, $-\overline{2u'v'}/U_\infty^2$, and $\overline{v'^2}/U_\infty$ from the hot-wire data.

The third program was used to compute the longitudinal energy spectrum $E(k)/\overline{u'^2}$ and wave number k from hot-wire data.

The correlation of Patel[15] was used to obtain estimates of wall shear stress from the Preston tube data. The sub-layer fence data was reduced by first finding the equivalent Preston tube reading from the fence zero pressure gradient calibration curve, and then using Patel's[15] correlation. No corrections for pressure gradient were made for either set of wall shear stress data.

E. Accuracy

The static pressure distribution could be determined to better than .5%. A few static taps read consistently high or low. These taps were generally neglected in reducing the data.

No corrections to the total pressure readings were made for the effects of turbulence, streamline displacement, or the wall. The linearity of the transducer used to record the velocity pressures is illustrated in Figure 11, where transducer Δp ratios are plotted against manometer board Δp ratios. The overall accuracy of the velocity measurements is estimated to be better than 5% except for measurements within 2 or 3 probe heights (.014") from the wall where due to the wall effect the accuracy should be somewhat poorer.

The pressure measurements presented no particular problem. The hot-wire measurements were more difficult due to such problems as linearity, drift, and orientation for the shear stress wire. The linearity problem was overcome by frequent calibration of the electronic equipment.

Drift was minimized by the effective filtering of large dust particles.

This was done by two fine mesh silk screens, (1) the main turbulence reduction screen in the settling chamber, and (2) a piece of the same material that was placed across the inlet of the fan. Another factor which greatly reduced the drift problem was the speed at which boundary layer traverses could be made. The use of the X-Y recorder made it possible to make a boundary layer traverse in about a minute.

Accurate shear stress measurements require accurate alignment of the shear stress measuring wire or wires with the mean flow. With a single wire probe, the axis of rotation of the probe must be aligned with the local mean flow direction so that the angle between the wire and the local mean velocity will change in sign only when the probe is rotated $180°$. To have done this at every measurement point would have required a prohibitive amount of time. Instead, some accuracy was sacrificed in the outer part of the layer where the shear stresses are generally small and the probe orientation was fixed for each traverse by the conditions existing near the wall at each longitudinal station. The Appendix presents a simplified analysis of shear stress errors due to misalignment of the measuring wire or wires.

A consideration of the errors entering the hot-wire measurements, along with cross checks made on the data, indicates the maximum error for the measurements presented is of the order of 5% for the u' measurements and 15% for the $\overline{u'v'}$ measurements, except in the outer 20% of the boundary layer were the $\overline{u'v'}$ measurements may be somewhat larger.

F. Experimental Results

Typical experimental results are shown in Figures 12 to 17. The mean flow quantities shown in Figures 12 and 13 include the pressure distribution in terms of the free stream velocity and the usual integral parameters, θ and H, which were determined from the measured velocity profiles. These values are shown as a function of x, the distance along the cylinder starting from the first pressure

tap, which was approximately the point of minimum pressure.

The three pressure distributions chosen to study the effects of upstream history are shown in Figure 12. Each consists of an initially adverse pressure gradient section followed by a zero pressure gradient section. Since the equilibrium boundary layer behavior in zero pressure gradient has been well documented, these pressure distributions allowed a study of the non-equilibrium zero pressure gradient behavior induced by the upstream history (initial adverse pressure gradient section). From this figure it is seen that the mean flow, as typified by the shape factor, appears to return to equilibrium at a rate which is proportional to the departure from equilibrium. Also apparent from Figure 12 is that it takes the mean flow on the order of 100 momentum thicknesses to return to equilibrium.

Two linear pressure distributions are shown in Figure 13. Pressure Distribution #5 is a linear gradient starting at x = 0 where the boundary layer is very thin and continuing on to separation. Pressure Distribution #6 is zero pressure gradient, followed by an adverse gradient driving the boundary layer to separation. Distribution #6 is much more severe than #5 for two reasons; first, the rate of pressure rise is faster and, second, the momentum thickness at the initiation of the adverse gradient is some three times larger. These two distributions were included in the study in an attempt to define the upstream history effect more thoroughly.

Figures 14a and b show a comparison of the various methods used to obtain wall shear stress for Pressure Distributions #3 and #5, respectively. Preston tube and sub-layer fence measurements are plotted as a function of longitudinal distance x along with values obtained from (a) a Clauser[5] type determination based upon the law of the wall and measured velocity profiles and (b) the Ludwig-Tillmann[14] correlation, Equation (5). In general, the agreement is good. For all of the pressure distributions studied, the Ludwig-Tillmann

correlation predicted values about 10% higher than those measured when the

Reynolds number R_θ was about 1,000, but gave values much closer to those

measured as R_θ increased. The sub-layer fences used in this study do not

seem to give any better results than the simple, relatively large, Preston

tube.

Measured longitudinal turbulence intensities for Pressure Distributions

#3 and #5 are presented in Figures 15a and b, respectively. From this figure

it is seen that in an adverse pressure gradient the distribution of u' across

the boundary layer develops a maximum which grows and moves away from the wall

as the boundary layer progresses downstream. Also apparent from Figure 15a

is that when the pressure gradient is removed this maximum decreases in the

downstream direction and eventually disappears as the boundary layer approach-

es equilibrium (althouth the test cylinder was not long enough for the bound-

ary layer of Pressure Distribution #3 to return fully to equilibrium, this

last remark was verified by measurements made for Pressure Distribution #4).

From a comparison of Figure 12 and Figure 15a it can be seen that H returns to

equilibrium faster then u'.

Typical hot-wire shear stress measurements are shown in Figures 16a and

b again for Pressure Distributions #3 and #5, respectively. To complete the

shear stress distributions, the shear stress at the wall, as determined from

the Preston tube and sub-layer fence measurements, has been added.

The shear stress behavior is similar to the longitudinal turbulence

intensity behavior in that in the adverse gradient section a maximum develops

and moves away from the wall and when the adverse gradient is removed this

maximum decays. Since the equilibrium shear stress distribution for zero

pressure gradient has a maximum at the wall only, it is apparent from Figure

16a that the shear stress distribution cannot be characterised by pressure

gradient alone.

Energy spectra for the longitudinal turbulence intensity are shown in Figures 17a, b, and c. Figures 17a and b present rectangular coordinate plots of normalized energy spectrum versus wave number for Pressure Distributions #3 and #5, respectively. These spectrum measurements were made with a hot-wire that was within .010 inch of the wall. The measurements indicate that in an adverse pressure gradient there is a substantial shift of energy from high to low frequency near the wall. Additional spectrum measurements indicate that this shift of energy from high to low frequency also occurs in the outer region of the boundary layer, but to a lesser extent. In Figure 17c some energy spectrum measurements for Pressure Distribution #5 are presented in the form which is generally found in the literature.

III. PRESENTATION AND DISCUSSION OF FINDINGS

A. Normal Stresses

A calculation of momentum thickness from the von Karman momentum int-
egral equation, Equation (2), was carried out for all six pressure distrib-
utions considered in this study, (Pressure Distribution #1 was the case of
zero pressure gradient used to verify measurements). In this calculation
the experimental values of wall shear stress, shape factor, and pressure
distribution were used. The results of this calculation, along with the
experimental data are shown in Figure 18. A significant difference between
the calculated values and the experimental values can be noted. Since this
difference is larger than would be expected, due to experimental errors, a
further study of the momentum integral equation was made.

The von Karman momentum integral equation, Equation (2), has within it
the assumption that the Reynolds normal stresses can be neglected, a fact
which has been disputed by a number of authors. In References 16 thru 20
the validity of this assumption, especially near separation, has been quest-
ioned. Without this assumption the momentum integral equation can be written
as

$$\frac{d\theta}{dx} = \frac{C_{fw}}{2} - (H + 2) \frac{\theta}{U_\infty} \frac{dU_\infty}{dx} + \frac{1}{U_\infty^2} \int_0^\infty \frac{\partial}{\partial x} (\overline{u'^2} - \overline{v'^2}) dy \qquad (6)$$

The term containing $\overline{u'^2}$ comes directly from the x momentum equation. The
$\overline{v'^2}$ term enters the equation through a static pressure variation across the
boundary layer.

In order to investigate the importance of these Reynolds normal stress-
es, the momentum thickness calculations were repeated. Estimates of the
first correction term

$$\frac{1}{U_\infty^2} \int_0^\infty \frac{\partial}{\partial x} \overline{u'^2} \, dy$$

evaluated directly from the experimental data were included.

An estimate of the second correction term

$$- \frac{1}{U_\infty^2} \int_0^\infty \frac{\partial}{\partial x} \overline{v'^2} \, dy$$

was also made from the experimental data. It was found that in general

$$\int_0^\infty \frac{\partial}{\partial x} v'^2 \, dy = \frac{1}{2} \int_0^\infty \frac{\partial}{\partial x} \overline{u'^2} \, dy \; . \tag{7}$$

Based upon this approximation the momentum thickness calculations were repeated, this time using the full equation as presented in Equation (6).

The results of these additional calculations are also shown in Figure 18. As can be seen, particularly in Figure 18c, the Reynolds normal stresses make a noticeable contribution to the calculated momentum thicknesses.

However, the normal stresses do not fully account for the momentum thickness behavior. The effects of longitudinal streamline curvature could explain the discrepancies shown in Figure 18. In a decelerating boundary layer the streamline curvature causes a pressure rise across the boundary layer ($\frac{dP}{dy} < 0$) which increases in the downstream direction causing the boundary layer to grow faster than would be predicted by assuming no static pressure variation across the boundary layer.

One possible reason why more experimenters have been unable to reach a definite conclusion regarding the importance of normal stresses is evident from Figures 18c and d: when the boundary layer is driven rapidly to separation the effect of normal stresses is not nearly as noticeable as when the boundary layer is driven close to separation and then allowed to return to some equilibrium condition away from separation.

Based upon the data generated in this study and the data presented in References 18, 21, and 22, a correlation for a normal stress correction (N.S.C.) to the von Karman momentum integral equation (Equation (2)) has

been generated. The correlation is as follows,

$$\text{N.S.C.} = .0365 (H - 1) \frac{d\delta^*}{dx} . \tag{8}$$

A comparison of the experimental data points and the correlation is shown in Figure 19. The scatter is rather large, but is to be expected since x derivatives of the data must be taken to determine the N.S.C. The results of using the correlation to predict θ are shown in Figure 18.

The correlation as proposed is somewhat similar to that suggested by Ross[19]

$$\text{N.S.C.} = \frac{.016}{U_\infty^2} \frac{d(\delta^* U_\infty^2)}{dx} \tag{9}$$

in that the correction depends upon the derivative of δ^* and leads to a singularity in the momentum integral equation. This can easily be seen if δ^* is replaced by θH in Equation (8) and if this equation is added to Equation (2)

$$\frac{d\theta}{dx} = \frac{\frac{C_{fw}}{2} - (H + 2) \frac{\theta}{U_\infty} \frac{dU_\infty}{dx} + .0365(H - 1)\theta \frac{dH}{dx}}{1 - .0365 H(H - 1)} \tag{10}$$

When H is approximately 5.7 $\frac{d\theta}{dx}$ goes to infinity. This singularity should not be a practical limitation since separation occurs well below H = 5.7.

B. Velocity Profiles

Reduced total head tube data for Pressure Distribution #3 is chosen to illustrate the behavior of the velocity profiles in an adverse pressure gradient and also in the relaxing region (zero pressure gradient region where initially disturbed boundary layer is returning to equilibrium). The velocity profile data is presented in two ways. First, Figure 20 shows $\frac{u}{U_\infty}$ plotted as a function of y at various longitudinal stations. Typically, in the adverse pressure gradient the defect in the velocity profile grows with the velocity being reduced rapidly in the vicinity of the wall and two apparent inflection points becoming evident in the profile at x = 16". In

the relaxing region the defect is slowly reduced and as equilibrium is approached the velocity profile takes on a shape characterized by two regions: one close to the wall where $\frac{u}{U_\infty}$ increases rapidly and another covering most of the boundary layer where $\frac{u}{U_\infty}$ increases slowly toward 1.

The second method for presenting the velocity profiles is shown in Figure 21 where $\frac{u}{u_\tau}$ is plotted as a function of $\frac{yu_\tau}{\nu}$. Also shown in the figure is a curve representing the laminar sub-layer velocity profile

$$\frac{u}{u_\tau} = \frac{yu_\tau}{\nu} \tag{11}$$

for $\frac{yu_\tau}{\nu}$ less than about 10 and a line representing the "universal" law of the wall

$$\frac{u}{u_\tau} = \frac{1}{B} \log \frac{yu_\tau}{\nu} + C \tag{12}$$

where constants B and C have been assumed to be those used by Coles[11]. All of the velocity profiles can be divided into a sub-layer region, a law of the wall region, and a wake region. In the former two regions, the expressions represented by Equations (11) and (12) fit all of the data reasonably well with the exception of the data for x = 24 inches which for some unknown reason falls somewhat low. The wake region grows in the pressure gradient as the wall shear stress decreases and then decays in the relaxing region.

Evidence that the velocity profile can be well represented by a single parameter family in a relatively small R_θ range, as suggested by von Doenhoff and Tetervin[32], Coles[11], and others, is given by Figure 22. In this figure the energy shape factor $\overline{H}$ is plotted as a function of H. All of the data taken in this study can be well represented by a single line. No distinction could be made between data points for the same shape factor in regions of rising or falling H (adverse pressure gradient or relaxing zero pressure gradient sections). The curve shown in Figure 22 which fits the data reasonably well

$$\overline{H} = \frac{3.6\ H}{2.78\ H - 1} \tag{13}$$

was obtained by juggling the constants in the expression for $\overline{H}$ vs H from power law velocity profiles. Another expression proposed by Nicoll & Escudier[23]

$$\overline{H} = 1.431 - \frac{.097}{H} + \frac{.773}{H^2} \qquad\qquad 1.25 \le H \le 2.8 \tag{14}$$

yields results within about 2% of Equation (13) and hence would fit the data in Figure 22 equally well.

The Reynolds number effect upon velocity profiles cannot be established from this study since the total range of R_θ covered was only

$$1,000 \le R_\theta \le 10,000$$

with most of the data falling below R_θ = 5,000. Using some form of logarithmic velocity profile, such as that proposed by Coles[11], there would be a slight downward shift of the curve of $\overline{H}$ vs H as Reynolds number increased.

C. Turbulent Shear Stress

To solve any turbulent boundary layer problem an assumption about the turbulent shear stress based upon empirical information must be made. Three basic approaches are usual.

First, correlate $\theta\frac{dH}{dx}$ empirically and directly, thus allowing a solution of the integral equations and hence implying something about the shear stress.

Second, utilize empirical data to specify the shear stress distribution either (a) directly, (b) in terms of an eddy viscosity, or (c) in terms of a mixing length. Then either:

  i) attempt a direct numerical solution of the partial differential equations

  ii) use the shear stress distribution to evaluate the shear stress at some point in the boundary layer and solve integral equations as described in Reference (3).

iii) evaluate shear stress integrals required for a solution. Most frequently, either the moment-of-momentum equation or mean-flow energy equations are used. For power-law mean velocity profiles the moment-of-momentum equation takes the form

$$\theta \frac{dH}{dx} = -\frac{H(H + 1)(H^2 - 1)}{2} \frac{\theta}{U_\infty} \frac{dU_\infty}{dx} + (H^2 - 1)\left[H \frac{C_{fw}}{2} \right.$$

$$\left. -\frac{(H + 1)}{\theta \rho U_\infty^2} \int_0^\infty \tau \ dy \right] \qquad \text{(Reference 6)} \qquad (15)$$

requiring $\int_0^\infty \tau \ dy$. The mean-flow energy equation, Reference 8,

$$\frac{d\bar{H}}{dH} \frac{dH}{dx} = (H - 1) \bar{H} \frac{\theta}{U_\infty} \frac{dU_\infty}{dx} - \frac{\bar{H}C_{fw}}{2} + C_D \qquad (16)$$

requires C_D which is defined as

$$C_D = \frac{2}{\rho U_\infty^2} \int_0^\infty \tau \frac{\partial \frac{u}{U_\infty}}{\partial y} \ dy \qquad (17)$$

Third, use empirical information to correlate directly either the shear stress at some specified location in the boundary layer[3] or one of the shear stress integrals.

Needless to say the first approach above is the poorest in terms of generality and in terms of providing some understanding of the turbulent process and hence will not be considered further. The second and third approaches, however, will be discussed in some detail in light of the data obtained in this study.

Before continuing with the discussion a result presented in an earlier section regarding the wall shear stress is repeated. Based upon all of the wall shear stress measurements made in this study the Ludweig-Tillmann[14] correlation

$$C_{fw} = \frac{.246}{R_\theta^{.268} 10^{.678H}} \qquad (5)$$

appears to be perfectly adequate for Reynolds numbers based upon momentum

thickness between 2 and 10 thousand.

C.1 Polynomial Representation

A number of attempts have been made to represent the turbulent shear stress distribution by a polynomial in terms of y/δ. Perhaps the first of these attempts was made by Fediaevsky[24] who, following the Pohlhausen method for laminar flow, expresses τ/τ_w in terms of a fourth order polynomial in y/δ and evaluates the coefficients to satisfy appropriate boundary conditions at the wall and at the free stream. Another attempt somewhat similar to Fediaevsky's was made by Ross and Robertson[25] who tried to include some upstream history in their shear stress distribution by making the boundary condition on $\frac{d}{dy}(\frac{\tau}{\tau_w})$ at $y = \delta$, a function of the initial value of $\frac{\tau_w}{\delta}$. The basic shortcomings of both of these attempts are discussed by Rotta[2] who finds poor agreement between calculated shear stress distributions and the data of Schubauer and Klebanoff[22].

Another approach which utilizes a polynomial representation for shear stress is that described by Libby, et al[25] for equilibrium boundary layers. In this approach, the boundary layer was broken up into (a) an inner region where the shear stress was obtained by integrating a law of the wall type logarithmic velocity profile and (b) an outer region where the shear stress was represented by a polynomial in y/δ. At the boundary between the two regions the velocity profile and the shear stress profile and its derivative were forced to be continuous. In addition, the eddy viscosity ε defined as

$$\varepsilon = \frac{-\overline{u'v'}}{\frac{\partial u}{\partial y}} \tag{18}$$

was assumed to be constant in the outer region. With experimental data for equilibrium boundary layers such as Clauser's[5] the empirical functions required in this approach were evaluated. This approach is not applicable

in the present situation since these authors were dealing only with equil-
ibrium boundary layers which, in essence, have no history.

Based upon the results of these previous studies, several unsuccessful
attempts were made to express the shear stress distributions in the relaxing
region of Pressure Distributions #2, #3, and #4, with polynomials.

C.2 Eddy Viscosity

The eddy viscosity as defined in Equation (18) has been used very often
to relate the turbulent shear stress to the mean velocity profile. Rotta[2]
presents a summary of eddy viscosity relations employed in the region near
the wall. Clauser[26] suggested that the eddy viscosity away from the wall
region can be assumed constant and also that

$$\frac{\varepsilon}{U_\infty \delta^*} = .018. \tag{19}$$

Based upon Clauser's work, Libby et al[25] and Mellor and Gibson[27] have
formulated methods for calculating equilibrium boundary layer behavior.
However, Bradshaw and Ferriss[9] have questioned the assumption of constant
eddy viscosity away from the wall and distributions evaluated from hot-wire
shear stress data do not usually exhibit this behavior.

Eddy viscosity distributions for Pressure Distributions #3 and #5 are
shown in Figs. (23) and (24), where $\frac{\varepsilon}{U_\infty \delta^*}$ is plotted against y with x as a
parameter. The eddy viscosity is zero at the wall, reaches a maximum some-
where near the middle of the boundary layer, and returns to zero at $y = \delta$.
The variations of $\frac{\varepsilon}{U_\infty \delta^*}$ at fixed y/δ are large particularly for Pressure
Distribution #3. In an adverse pressure gradient $\frac{\varepsilon}{U_\infty \delta^*}$ decreases. When the
pressure gradient is removed it then increases rapidly. This behavior was
found to be typical for all of the pressure distributions considered in this
study.

An attempt was made to determine a more appropriate normalization for

eddy viscosity. For this attempt a mean value of eddy viscosity in the central portion of the boundary layer was estimated from the data at each measurement station. The results of these calculations are summarized in Table I which presents the maximum and minimum values for four different normalizations of eddy viscosity. In all cases the distribution of values between the maximum and minimum was fairly uniform.

Table I Eddy Viscosity Variations

	$\dfrac{\varepsilon}{U_\infty \delta^*}$	$\dfrac{\varepsilon}{U_\tau \delta^*}$	$\dfrac{\varepsilon}{U_\infty \theta}$	$\dfrac{\varepsilon}{U_\tau \theta}$
Maximum Value	.028	.79	.039	1.4
Minimum Value	.0048	.26	.014	.51

The parameter $\dfrac{\varepsilon}{U_\infty \delta^*}$ suggested by Clauser shows a somewhat larger variation than the other three parameters. Clauser was primarily concerned with equilibrium boundary layers, whereas the boundary layers in this study were generally not in equilibrium. However, even the best of these four has a ratio of about 3 between the maximum and minimum values.

C.3 Mixing Length

The mixing length as defined by Prandtl

$$\ell = \left[\frac{\tau}{\rho \left(\frac{\partial u}{\partial y} \right)^2} \right]^{1/2} \qquad (20)$$

also has been used to relate the turbulent shear stress to the mean velocity profile. Rotta[2] once again presents a summary of expressions for mixing lengths proposed for use in regions close to the wall. Escudier and Spalding[28] have recently published an approximate expression for the mixing length distribution which says that the mixing length is constant in the outer 81% of the boundary layer and equal to .075 δ.

Figures 25 and 26 show mixing length distributions for Pressure Distributions #3 and #5, evaluated from experimental shear stress and velocity

data. In general, the shape of the distributions agrees reasonably well with the Escudier and Spalding[28] assumption of constant mixing length over most of the boundary layer. However, the magnitude of this constant level varies considerably. In the adverse pressure gradient $\frac{\ell}{\delta*}$ decreases. When the pressure gradient is removed $\frac{\ell}{\delta*}$ grows rapidly. A study of the variations of $\frac{\ell}{\delta*}$, $\frac{\ell}{\theta}$, and $\frac{\ell}{\delta}$ for the data of this study indicates that $\frac{\ell}{\delta}$ shows somewhat less variation than either $\frac{\ell}{\delta*}$ or $\frac{\ell}{\theta}$. Similar to the variations found for the eddy viscosity, the maximum and minimum values of $\frac{\ell}{\delta}$ differed by a factor of approximately three. Table II presents the limiting values of the mean mixing length over the outer portion of the boundary layers for Pressure Distributions #3 and #5. Once again the values were fairly well distributed between the maximum and minimum values.

Table II   Mixing Length Variations

	$\frac{\ell}{\delta*}$	$\frac{\ell}{\theta}$	$\frac{\ell}{\delta}$
Maximum Value	.55	.75	.10
Minimum Value	.10	.22	.04

C.4 Shear Stress Integrals

The shear stress integrals required in the moment-of-momentum and the mean-flow energy integral equations have been evaluated from the hot-wire shear stress data. These are presented in Table III along with the Reynolds number based upon momentum thickness and the shape factor. As seen the variations of these integrals over the range of test conditions is not large. Some of this variation is undoubtedly due to experimental errors and some to real variations. The effects of variations in the shear stress integrals are magnified in the equations for $\theta \frac{dH}{dx}$ (for example, at H = 1.5 a 10% change in either integral produces more than a 30% change in $\theta \frac{dH}{dx}$, and at higher shape factors even greater changes). The difficulty of obtaining a valid corr-

Table III Shear Stress Integrals Based Upon

Hot-Wire Shear Stress Measurements

Pressure Distribution	x in	R_θ	H	$\int_0^\delta \frac{\tau}{\rho U_\infty^2} \, d\frac{y}{\delta^*}$	$\int_0^\delta \frac{\tau}{\rho U_\infty^2} \frac{\partial \frac{\overline{u}}{U_\infty}}{\partial y} \, dy$
		$\times 10^{-3}$		$\times 10^2$	$\times 10^3$
1	20	2.5	1.33	.79	1.71
	42	4.1	1.33	.58	1.56
2	4	1.2	1.41	.82	2.08
	8	1.9	1.47	.80	1.85
	12	2.8	1.61	.85	1.85
	16	3.9	1.78	.90	1.85
	20	4.4	1.72	.83	1.76
	24	4.6	1.58	.97	1.93
	28	4.7	1.49	.79	1.58
	32	4.8	1.43	.82	1.58
	36	4.9	1.36	.88	1.52
	40	5.0	1.35	.84	1.41
3	4	1.2	1.42	.68	1.91
	8	1.8	1.47	.51	1.41
	12	2.9	1.72	.36	1.0
	14	3.5	1.98	.46	1.54
	16	4.3	2.15	.50	1.84
	18	4.7	2.25	.60	2.25
	20	5.0	2.15	.63	2.37
	22	5.2	1.93	.77	2.05
	24	5.4	1.80	.85	1.74
	28	5.6	1.60	.90	1.67
	32	5.7	1.48	1.02	1.56
	36	5.8	1.42	.97	1.46
4.	4	1.2	1.45	.41	1.69
	8	1.8	1.44	.41	1.33
	12	2.3	1.46	.38	1.48
	16	2.8	1.46	.53	1.52
	20	3.1	1.42	.53	1.43
	24	3.3	1.39	.47	1.39
	28	3.5	1.37	.52	1.44
	32	3.7	1.36	.50	1.46
	36	3.8	1.34	.50	1.41
5	4	1.2	1.39	.45	1.86
	8	1.6	1.42	.37	1.79
	12	2.1	1.42	.65	1.80
	16	2.6	1.44	.54	1.66
	20	3.2	1.48	.59	1.60
	24	4.0	1.54	.52	1.35
	28	5.0	1.63	.52	1.37

TABLE III   Continued...

5	32	6.3	1.75	.52	1.46
	36	7.9	1.84	.51	1.58
	40	10.0	2.17	.34	1.44
6	8	1.5	1.38	.78	2.20
	12	1.8	1.36	.78	2.07
	16	2.1	1.34	.72	1.85
	20	2.4	1.34	.70	1.82
	24	2.8	1.37	.60	1.71
	32	3.8	1.43	.49	1.30
	34	4.6	1.54	.55	1.44
	36	6.0	1.76	.47	1.42
	38	7.6	2.22	.60	2.35

elation of the data can be seen. What might normally be accepted as a reasonable correlation for the experimental data may actually mask important behavior.

Several attempts were made to determine the uncertainties in the values presented in Table III. The first of these was to evaluate the shear stress integrals from Equations (15) and (16) and also from

$$\frac{1}{U_\infty{}^3} \frac{d \, \delta^{**} U_\infty{}^3}{dx} = 2 \int_0^\infty \frac{\tau}{\rho U_\infty{}^2} \frac{\partial \frac{u}{U_\infty}}{\partial y} \, dy \tag{21}$$

(another form of the mean flow energy equation) using velocity profile data. This attempt was not very successful since it was found that uncertainties in the x derivatives were such that almost any level of agreement could be obtained between the values in Table III and those calculated from velocity profile data.

For the second attempt the energy thickness δ^{**} was calculated from Equation (21) using the dissipation integrals (shear stress integral required for the mean-flow energy equation) listed in Table III and then compared with those values obtained from velocity profile data. This comparison is shown in Figure 27. The differences shown in this figure can be explained in part by normal stresses which were shown to be of some importance in an earlier section but which are neglected in Equation (21). Although these calculations do not allow a quantitative statement concerning the accuracy of the integrals listed in Table III, they do imply that on the average at least the values are reasonable.

D. Evidence of Upstream History

Once again the effects of upstream development are demonstrated by the behavior of the shape factor H. The normalized rate of decay of H with distance, $- \theta \frac{dH}{dx}$ is plotted in Figure 28 as a function of H for the relaxing regions of Pressure Distributions #2, #3, and #4. From this figure it is

seen that at the same shape factor the decay rate is larger for #3 which was driven closer to separation before being allowed to relax than it is for #2. A similar comparison can be made for #2 with respect to #4. Therefore, it follows that the mean turbulent shear stress at the same shape factor must also be larger for #3 than for #2 and likewise for #2 with respect to #4. It was shown in the previous section that the mean velocity profiles are a function of H alone (within this limited Reynolds number range). Therefore, the mean velocity profile at any station is not sufficient to determine the turbulent shear stress at that station. Hence the local mean velocity profile is not sufficient to fully determine the downstream behavior of the boundary layer. More information is needed concerning what has gone before, i.e. concerning the upstream history of the flow.

The intuitive argument used earlier in this report, whereby the turbulent fluctuations are built up in the adverse pressure gradient section and then decay slowly when the pressure gradient is removed, would still seem to be pertinent. By specifying, in addition to the mean velocity profile at some station, some measure of the initial turbulence level (actually the initial turbulent shear stress) and of its subsequent rate of decay, it should be possible to calculate the downstream development of the boundary layer.

For the usual integral parameter methods the shape factor behavior is described by Equation (3), which for zero pressure gradient simply becomes

$$\Theta \frac{dH}{dx} = f_2(H, R_\Theta) \tag{22}$$

It has been clearly shown with the data of Moses[3] and the data generated in this study that this description (Eq. (3) or Eq. (22)) is not adequate. In addition, it has been indicated that the reason for this inadequacy is the failure to account fully for the upstream history of the boundary layer. Therefore, the conclusions reached by Rotta[2] and by Bradshaw and Ferriss[9]

concerning the need to account for more upstream history than that implied by the mean velocity profile in boundary layer calculations are substantiated.

E. Proposed Calculation Method

Based upon (a) the conclusion that the apparent or turbulent shear stress is not uniquely determined by the local velocity profile and (b) the realization that an accurate specification of the complete shear stress distribution is extreemly difficult, attention was focused upon the problem of including more upstream history in an integral method for predicting downstream boundary layer behavior. The mean-flow energy integral equation was chosen over the moment-of-momentum integral equation because of its somewhat simpler form. The moment-of-momentum equation with a set of velocity profiles somewhat more appropriate than power law profiles, such as Cole's[11] universal profiles, becomes rather complicated. Therefore, a study of the behavior of the dissipation integral C_D was made. The relaxing regions for Pressure Distributions #2, #3, and #4 were chosen for the initial study since 1) this eliminated consideration of the pressure gradient and, 2) equilibrium behavior in zero pressure gradient is well documented.

It was found that a relatively simple diffusion type equation,

$$\theta \frac{dC_D}{dx} = K \left(C_{D_{F.P.}} - C_D \right) \tag{23}$$

could be used to represent the data. The value of $C_{D_{F.P.}}$ was assumed to be the equilibrium value of the zero pressure gradient dissipation integral, as given by Truckenbrodt's[29] correlation

$$C_D = \frac{.0112}{R_\theta^{1/6}} \tag{24}$$

which represents flat plate data well. In order to use Equation (23) to calculate C_D at any down stream station the initial value of C_D which reflects the effect of the upstream history on the turbulent fluctuations must be specified.

The results of using Equation (23) along with the mean-flow energy integral equation to calculate the shape factors in the relaxing regions of Pressure Distributions #2 and #3 are shown in Figure 29 for K = .009. The initial values of C_D used for these calculations were estimated from the integrated hot-wire data. Wall shear stresses were calculated from the Ludwieg-Tillmann correlation Equation (5). Pressures and momentum thicknesses were taken from the data, and a 2 step Runge-Kutta[30] method was used to march the solution downstream. Also shown in Figure 29 are predictions made using the equilibrium value for C_D, $C_{D_{F.P.}}$, throughout the relaxing region, and those made with the method of Escudier and Spalding[28]. The predictions made with Equation (23) give much better agreement with the data than either of the other two. However, this was to be expected here since Equation (23) was derived from the data with which it is compared.

Although the results of only two other methods are shown in Figure 29, a host of other methods were considered in the study, including the following:

Head's[31] method

Von Doenhoff and Tetervin[32] method

Garner[33] method

Rubert and Persh[16] method

Schuh[34] method

Spence[35] method

Moses[3] method.

For all of the pressure distributions considered in the study and in particular for distributions #2 and #3 the method of Escudier and Spalding[28] gave the best agreement with the data. Therefore, this method has been used in Figure 29 and will be used for comparisons between the "best" method based upon the local velocity profile hypothesis (shear stress distribution dependent upon local velocity profile only) and the proposed method which

attempts to account for an upstream history effect upon the shear stress distribution.

Extension of the proposed behavior of C_D, Equation (23), to pressure gradient regions was simply made by changing $C_{D_{F.D.}}$ to the equilibrium value of C_D based upon the local conditions. Thus,

$$\theta \, \frac{d \, C_D}{dx} = K \, (C_{D_{equi}} - C_D) \tag{25}$$

This simple approach preserves the intuitive diffusive type behavior of the integrated turbulent fluctuations and also insures that at least at equilibrium the correct value of C_D will be obtained.

In order to obtain estimates for $C_{D_{equi}}$ the equilibrium data of Clauser[5] and Herring and Norbury[36], as well as Townsend's[37] zero wall shear stress estimate and flat plate data were used to calculate C_D from the mean-flow energy equation. The values of $C_{D_{equi}}$ calculated in this way are shown plotted in Figure 30 as a function of normalized pressure gradient. The ordinate has been divided by $C_{D_{F.D.}}$, Equation (24), to approximately account for Reynolds number effects. Using these data points, various relationships were assumed between $C_{D_{equi}}/C_{D_{F.D.}}$ and $\frac{\theta}{U_\infty} \frac{dU_\infty}{dx}$, four of which are represented in Figure 30. These functions were then used to calculate the shape factors from the mean-flow energy integral equations for the following pressure distributions:

    (a) Pressure Distributions #2, #3, #4, #5 and #6 of this study,

    (b) The three pressure distributions of Moses[3] shown in Figure 1,

    (c) Bradshaw and Ferriss[9] pressure distribution which has a relaxing

          region.

In these calculations, the experimental pressure and momentum thicknesses as well as Ludwieg Tillmann[14] wall shear stresses were used. The initial values of C_D were assumed to be the equilibrium values for the pressure distributions

indicated in (a) and (b) above. Since these boundary layers were very thin at the start of the calculations the initial values of C_D chosen were not very important since these boundary layers returned to equilibrium very quickly. For the Bradshaw and Ferriss[9] calculation the initial value of C_D was estimated from the hot-wire data presented in Reference 9. Once again a two step Runge-Kutta method was used to march the solutions downstream. Various constant values of K were used in these calculations.

The results obtained for K = .009 and for

$$C_{D_{equi}} = [1 - 2.5 \times 10^7 (\frac{\theta}{U_\infty} \frac{dU_\infty}{dx})^3 - 10^2 \frac{\theta}{U_\infty}][\frac{.0112}{R_\theta^{1/6}}] \tag{26}$$

gave the best overall agreement with the data. These results are presented in Figure 31 along with the predictions made with a similar calculation using the Escudier and Spalding[28] correlation for C_D. In general, the calculations made using Equation (25) give a better fit with the data.

Based on these very encouraging results, the following integral equations are proposed for the prediction of turbulent boundary layer behavior:

Momentum integral equations

$$\frac{d\theta}{dx} = \frac{C_{fw}}{2} - (H + 2) \frac{\theta}{U_\infty} \frac{dU_\infty}{dx} + N.S.C. \tag{27}$$

Mean-flow energy integral equation

$$\theta \frac{dH}{dx} = [(H - 1)\bar{H} \frac{\theta}{U_\infty} \frac{dU_\infty}{dx} - \bar{H} \frac{C_{fw}}{2} + C_D] \frac{dH}{d\bar{H}} \tag{16}$$

And dissipation integral diffusion equation

$$\theta \frac{dC_D}{dx} = K(C_{D_{equi}} - C_D) \tag{25}$$

Best estimates for the normal stress correction (N.S.C.), K, and $C_{D_{equi}}$
are at present

$$N.S.C. = .0365 \ (H - 1) \ \frac{d\delta^*}{dx} \tag{9}$$

$$K = .009 \tag{28}'$$

and

$$C_{D_{equi}} = [1 - 2.5 \times 10^7 (\frac{\theta}{U_\infty} \frac{dU_\infty}{dx})^3 - 10^2 \frac{\theta}{U_\infty} \frac{dU_\infty}{dx}][\frac{.0112}{R_\theta^{1/6}}] \tag{26}$$

Although reasonable results were achieved with Equations (28) and (26) for
the limited number of cases considered, these equations can be revised as
more experimental data is examined. One possibility that has been considered
but not investigated to any extent is that K may not be a constant but some
function of local conditions.

Specification of initial values for C_D, which is required for the
proposed method, may be a problem. Unless the calculation is started at a
station in the flow where the boundary layer is at or near equilibrium,
measurements or guesses based upon past experience will have to be used to
establish the initial C_D.

The proposed method adds little complication to the boundary layer
calculations and appears to describe the mean turbulence behavior correctly.
The diffusive nature of Equation (25) is very satisfying to the intuition and
given the correct values of $C_{D_{equi}}$ will always give the correct solution at
equilibrium. A failing which is inherent in some of the proposed prediction
methods is thus avoided.

When a computer is available for the boundary layer calculations,
inclusion of Equation (25) into the calculation is simple and adds only slightly
to the time required to obtain a solution. If the calculations are being made
by hand then it may be desirable to use the following approximate criterion

for deciding whether or not Equation (25) need be included in the calculation:
For

$$\theta \frac{d}{dx} \left(\frac{\theta}{U_\infty} \frac{dU_\infty}{dx} \right) < 7 \times 10^{-5}$$

Equation (25) can probably be neglected and the Escudier and Spalding[28]
correlation

$$C_D = .547 \, C_{fw} + .004214 \, H - .004572 \tag{29}$$

used to determine C_D. This criterion was only investigated for adverse
pressure gradients and needs verification in accelerating pressure gradients.
Also, the limiting value was established somewhat arbitrarily since no
quantitative statement of the required prediction accuracy was made.

IV. CONCLUSIONS

Based upon the experimental and analytic programs described in the preceding sections, the following is a summary of the significant conclusions reached. Conclusions #2 and #3 are not new but add additional support to previous conclusions and provide alternate correlations of experimental data. Conclusion #5 is by far the most significant.

1. In zero and adverse pressure gradients Preston tubes are as good as sub-layer fences for measuring wall shear stress.

2. The Reynolds normal stresses which are usually neglected in turbulent boundary layer calculations do have a significant effect upon momentum thickness calculations for rapidly growing boundary layers. An approximate correction for normal stresses can be made in the two-dimensional, incompressible, momentum integral equation with the following correlation:

$$N.S.C. = .0365 \ (H - 1) \ \frac{d\delta^*}{dx} . \tag{9}$$

3. In the Reynolds number range

$$1000 < R_\theta < 10,000$$

the velocity profiles in two-dimensional, incompressible, turbulent boundary layers can be represented by a one parameter family. A characteristic of this family is that $\bar{H}$, the energy thickness factor, can be related to H, the shape factor δ^*/θ, in the range

$$1.3 < H < 2.3$$

by one of the following expressions

$$\bar{H} = \frac{3.6 \ H}{2.78 \ H - 1} \tag{13}$$

or

$$\bar{H} = 1.431 - \frac{.097}{H} + \frac{.775}{H^2} \qquad \text{(Reference 23)} \tag{14}$$

4. The turbulent shear stress is not uniquely related to the local velocity profile but also depends upon upstream history. The eddy viscosity and mixing length vary considerably in non-equilibrium boundary layers and cannot be well represented by the available correlations.

5. The behavior of the dissipation integral C_D defined as

$$C_D = \int_o^\infty \frac{2\,\tau}{\rho U_\infty^2} \; \frac{\partial \frac{u}{U_\infty}}{\partial y} \; dy \tag{17}$$

can be well represented with a simple diffusion-like equation,

$$\theta \, \frac{d\,C_D}{dx} = K\,(C_{D_{equi}} - C_D) \tag{25}$$

This equation can be used in conjunction with the mean-flow energy and momentum integral equations to obtain a practical method for predicting the behavior of two-dimensional, incompressible, turbulent boundary layers which accounts for upstream history.

Best estimates for K and $C_{D_{equi}}$ at the present time are

$$K = .009 \tag{28}$$

and

$$C_{D_{equi}} = [1 - 2.5 \times 10^7 (\frac{\theta}{U_\infty} \frac{d\,U_\infty}{dx})^3 - 10^2 \frac{\theta}{U_\infty} \frac{d\,U_\infty}{dx}][\frac{.0112}{R^{1/6}}] \tag{26}$$

V. RECOMMENDATIONS FOR FURTHER WORK

Due to the necessity for using empirical correlations in turbulent boundary layer calculations, the generality of any calculation method must be suspect until many successful comparisons have been made between predicted and measured behavior. Therefore, the proposed method should be tested and the suggested empirical correlations modified whenever additional two-dimensional, turbulent boundary-layer data is generated.

Because of the limited amount of equilibrium data available the validity of any correlations for equilibrium shear stress distributions or integrals cannot be established. More experimental data including hot-wire measurement of turbulence quantities for equilibrium turbulent boundary layers would be highly desirable.

REFERENCES

1. Stewart, C. C. - "A Comparison of Turbulent Boundary Layer Theories" - Gas Turbine Laboratory Report #57 - M. I. T. - 1960.

2. Rotta, J. C. - *"Turbulent Boundary Layers in Incompressible Flow"*- Progress in Aeronautical Sciences - Ed., A. Ferri, D. Kuchemann and L. H. G. Sterne - Pergamon Press - 1962.

3. Moses, H. L. - "The Behavior of Turbulent Boundary Layers in Adverse Pressure Gradients" - Gas Turbine Laboratory Report #73 - M. I. T. - 64.

4. B. G. J. Thompson - "A Critical Review of Existing Methods of Calculating the Turbulent Boundary Layer " - A. R. C. 26 109, F. M. 3492 - 1964.

5. Clauser, F. H. - "Turbulent Boundary Layers in Adverse Pressure Gradients" - Jour. Aero. Sciences, Vol. 21, pp. 91-108 - 1954.

6. Tetervin, N. and Lin, C. C. - "A General Integral Form of the Boundary Layer Equation for Incompressible Flow with an Application to the Calculation of the Separation Point of Turbulent Boundary Layers" - NACA Report 1046 - 1951.

7. Schubauer, G. B. and Tchen, C. M. - *"Turbulent Flow"* - Princeton University Press - Princeton, N. J. - 1961.

8. Schlichting, H. -*"Boundary Layer Theory"* - McGraw-Hill Book Co. - New York - 1960.

9. Bradshaw, P. and Ferriss, D. H. - "The Response of a Retarded Equilibrium Turbulent Boundary Layer to the Sudden Removal of Pressure Gradient" - N. P. L. Aero Report 1145 - 1965.

10. McDonald, H. and Stoddart, J. A. P. - "On the Development of the Incompressible Boundary Layer" - British Aircraft Corp., (Preston) Aero Report Ae 223 - 1965.

11. Coles, D. - "The Law of the Wake in the Turbulent Boundary Layer" - Jour. Fluid Mechanics, Vol. 1, pp. 191-226 - 1956.

12. Bradshaw, P., Ferriss, D. H. and Atwell, N. P. - "Calculation of Boundary Layer Development Using the Turbulent Energy Equation" - NPL Aero Report 1182, A. R. C. 27 667, F. M. 3678 - 1966.

13. Klebanoff, P. S. - "Characteristics of Turbulence in a Boundary Layer with Zero Pressure Gradient" - NACA Report 1247 - 1955.

14. Ludwieg, H. and Tillmann, W. - "Investigation of the Wall Shearing Stress in Turbulent Boundary Layers" - NACA TM 1285 - 1950.

15. Patel, V. C. - "Calibration of the Preston Tube and Limitations on Its Use in Pressure Gradients" - Jour. Fluid Mechanics, Vol. 23, Part I - 1965.

16. Rubert, K. J. and Persh, J. - "A Procedure for Calculating the Development of Turbulent Boundary Layers Under the Influence of Adverse Pressure Gradients" - NACA TN 2478 - 1951.

17. Bidwell, J. M. - "Application of the von Karman Momentum Theorem to Turbulent Boundary Layers" - NACA TN 2571 - 1951.

18. Newman, B. G. - "Some Contributions to the Study of the Turbulent Boundary Layer Near Separation" - Report ACA-53-Australian ARC - 1951.

19. Ross, D. - "Evaluation of Momentum Integral Equation for Turbulent Boundary Layers" - Jour. Aero. Sciences, Vol. 19 - 1953.

20. VanLe, N. - "The von Karman Integral Method as Applied to a Turbulent Boundary Layer" - Jour. Aero. Sciences, Vol. 19 - 1953.

21. Sandborn, V. A. and Slogar, R. J. - "Study of the Momentum Distribution of Turbulent Boundary Layers in Adverse Pressure Gradients" - NACA TN 3264 - 1935.

22. Schubauer, G. B. and Klebanoff, P. S. - "Investigation of Separation of the Turbulent Boundary Layer" NACA Report #1030 - 1951.

23. Nicoll, W. B. and Escudier, M. P. - "Empirical Relationships Between the Shape Factors H_{32} and H_{12} for Uniform-Density Turbulent Boundary Layers and Wall Jets" - Mech. Eng. Dept., Imperial College, London, TWF/TH/3 - 1965.

24. Fediaevsky, K. - "Turbulent Boundary Layer on an Airfoil" - Jour. Aero. Sciences, Vol. 4 - 1964.

25. Libby, P. A., Baronti, P. O. and Napolitana, L. - "Study of the Incompressible Boundary Layer with Pressure Gradient" - AIAA Jour., Vol. 2, No. 3 - 1964.

26. Clauser, F. H. - "The Turbulent Boundary Layer" - Advances in Appl. Mechanics, Vol. 4 - 1956.

27. Mellor, G. L. and Gibson, D. M. - "Equilibrium Turbulent Boundary Layers" Princeton University M. E. Dept., Rpt. FLD 13 - 1963.

28. Escudier, M. P. and Spalding, D. B. - "A Note on the Turbulent Uniform-Property Hydrodynamic Boundary Layer on a Smooth Impermeable Wall; Comparisons of Theory with Experiment" - M. E. Dept., Imperial College, London - 1965.

29. Trückenbrodt, E. - "A Method of Quadrature for Calculation of the Laminar and Turbulent Boundary Layer in Case of Plane and Symmetric Flow" - NACA TM 1379 - 1955.

30. Hildebrand, F. B. - *"Advanced Calculus for Applications"* - Prentice-Hall - New Jersey - 1963.

31. Head, M. R. - "Entrainment in the Turbulent Boundary Layer" - Reports & Memoranda of the A. R. C., R&M #3152 - 1960.

32. von Doenhoff, A. E. and Tetervin, N. - "Determination of General Relationships for the Behavior of Turbulent Boundary Layers" - NACA Report #772 - 1943.

33. Garner, H. C. - "The Development of Turbulent Boundary Layers - R&M #2133 - British ARC - 1944.

34. Schuh, H. - "On Determining Turbulent Boudnary Layer Separation in Incompressible Flow" - Jour. Aero. Sciences, Vol. 22 - 1955.

35. Thwaites, B. - *"Incompressible Aerodynamics II"* - The Calculation of the Boundary Layer - (from a contribution by Spence) - Oxford University Press - Britain - 1960.

36. Herring, H. J. and Norbury, J. F. - "Some Experiments on Equilibrium Turbulent Boundary Layers in Favorable Pressure Gradients" - Princeton Universtiy. Dept. of Aerospace and Mech. Sci., FLD #15 - 1963.

37. Townsend, A. A. - "The Development of Turbulent Boundary Layers with Negligible Wall Stress" - Jour. Fluid Mechanics, Vol. 8 - 1960.

APPENDIX

Effect of Hot-Wire Misalignment on Shear

Stress Measurements

Two cases are considered: The first of these is sketched below.
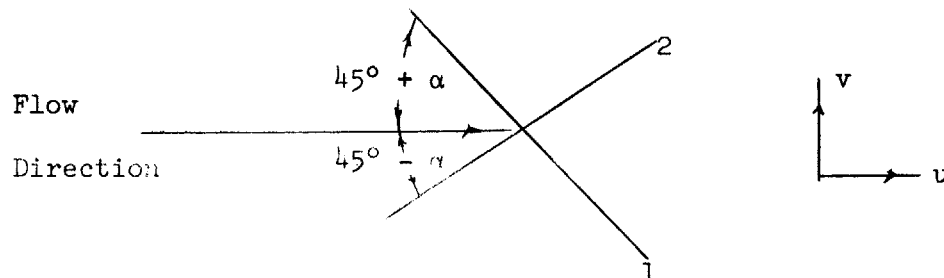
In position 1 the wire is at 45 plus α degrees to the mean flow direction and in position 2, 45 minus α degrees. Assuming α to be small and neglecting the cooling effect of flow parallel to the wires, the linearized fluctuating output voltages for the two positions are

$$e_1 = K_e \ [u' \ (\frac{1 + \alpha}{\sqrt{2}}) + v' \ (\frac{1 - \alpha}{\sqrt{2}})] \qquad (A.1)$$

and

$$e_2 = K_e \ [u' \ (\frac{1 - \alpha}{\sqrt{2}}) - v' \ (\frac{1 + \alpha}{\sqrt{2}})] \qquad (A.2)$$

where K_e is a proportionality constant. The turbulent shear stress coefficient is normally obtained by dividing the difference between the squared RMS values of e_1 and e_2 by the averaged mean-squared free stream reading e_∞ of the two wires,

$$- 2 \ \frac{\overline{u'v'}}{U_\infty^2} = \frac{\overline{e_1^2} - \overline{e_2^2}}{2 \ \overline{e_\infty^2}} \qquad (A.3)$$

For the case depicted in the sketch the usual approach would give, according to Equations (A.1) and (A.2),

$$- \frac{2 \ \overline{u'v'}}{U_\infty^2} = - \frac{\overline{e_1^2} - \overline{e_2^2}}{2 \ \overline{e_\infty^2}} + 2 \ \alpha \ \frac{\overline{u'^2} - \overline{v'^2}}{U_\infty^2} \qquad (A.4)$$

Therefore, the error which results from not correcting for the misalignment is

$$\% \ ERROR \simeq 100 \ \alpha \ \left(\frac{\overline{u'^2} - \overline{v'^2}}{-\ \overline{u'v'}}\right) \tag{A.5}$$

where α^2 has been neglected with respect to 1. For typical values

$$\frac{\overline{u'^2}}{U_\infty} = .01 \tag{A.6}$$

$$\frac{\overline{v'^2}}{U_\infty} = .0025 \tag{A.7}$$

and

$$-\ \frac{\overline{u'v'}}{U_\infty^2} = .002 \tag{A.8}$$

which could be expected in turbulent boundary layers, a 1 degree misalignment ($\alpha = 1°$) produces about a 6.5% error in shear stress coefficient. Thus indicating one of the reasons why accurate shear stress measurements are difficult to obtain.

The second case to be considered is sketched below.

Flow Direction

$45° + \alpha$

$45° + \alpha$

2

1
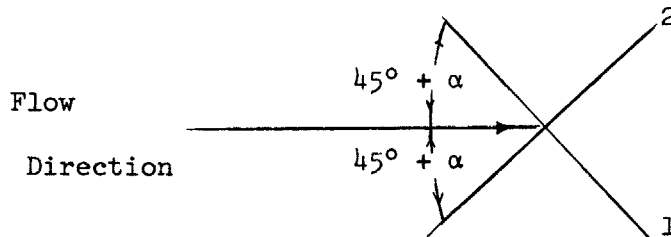
Following a procedure similar to that described above, the error in shear stress coefficient produced by neglecting α is found to be

$$\% \ ERROR = \frac{200\alpha}{1 + \alpha} \tag{A.9}$$

Therefore, for this case a 1 degree error ($\alpha = 1°$) produces a 3.4% error in shear stress coefficient.
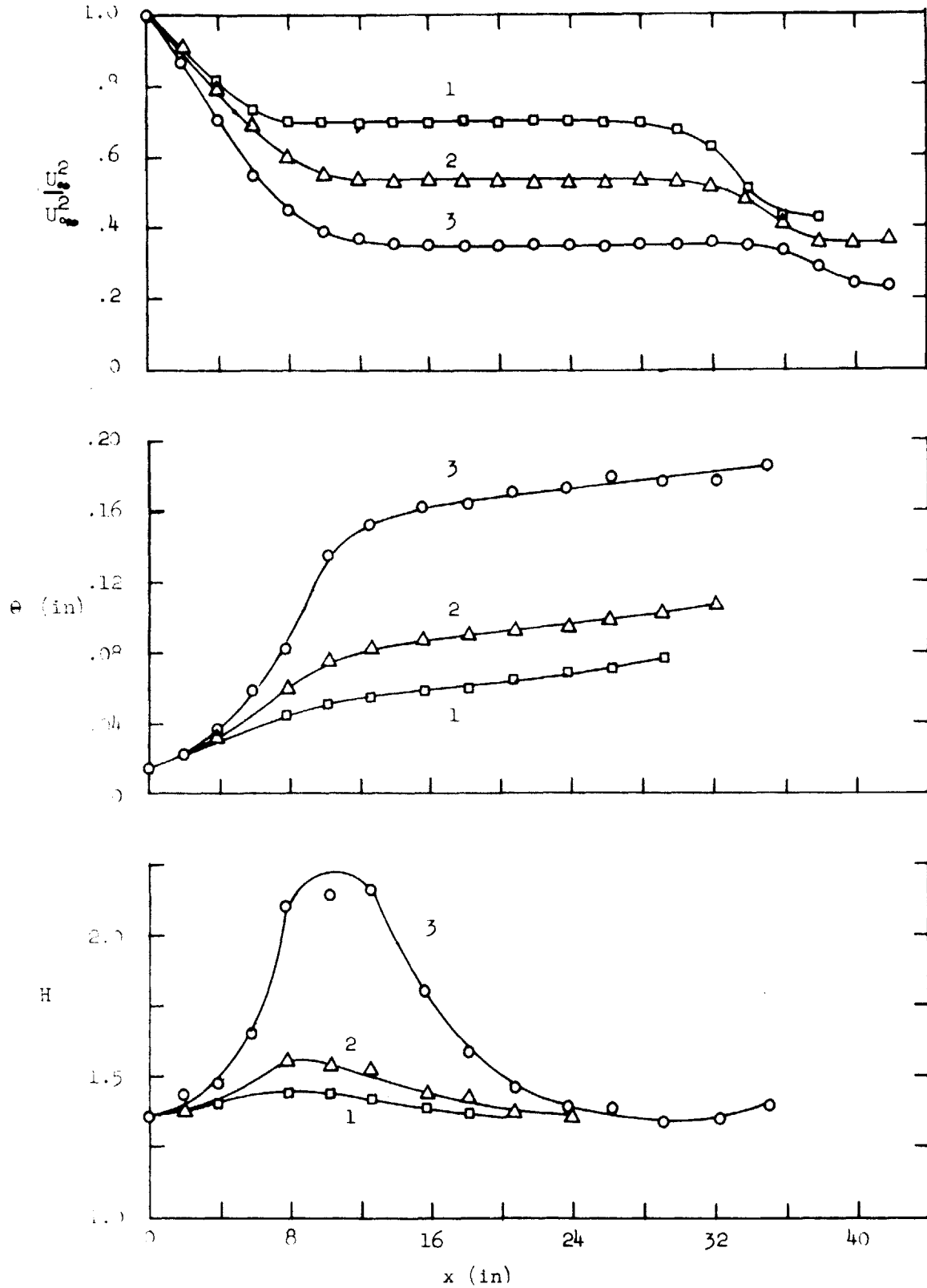
Figure 1   Experimental Values of Free Stream Velocity, Momentum Thickness, and Shape Factor from Reference 3
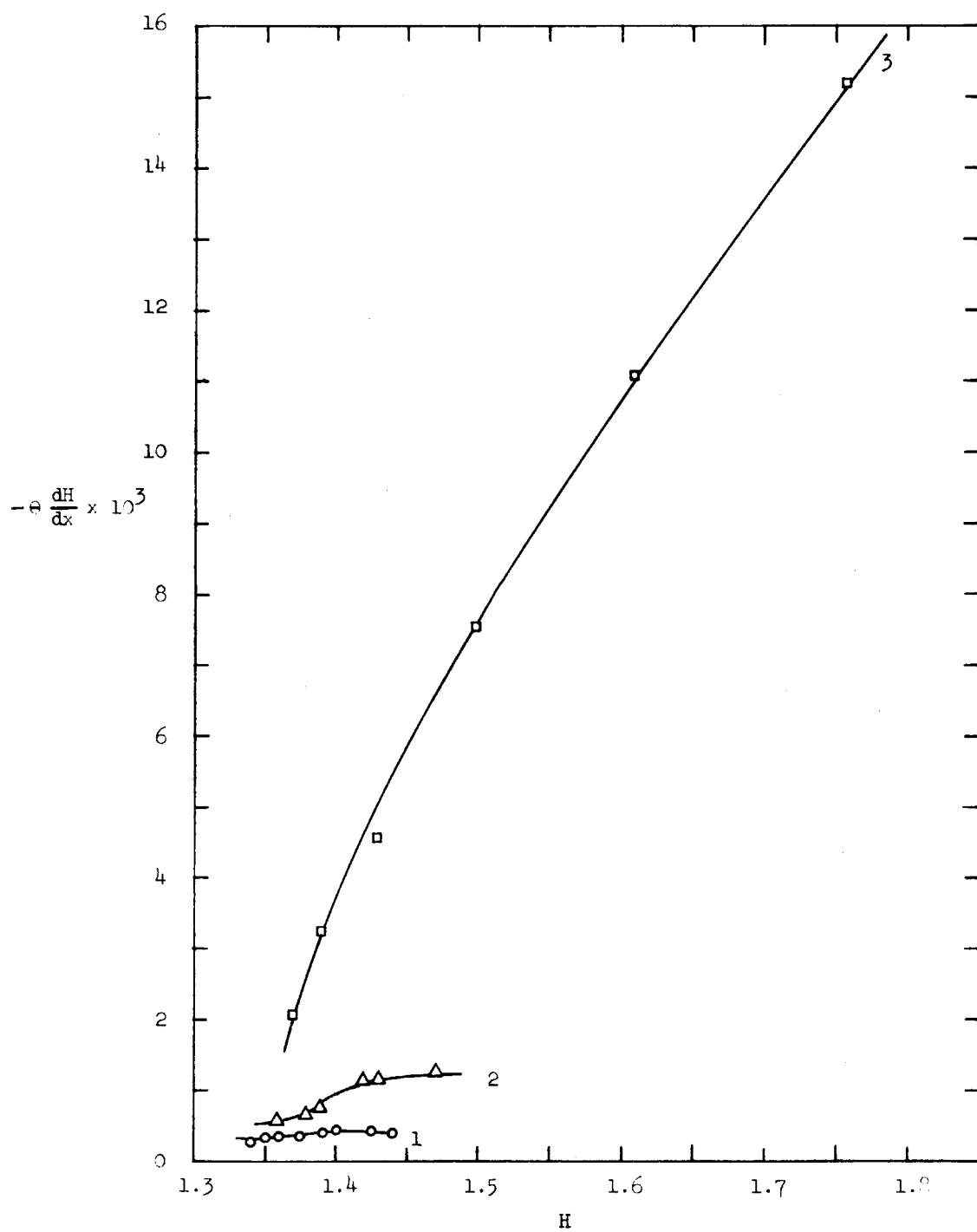
Figure 2 Shape Factor Decay Rate in Relaxing Region for Experimental Data of
Reference 3
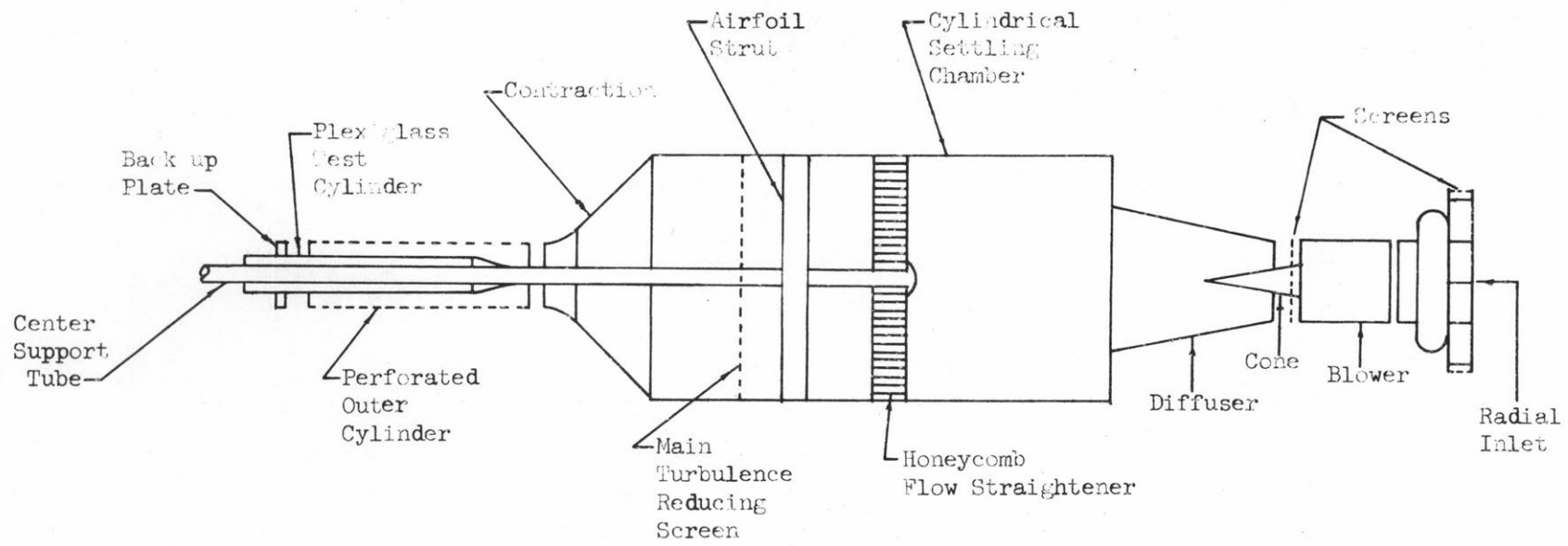
Figure 3 Schematic of Test Apparatus
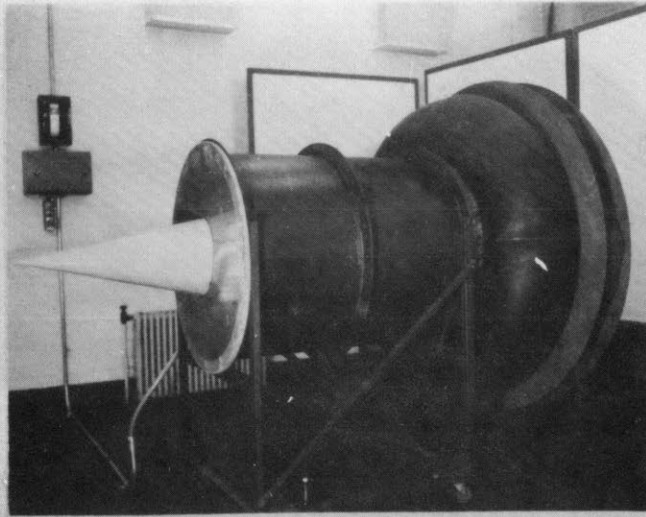
(a) Blower with Radial Inlet and Exit Cone
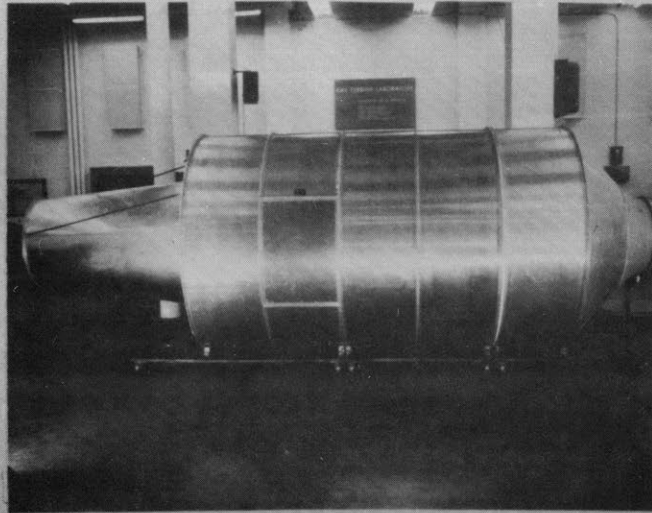
(b) Settling Chamber

Figure 4.   Photograph of Test Apparatus
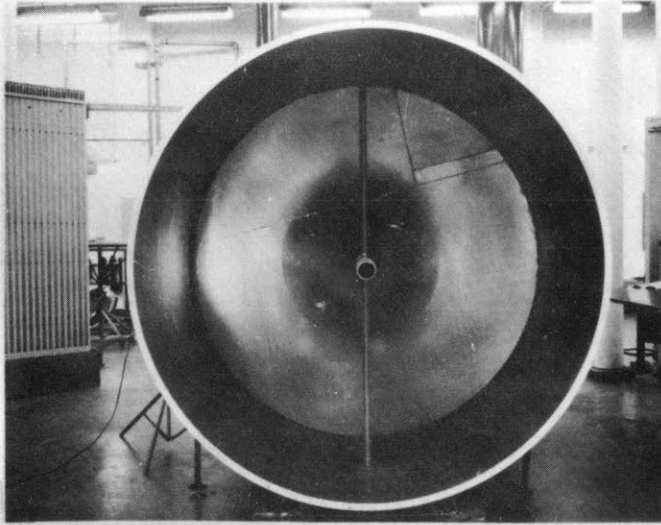
(c) Airfoil Strut, Center Tube, and Honeycomb
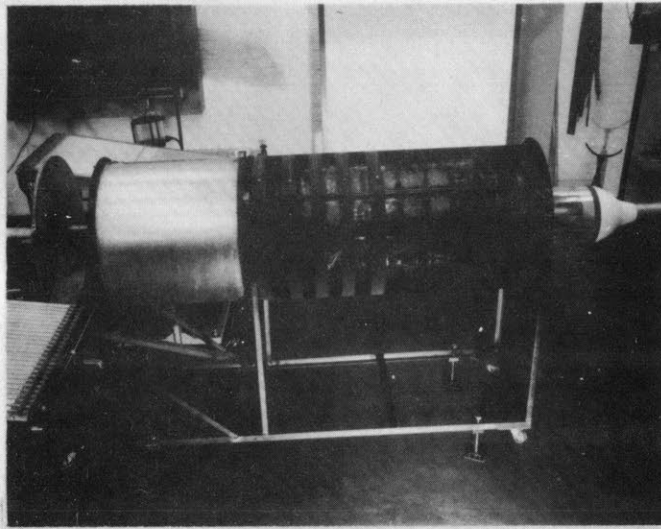
(d) Test Section

Figure 4. continued
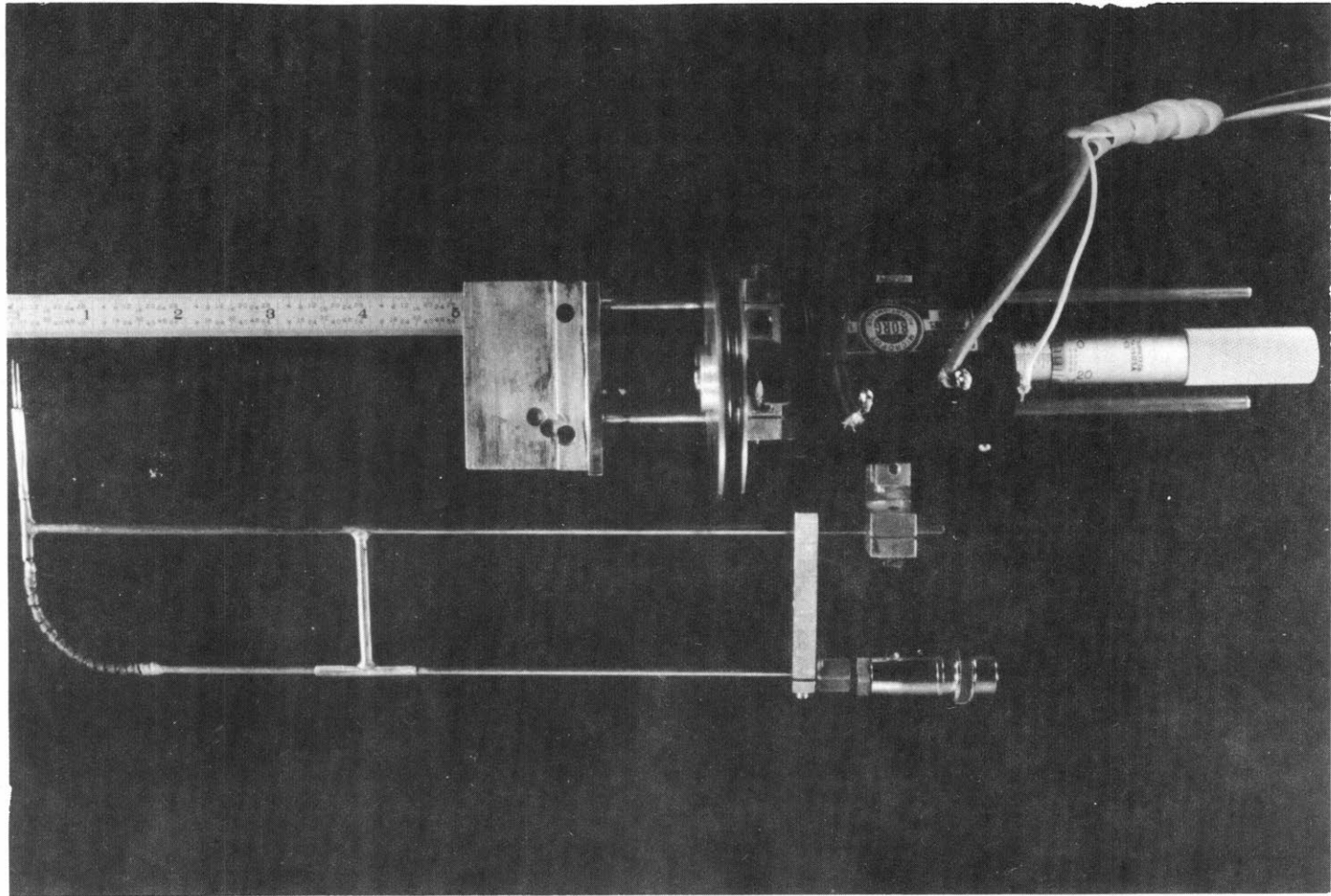
Figure 5. Hot-Wire Shear Stress Probe and
Micrometer Traversing Mechanism
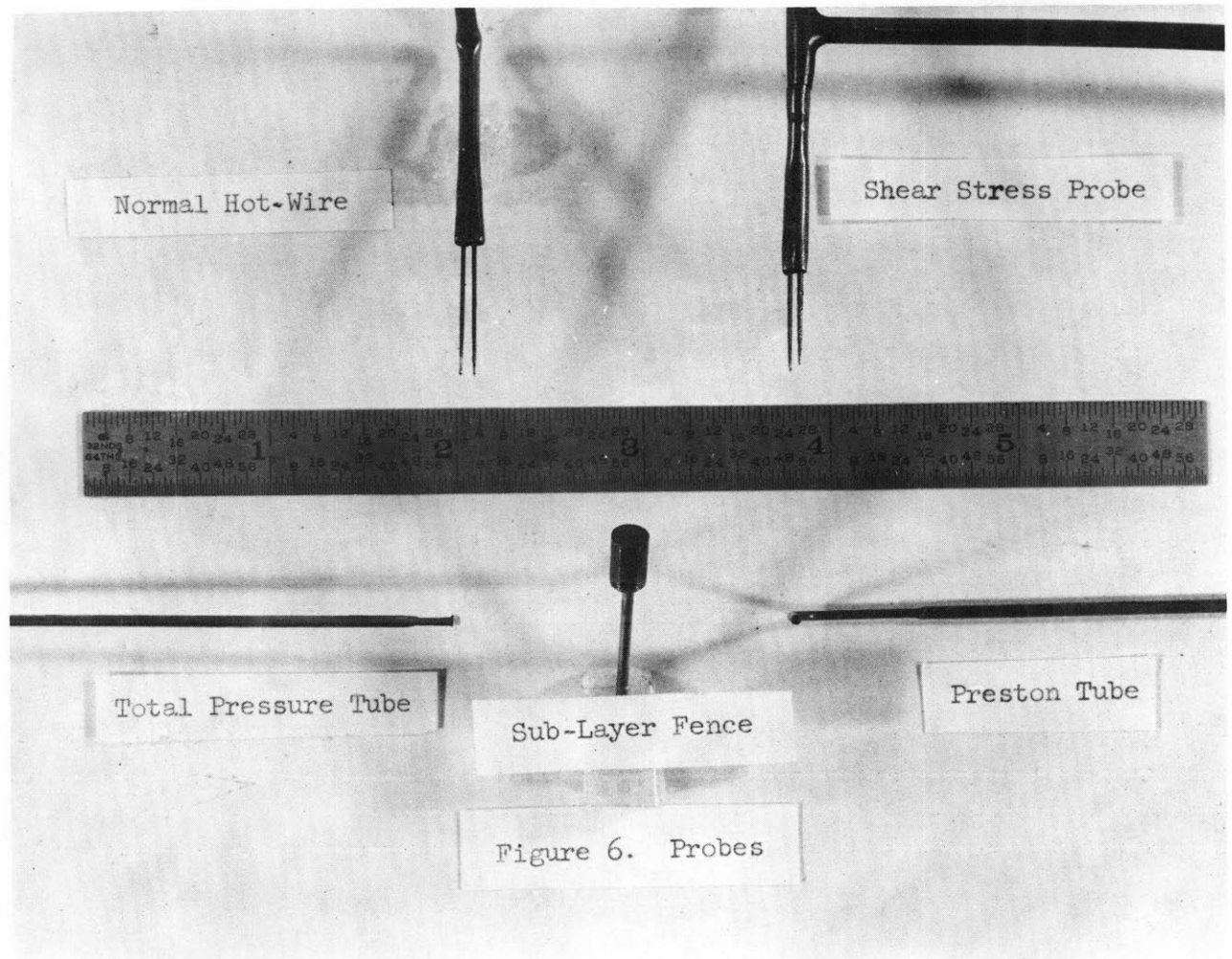
Normal Hot-Wire

Shear Stress Probe

Total Pressure Tube

Sub-Layer Fence

Preston Tube

Figure 6.   Probes
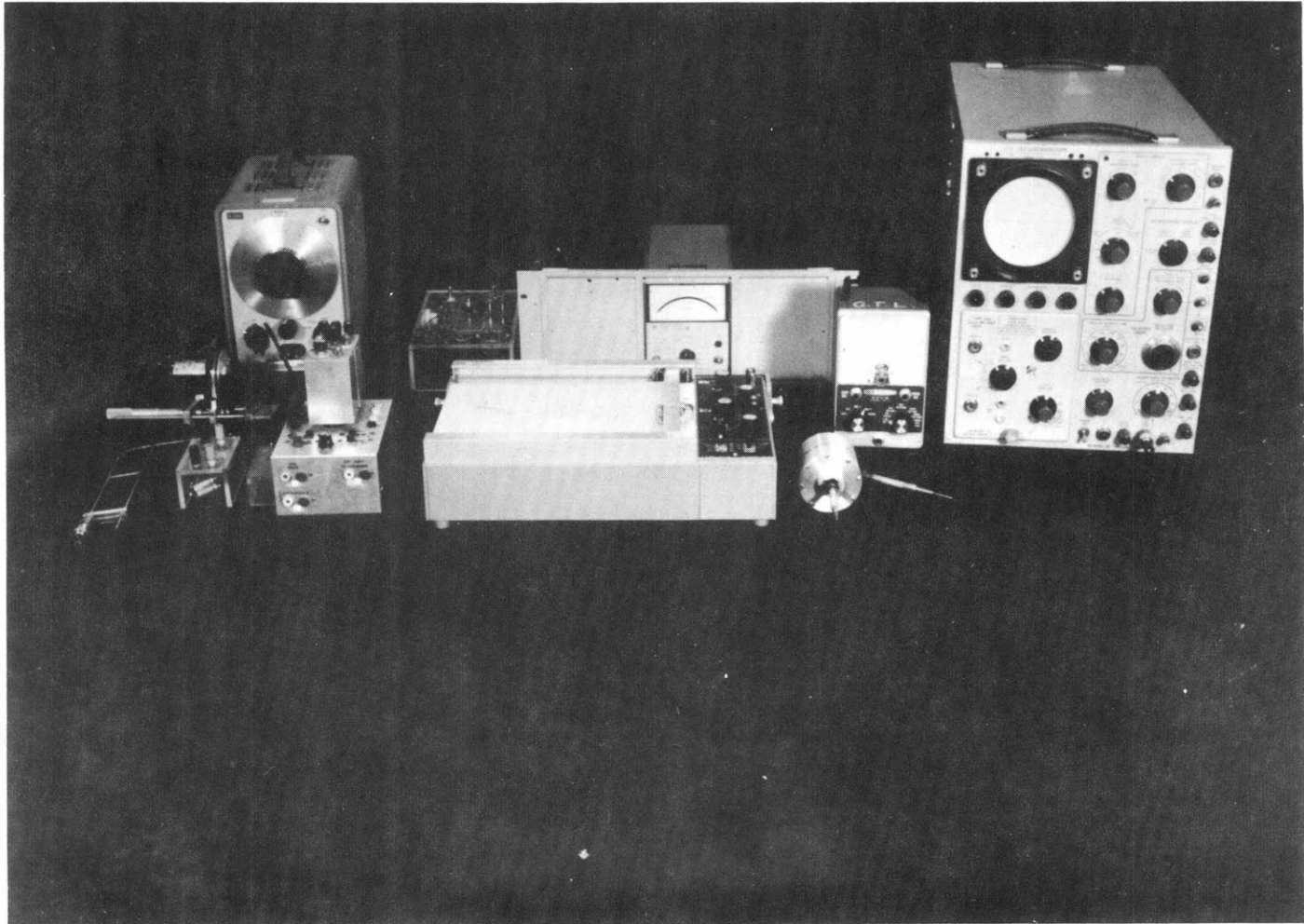
Figure 7.   Instrumentation
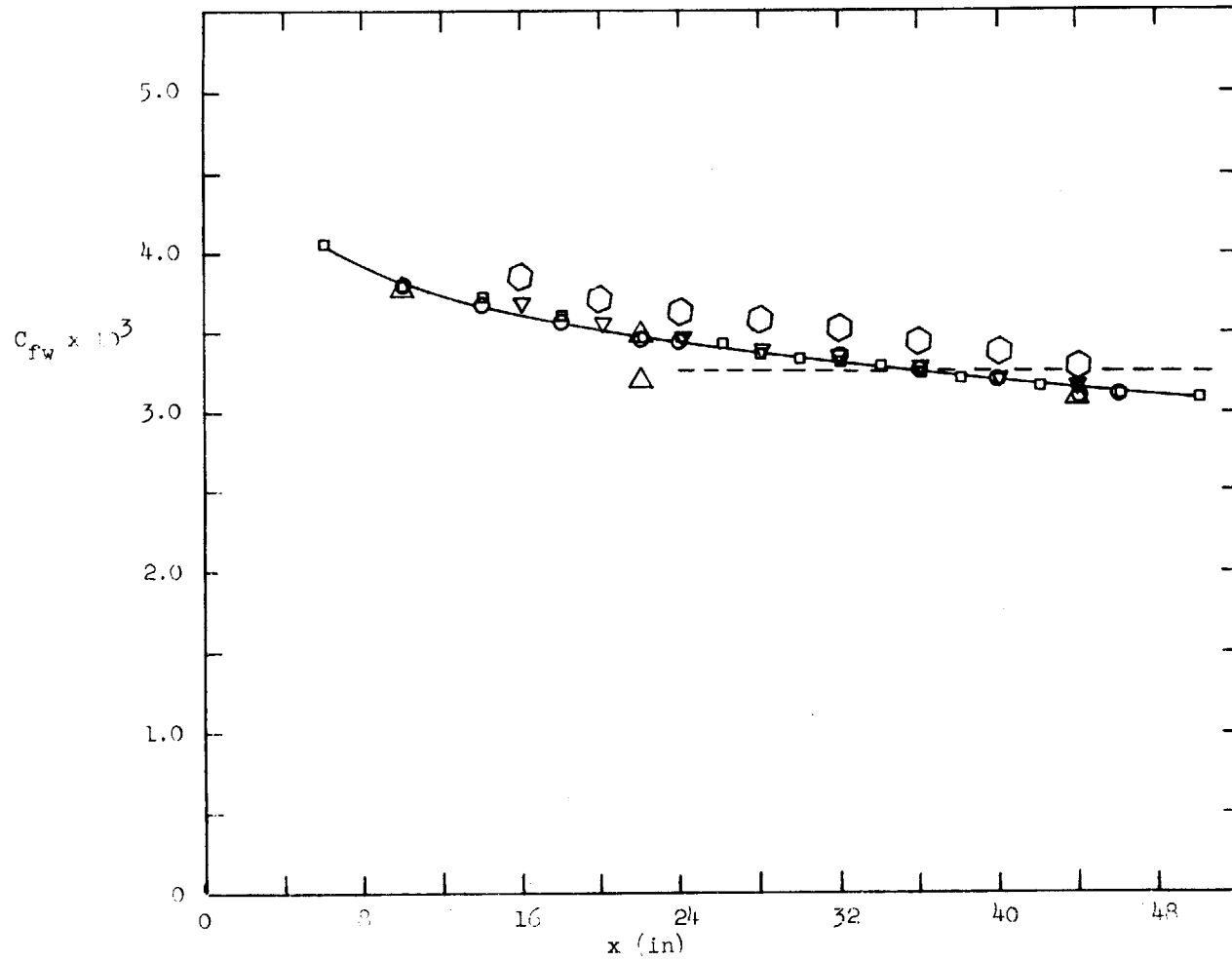
Figure 3 Wall Shear Stress in Zero Pressure Gradient

□ Preston Tube Patel Correlation[5]   ---- 2-D Momentum Eq. (2)
○ Clauser Method[5]   ▽ Ludwieg Tillmann 1
△ Shear Stress Extrapolated to Wall   ⬡ Ludwieg Tillmann 2
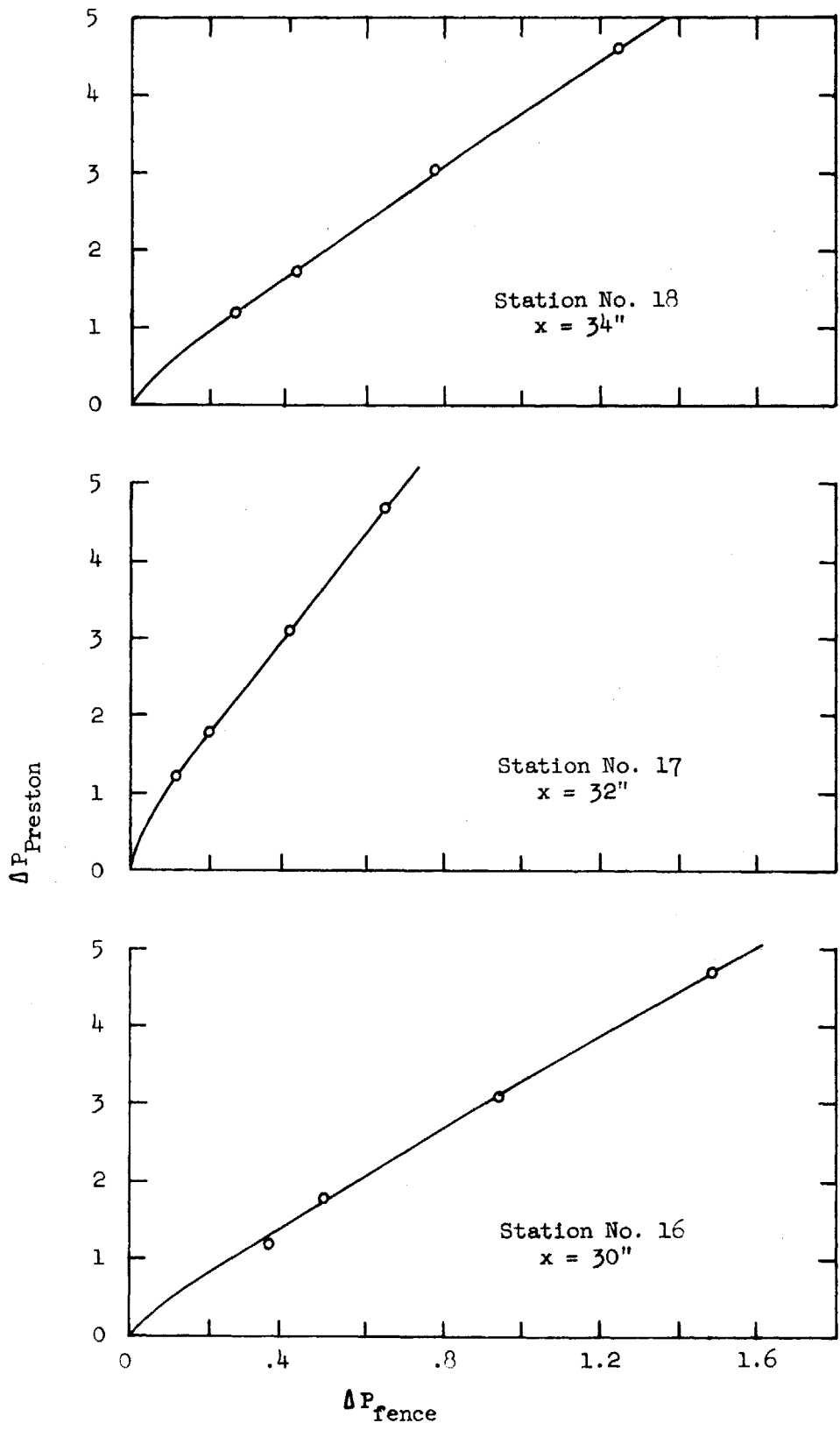
Figure 9 Sub-Layer Fence Calibration

Figure 1) Typical Raw Data
Pressure Distribution No.3

(a) ∆P Transducer Output
Velocity Pressure

0.1"

Station No. 17

y

u

Station No. 18   Station No. 19   Station No. 20   Station No. 21
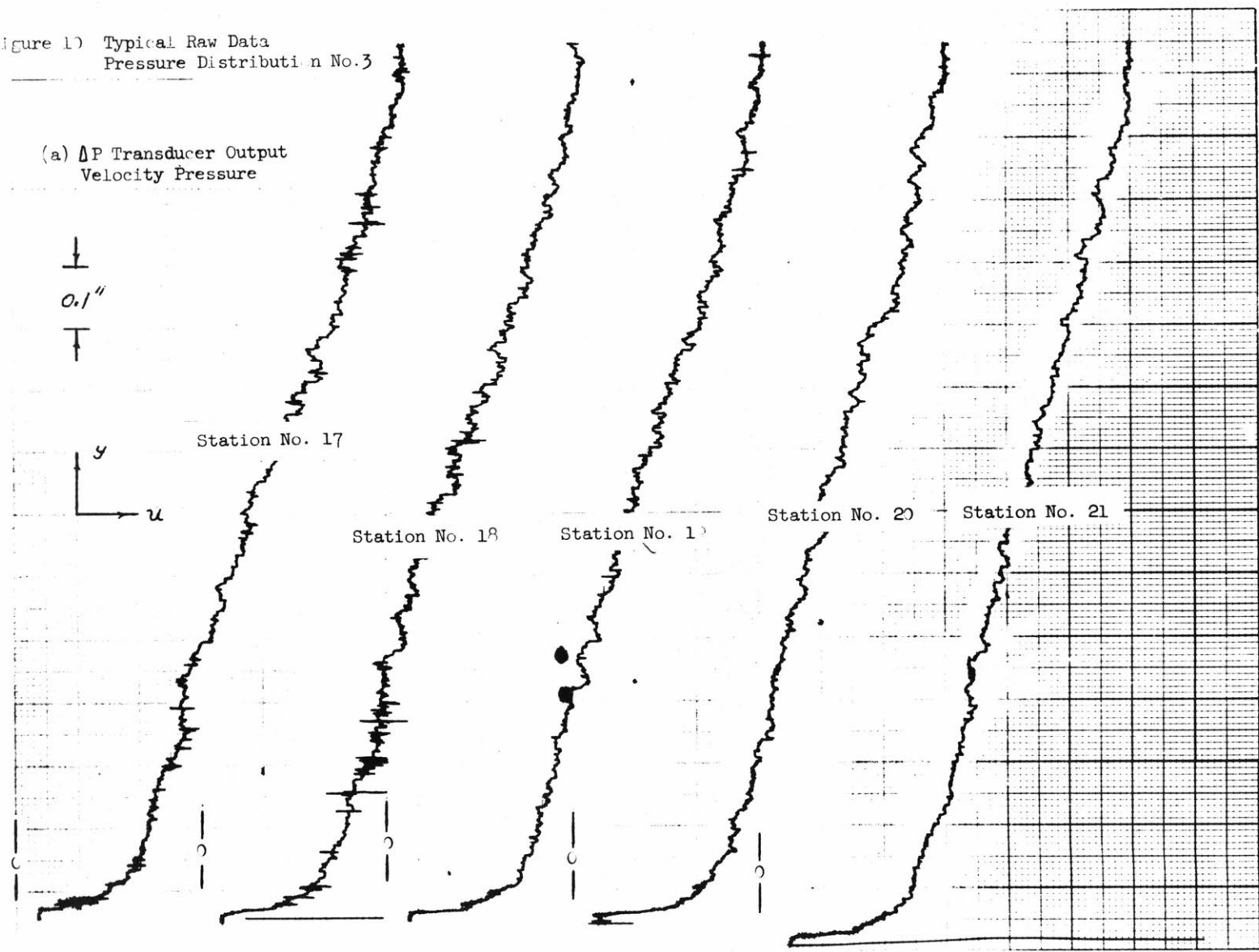
Figure 10 (b) Normal Hot wire Output
Mean Velocity and RMS of
Longitudinal Fluctuations

$\sqrt{u'^2}$

Station No. 10

RMS Voltage

Mean Voltage

u

$0.1''$

y

$u \, \& \, \sqrt{u'^2}$

Figure 1) (e) Shear Stress Probe Output
Mean and RMS

Position 0°   Position 180°   45 ½° wire ?

Mean Voltage

RMS Voltage

av"

Station No. 5

y

e

Position 180°   Position 0°
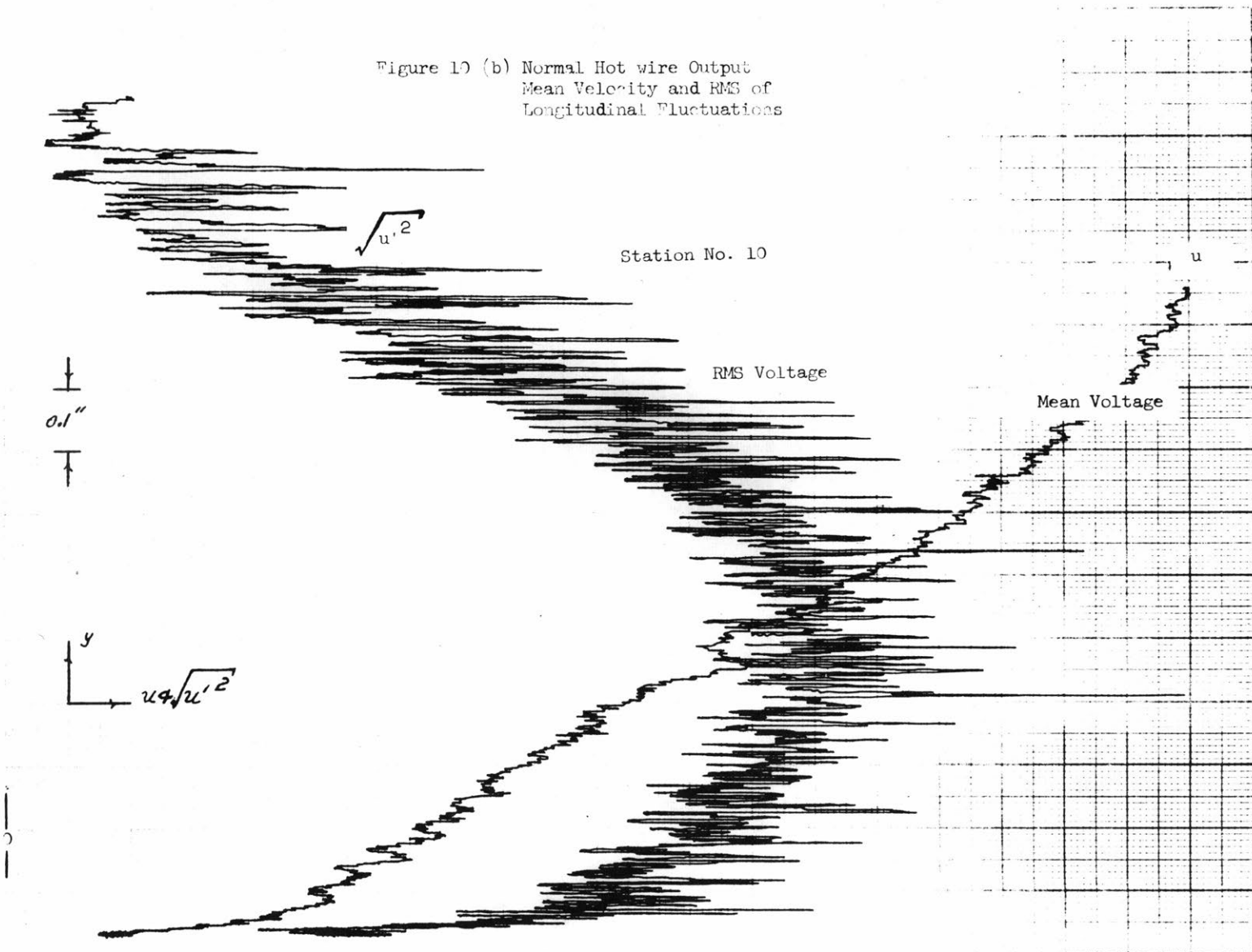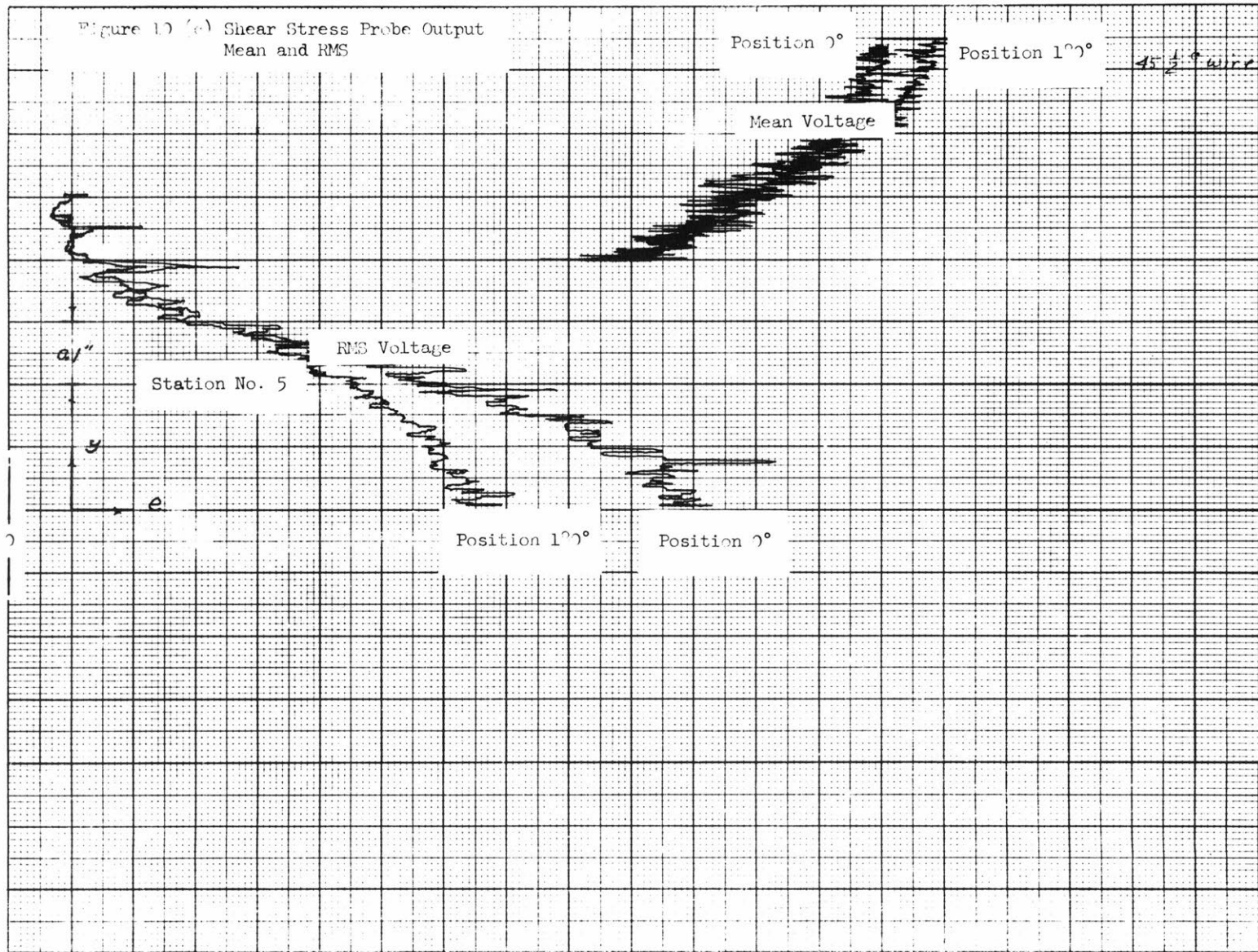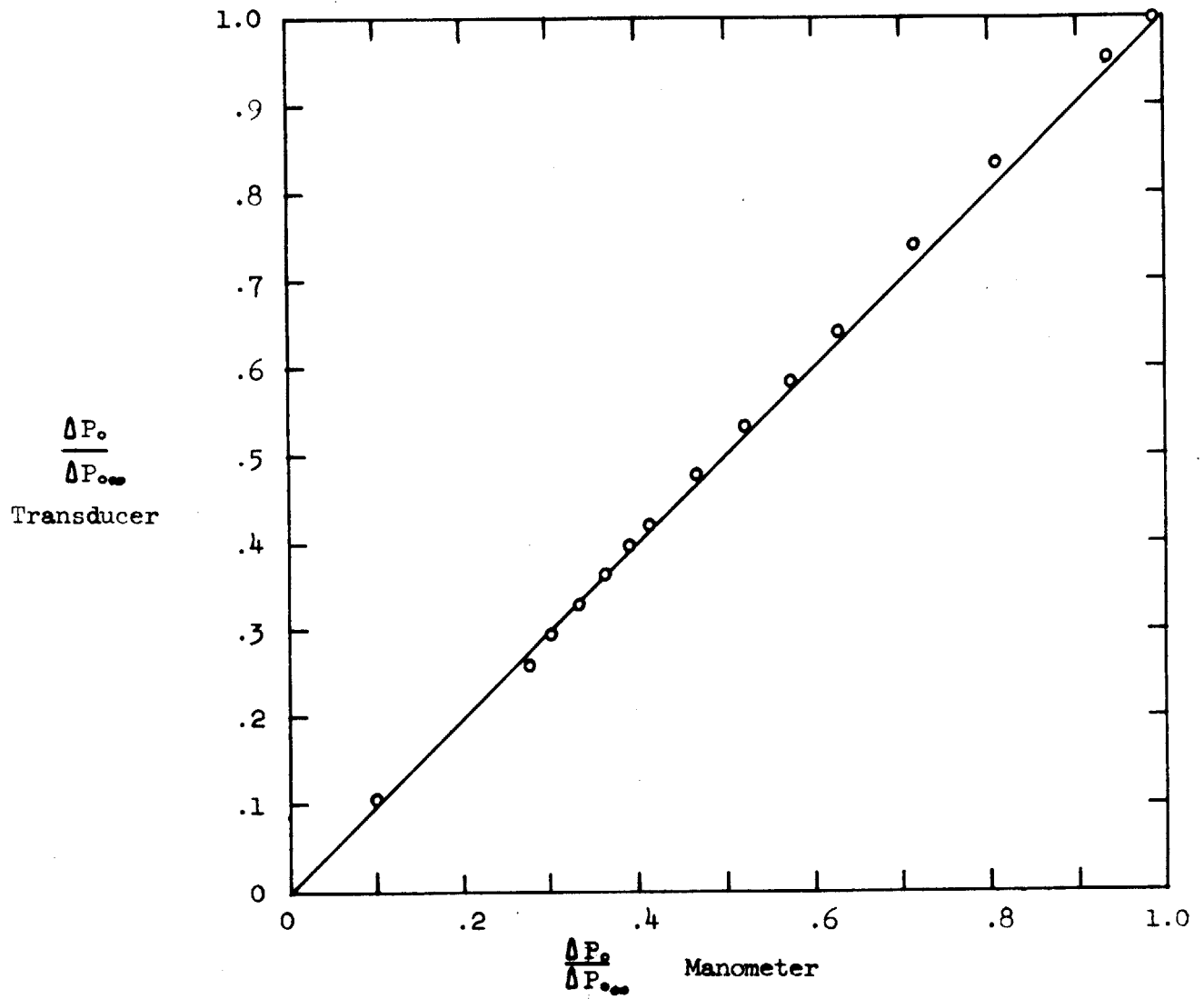
Figure 11 ΔP Transducer Linearity Pressure Distribution No. 6
Station No. 17   x = 32"

Figure 12 Experimental Values of Free Stream Velocity,Momentum Thickness, and Shape Factor – Pressure Distributions 2,3, and 4
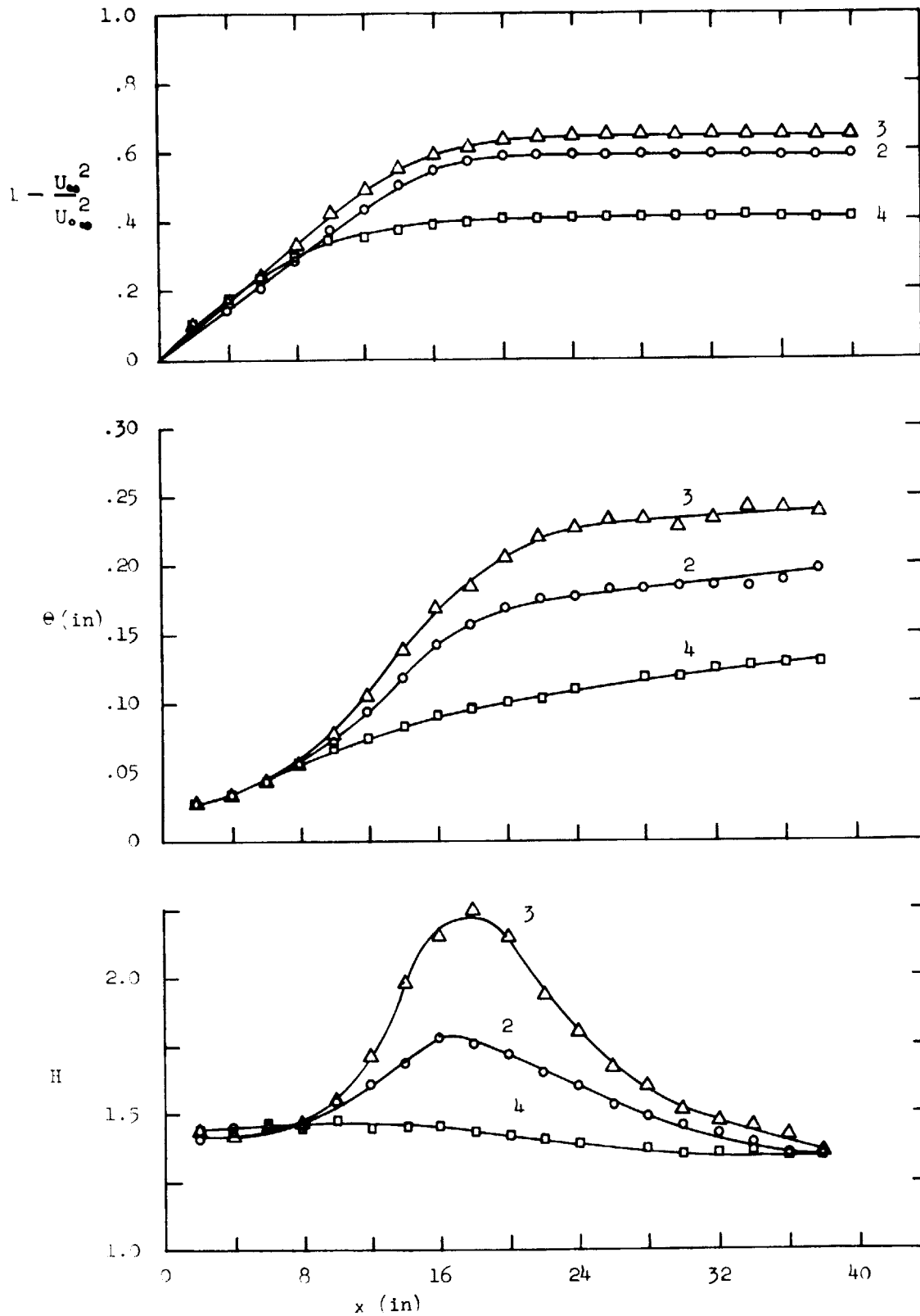
Figure 13 Experimental Values of Free Stream Velocity, Momentum Thickness, and Shape Factor – Pressure Distributions 5 and 6
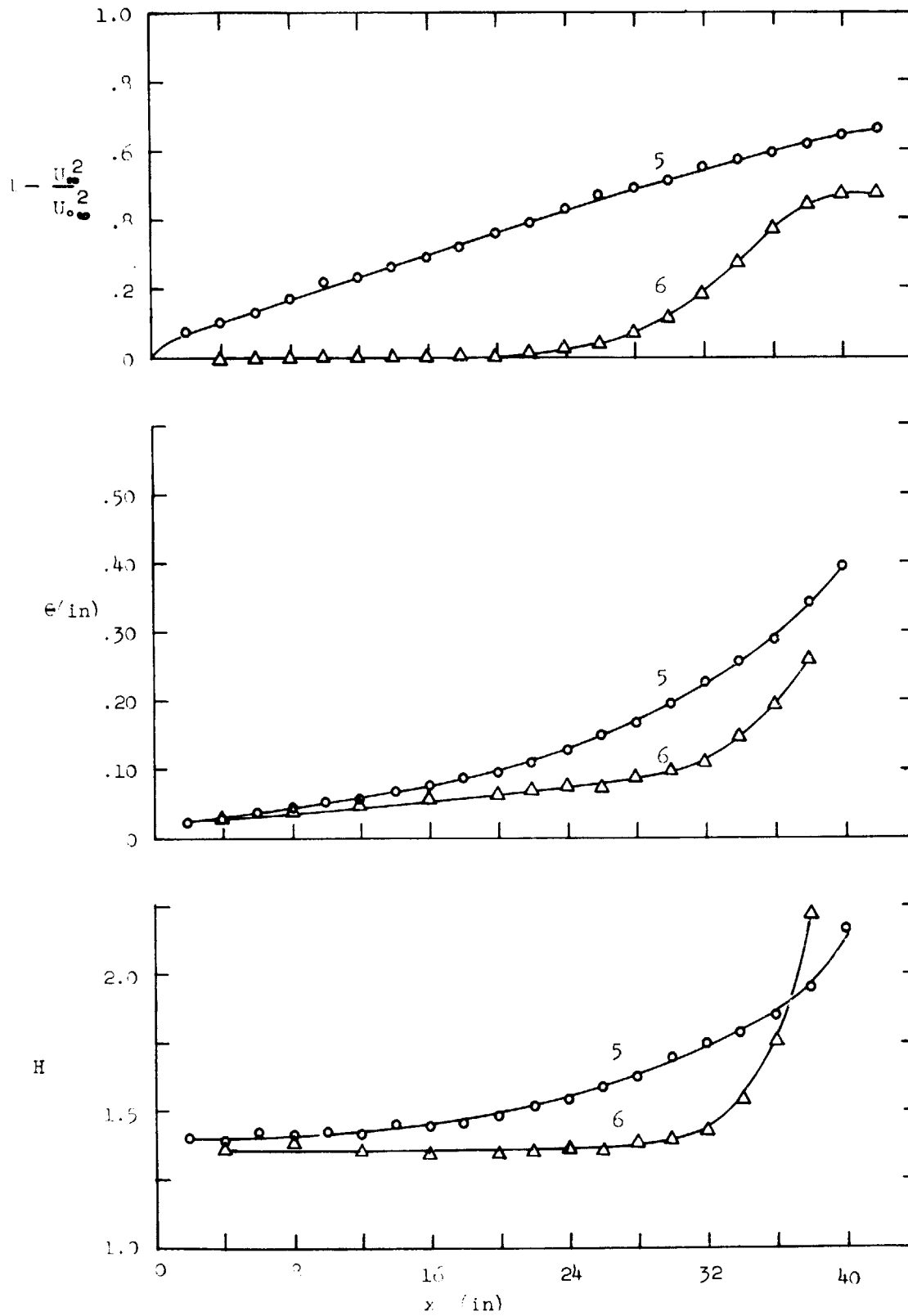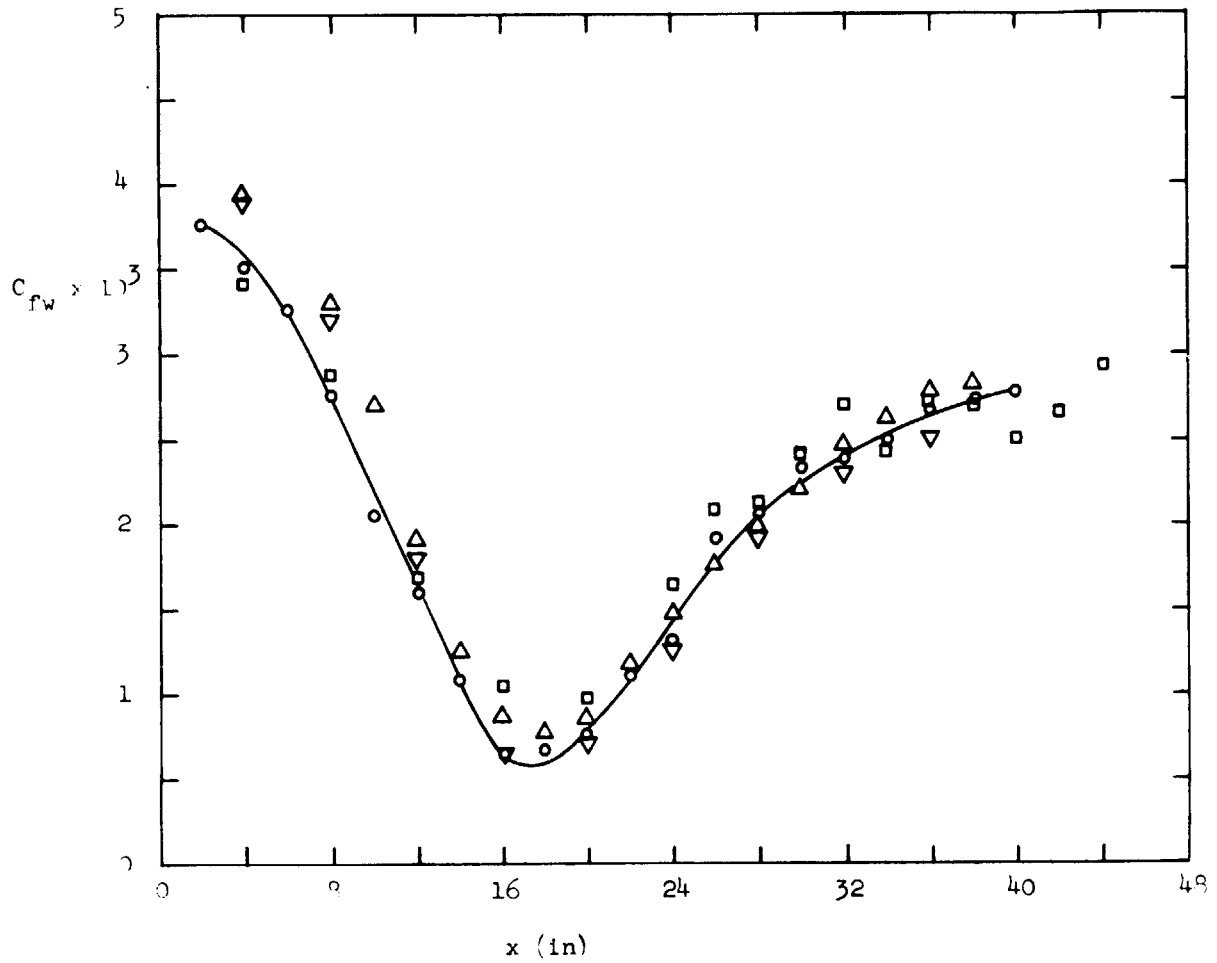
Figure 14   Experimental Wall Shear Stress   (a) Pressure Distribution No. 3

□   Sub-Layer Fence   ▽   Clauser Method [5]
○   Preston Tubes   △   Ludwieg Tillmann [14]
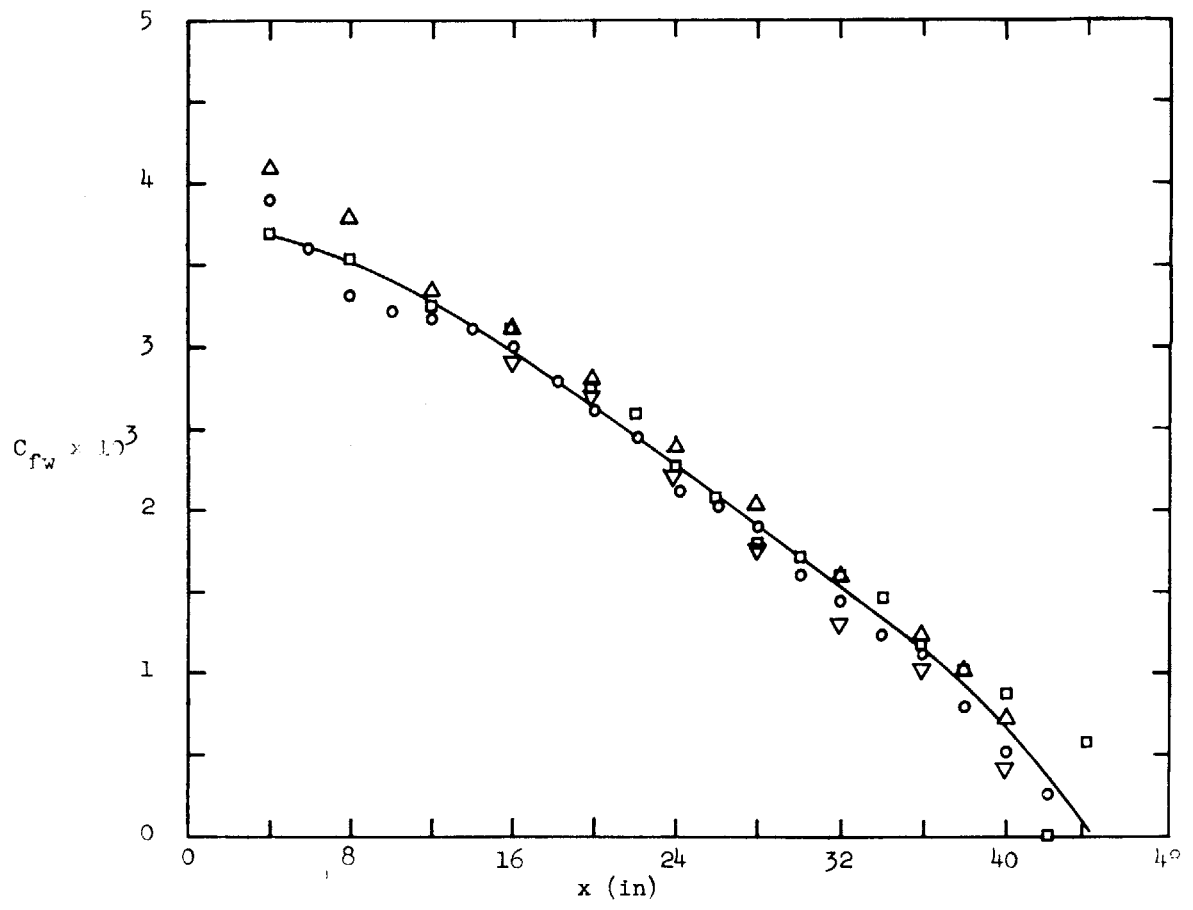
Figure 14 Experimental Wall Shear Stress (b) Pressure Distribution No. 5

◻ Sub-Layer Fences   ▽ Clauser Method[5]
o Preston Tubes   △ Ludwieg Tillmann[14]
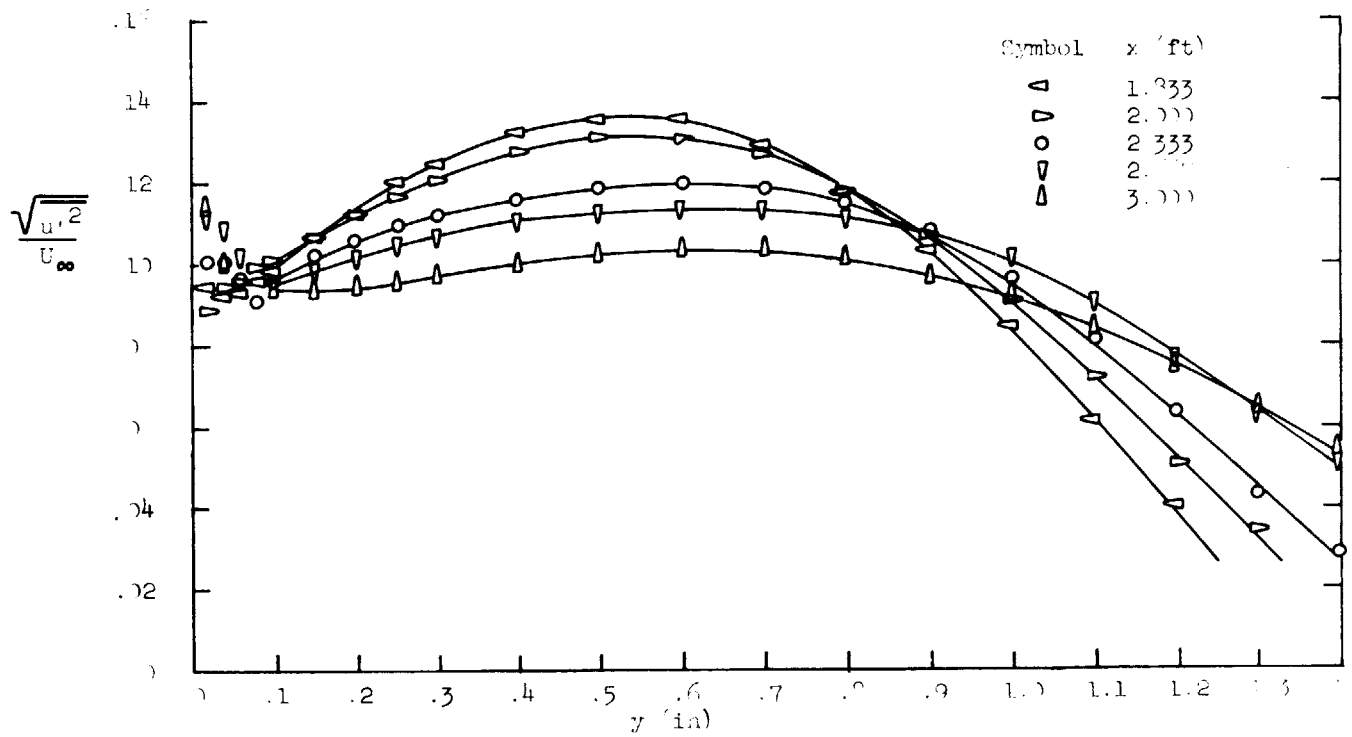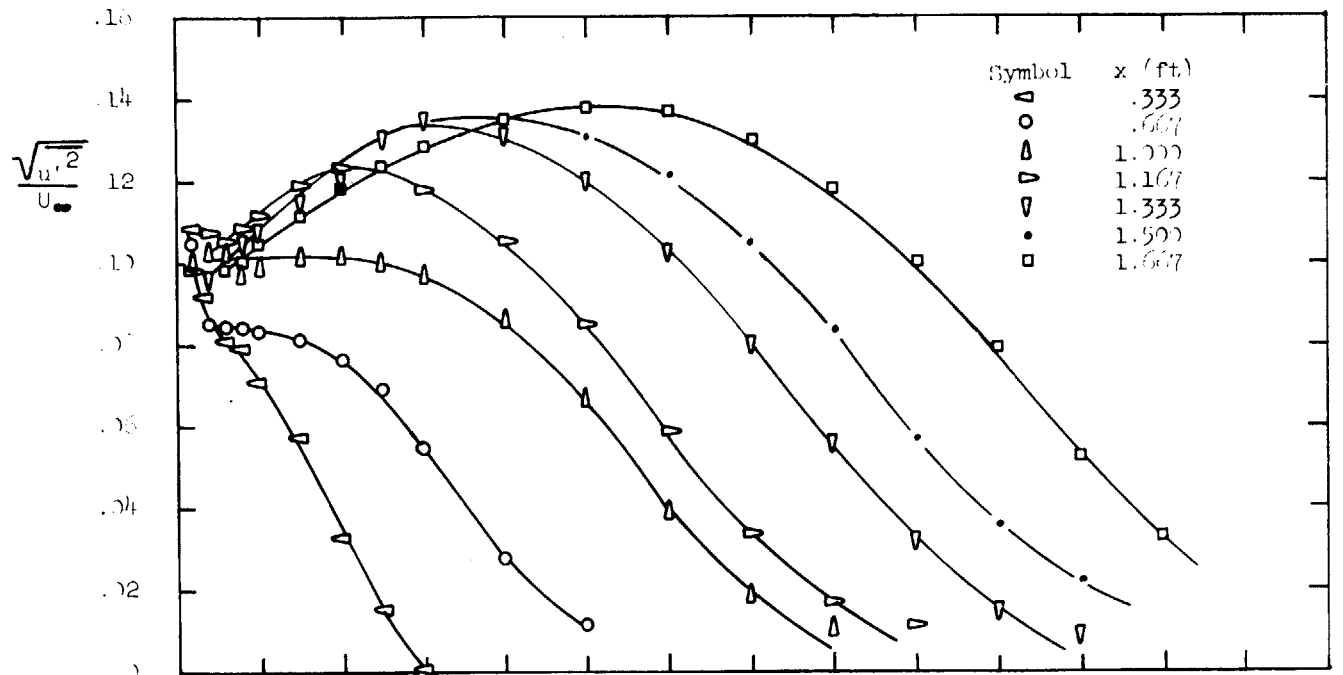
Figure. Experimental Longitudinal Turbulence Intensity. (a) Pressure Dis...
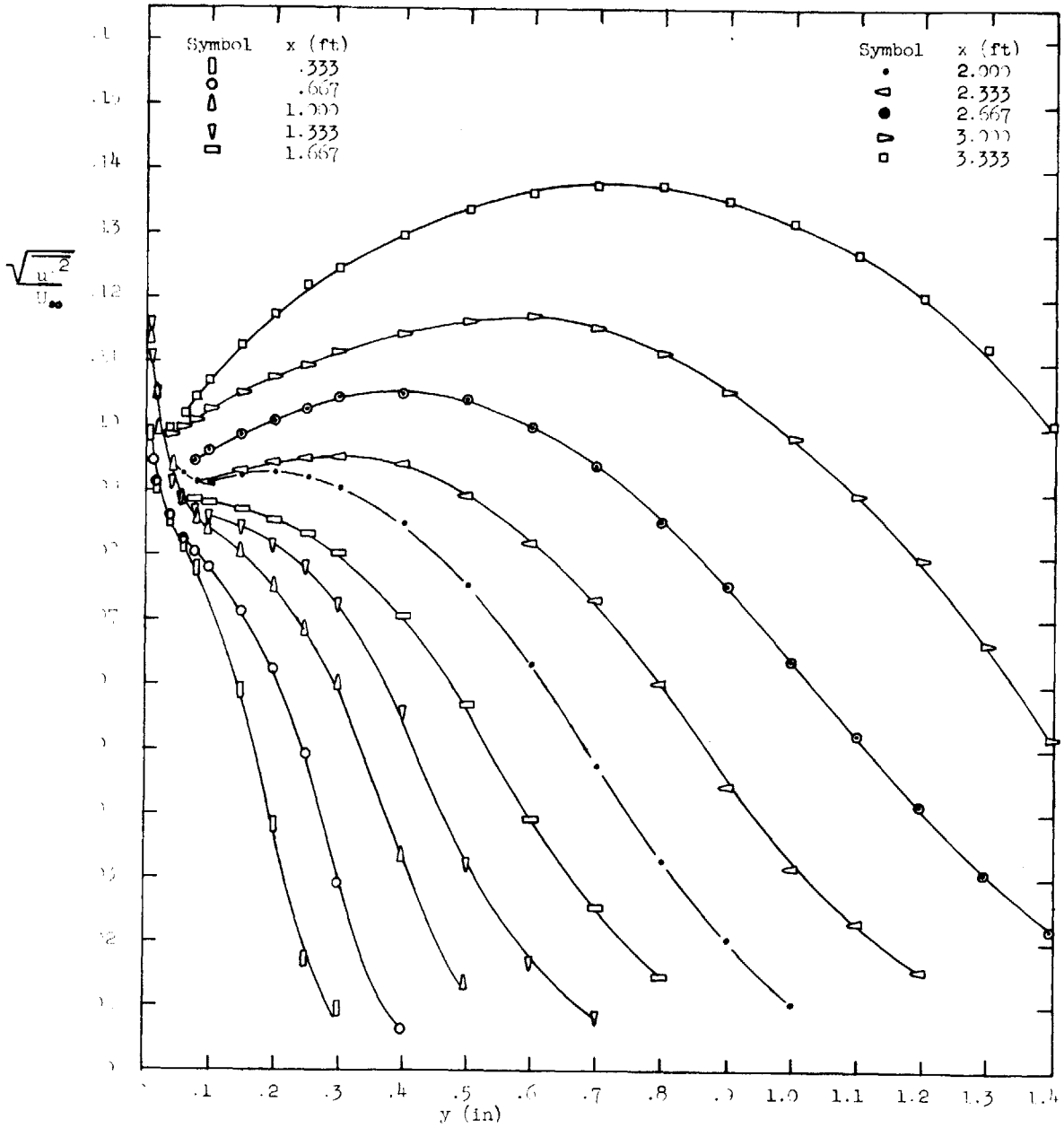
Figure 15 Experimental Longitudinal Turbulence Intensity (b) Pressure Distribution
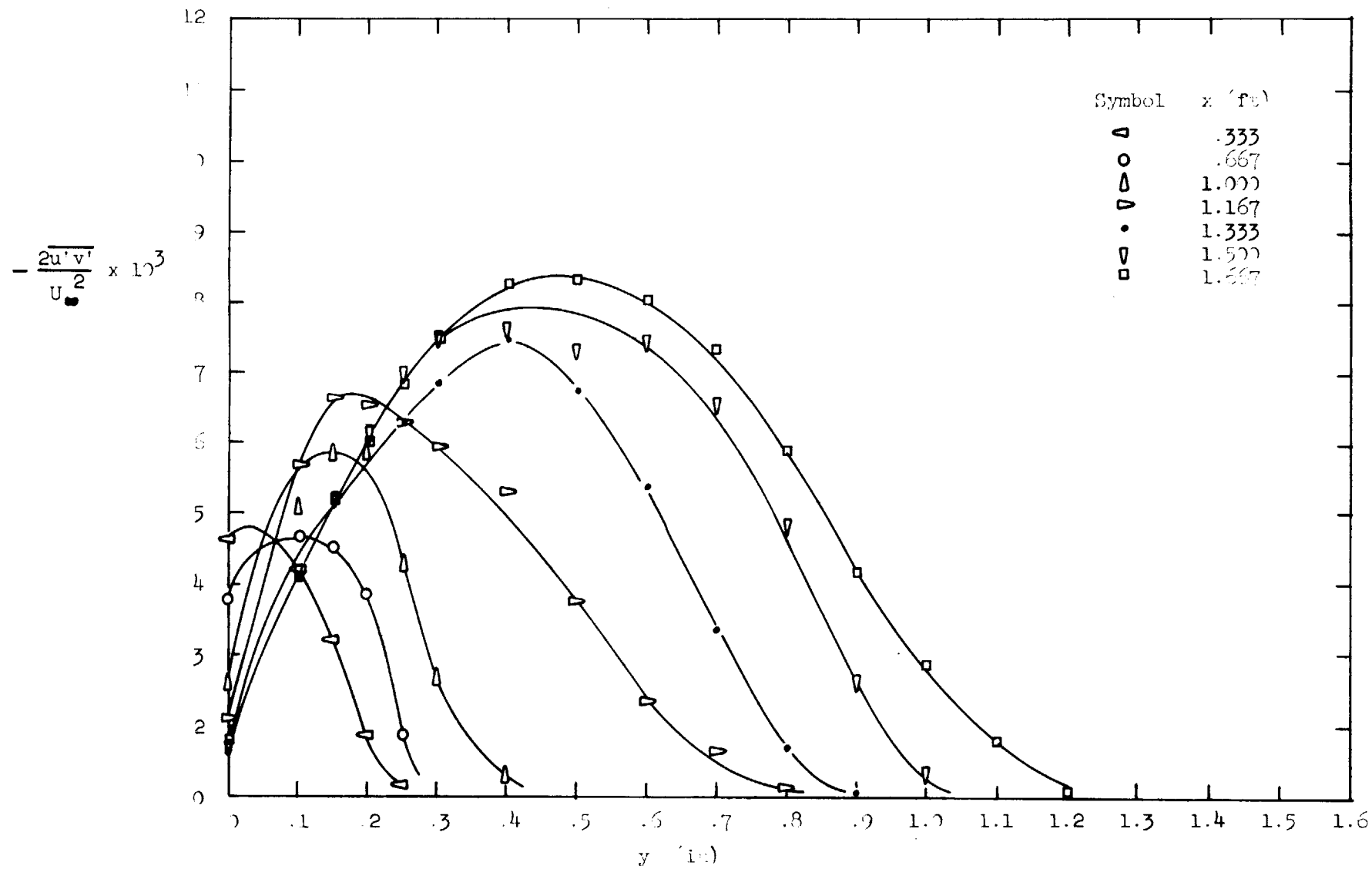
Figure 18 Experimental Shear Stress Distributions (a) Pressure Distribution No. 3
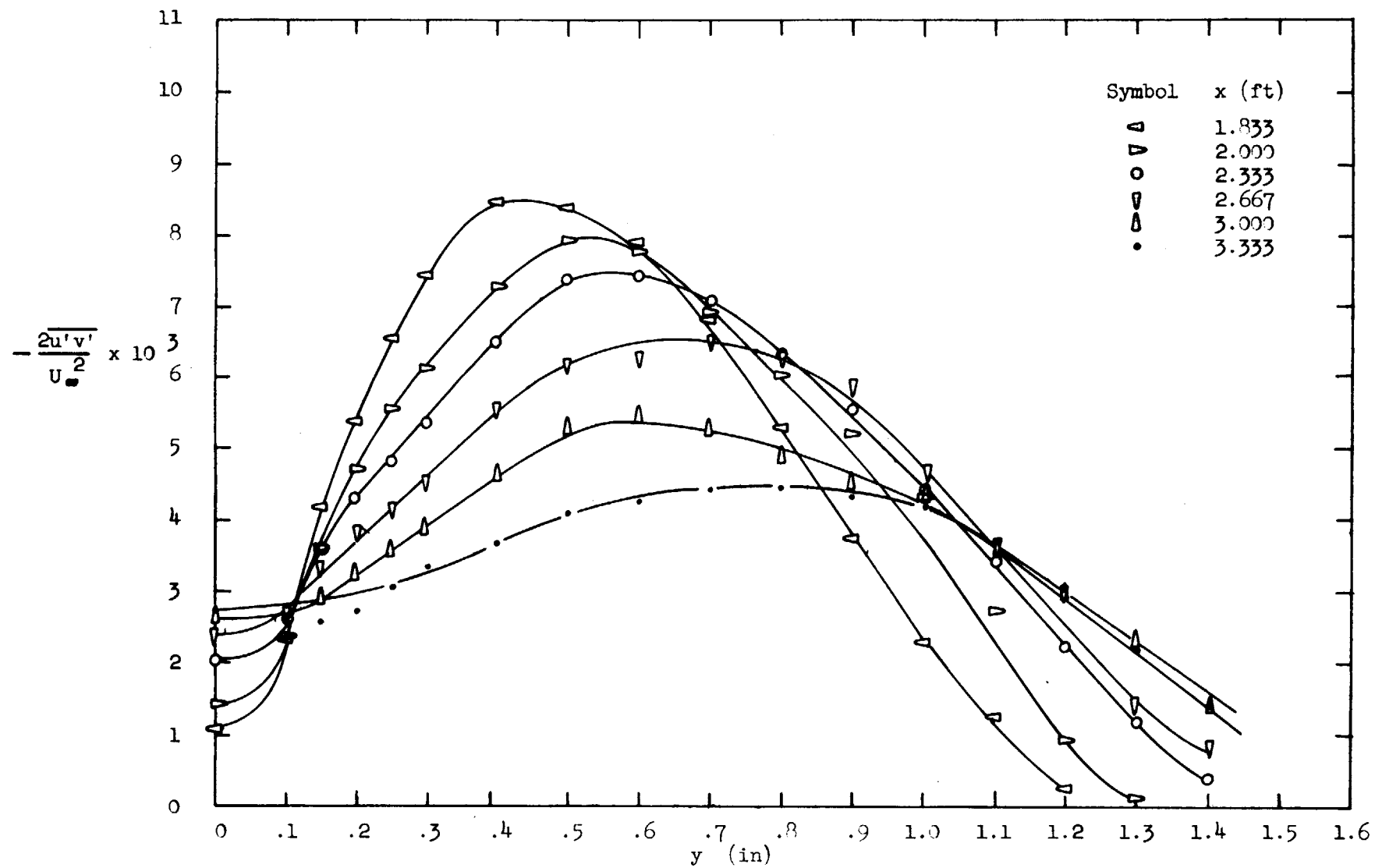
Figure 16 (a) Continued
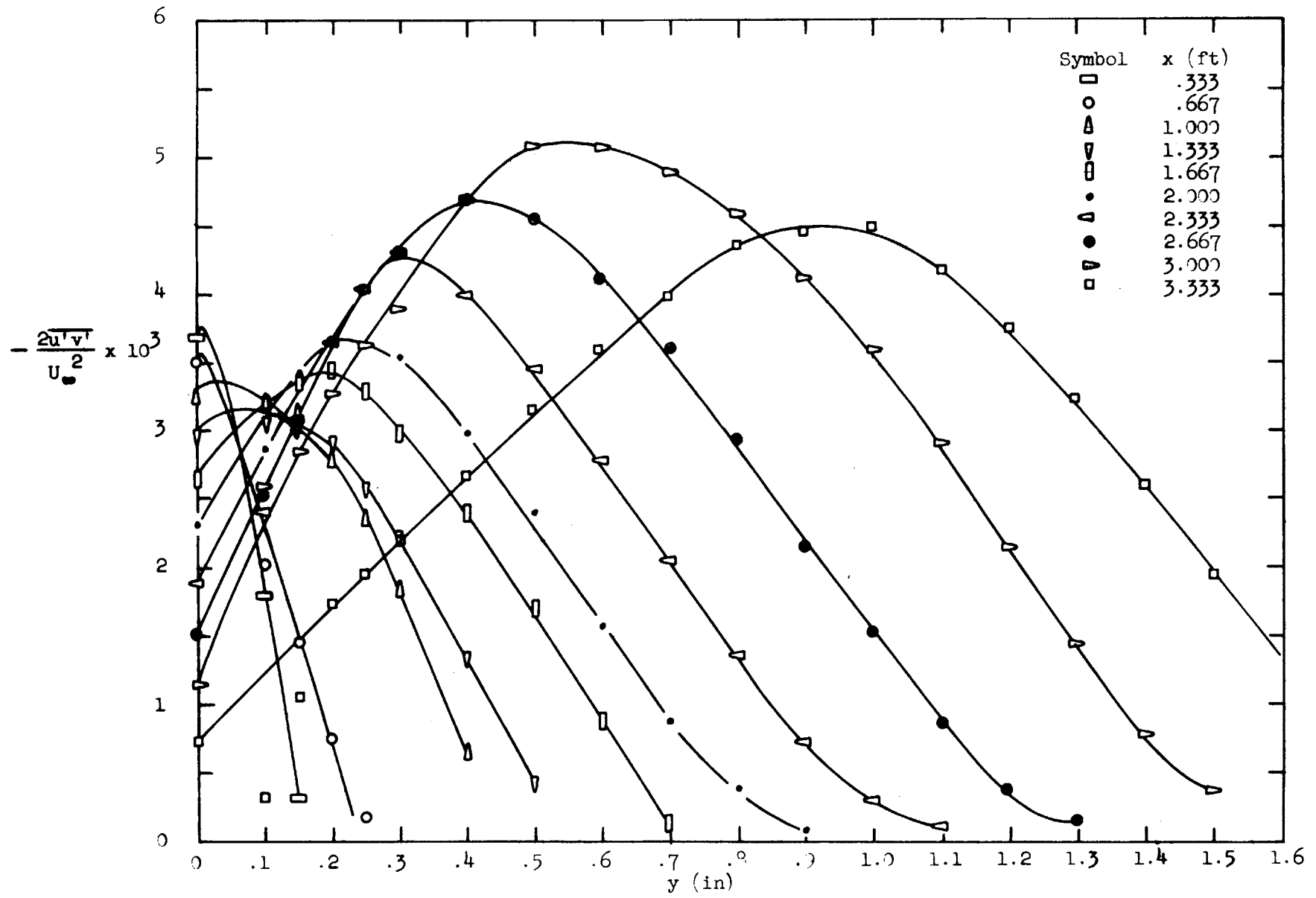
Figure 16 Experimental Shear Stress Distributions (b) Pressure Distribution No. 5
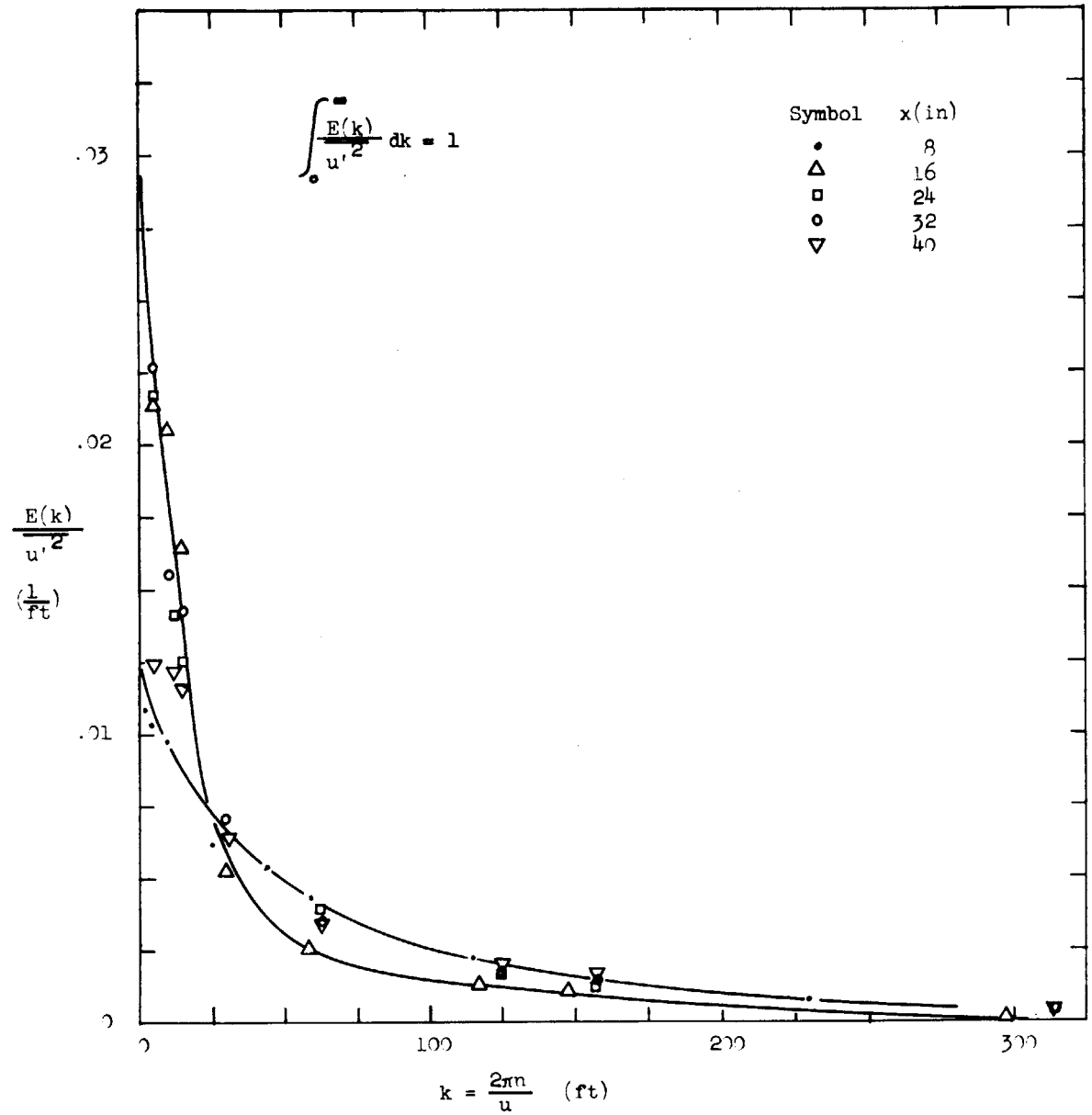
Figure 17 Normalized Energy Spectrums for Longitudinal Turbulence Intensity
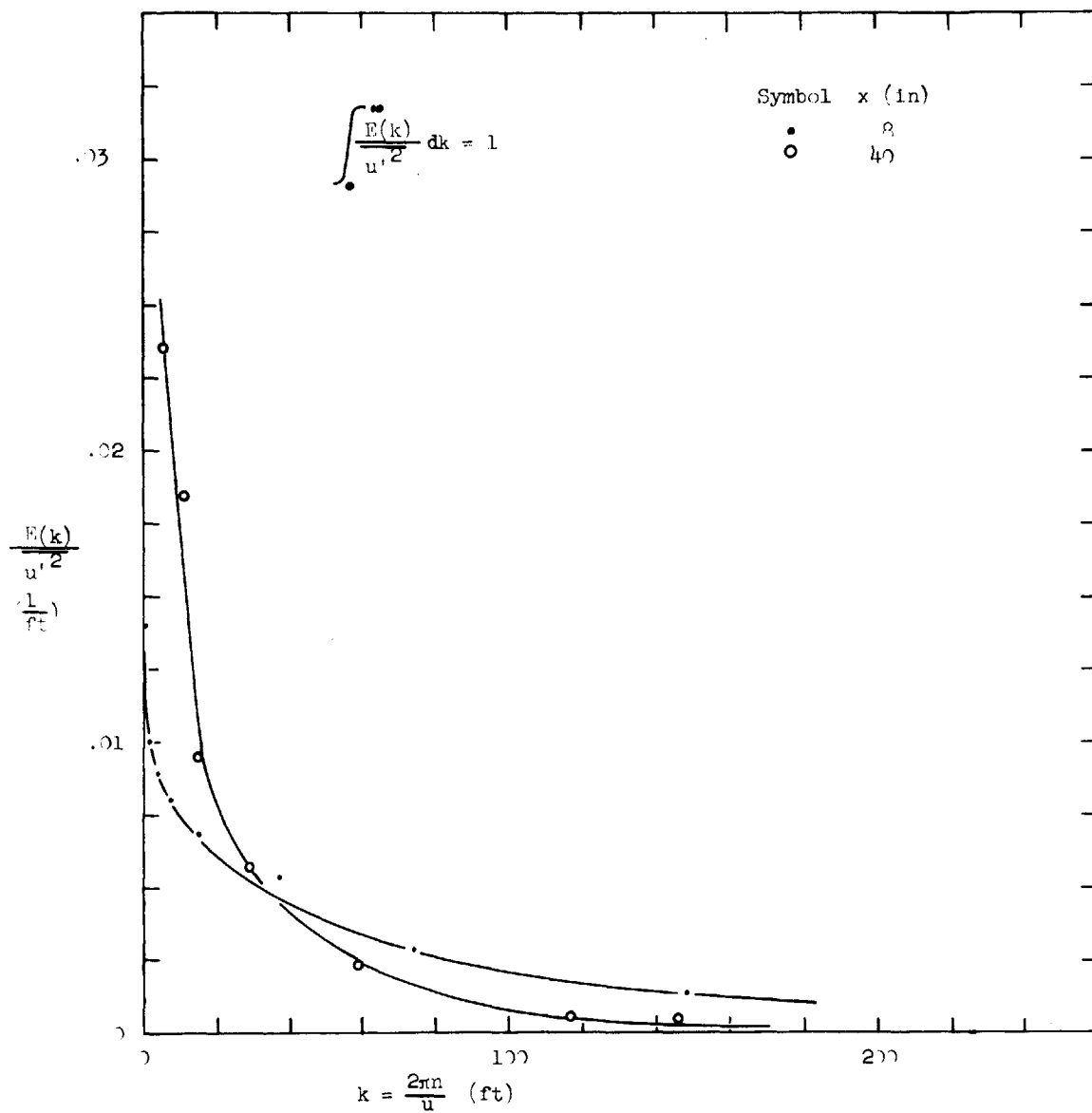(a) Pressure Distribution No. 3 Near Wall

$$\int_{\bullet}^{\infty} \frac{E(k)}{u'^2} \, dk = 1$$

Symbol   x (in)
•   8
o   40

$\frac{E(k)}{u'^2}$

$(\frac{1}{ft})$

.03

.02

.01

0

0   100   200

$k = \frac{2\pi n}{u}$ (ft)

Figure 17 (b)   Pressure Distribution No.5 Near Wall

$$\int_0^\infty \frac{E(k)}{u'^2} \, dk = 1$$

Symbol	y (in)
□	.33
○	.13
△	.0015

$k = \dfrac{2\pi n}{u}$ (ft)
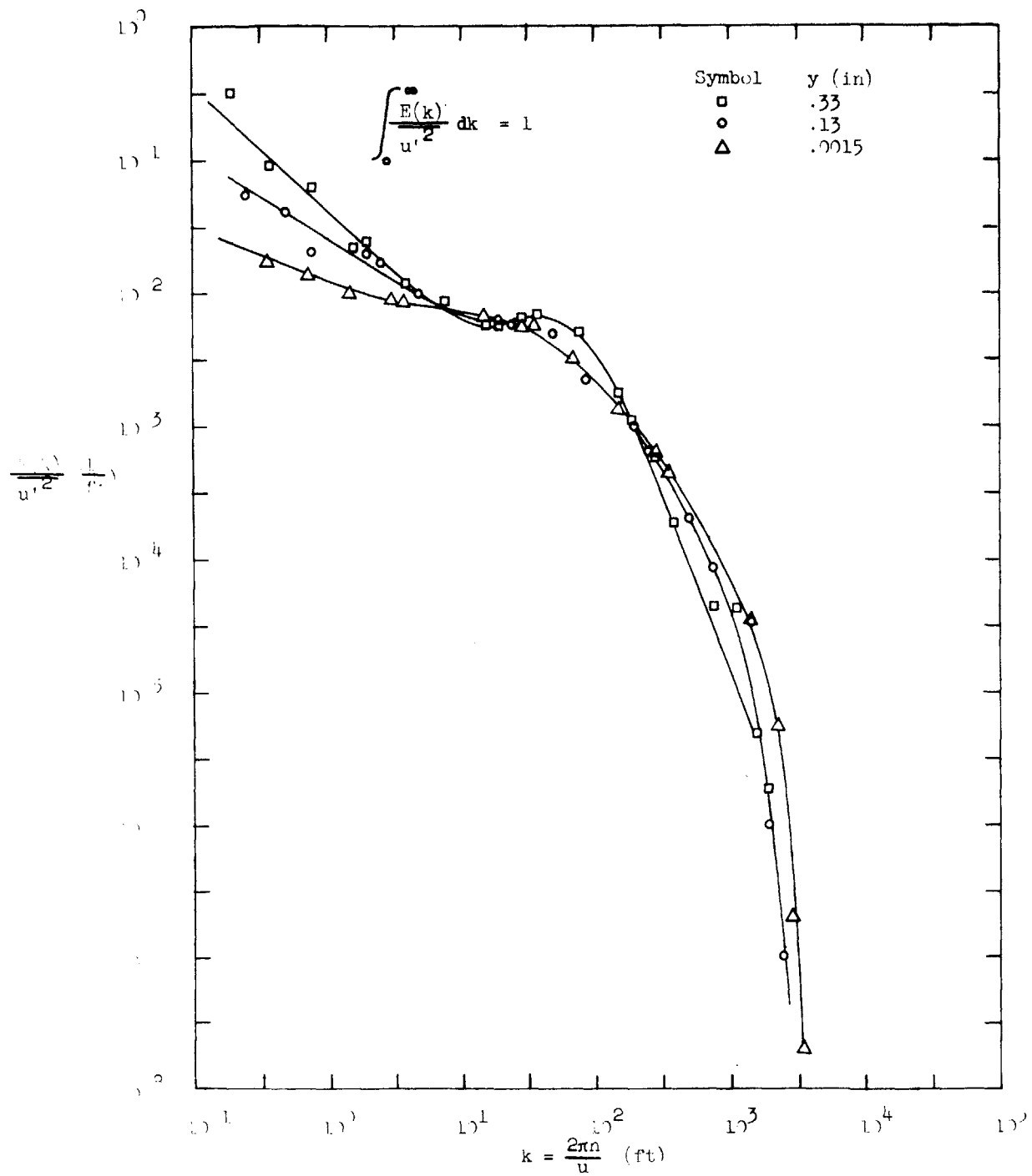
Figure 17 Normalized Energy Spectrums for Longitudinal Turbulence Intensity
(c) Variation Across Boundary Layer for Pressure Distribution
No. 5 at x = 8"

(a) Pressure Distribution No. 1

$\circ$ Data

$\triangle$ 2-D Mom. Eq. + Empirical N.S.C.

(b) Pressure Distribution No. 2

$---$ 2-D Mom. Eq. No Normal Stresses

$-\!\!-\!\!-$ 2-D Mom. Eq. $+ \dfrac{1}{U^2}\displaystyle\int_0^\infty \dfrac{\partial}{\partial x}(\overline{u'^2})\,dy$ from Experimental Data

$-\!\cdot\!-$ 2-D Mom. Eq. $+ \dfrac{1}{2U^2}\displaystyle\int_0^\infty \dfrac{\partial}{\partial x}(\overline{u'^2})\,dy$ from Experimental Data

x (in)
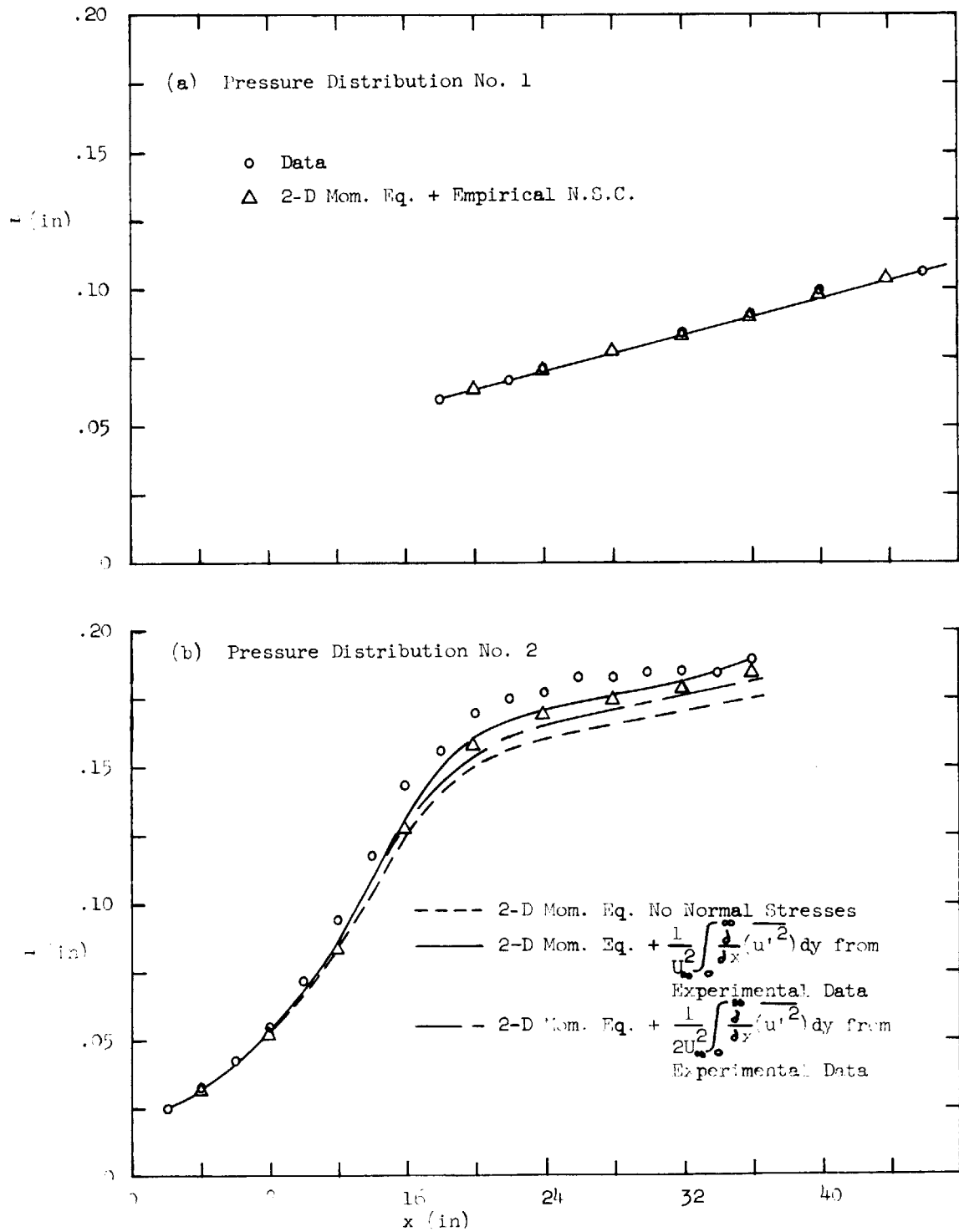
Figure 18 Comparisons of Momentum Thickness Calculations with Data

(c) Pressure Distribution No. 3

(d) Pressure Distribution No. 4

Continued

(e) Pressure Distribution No. 5
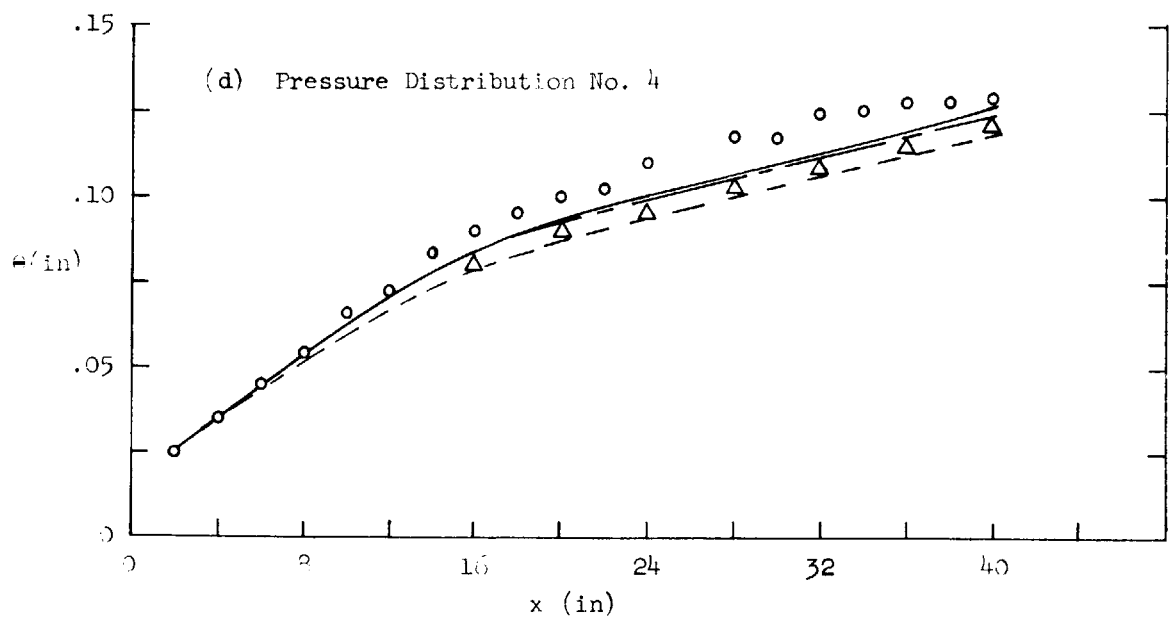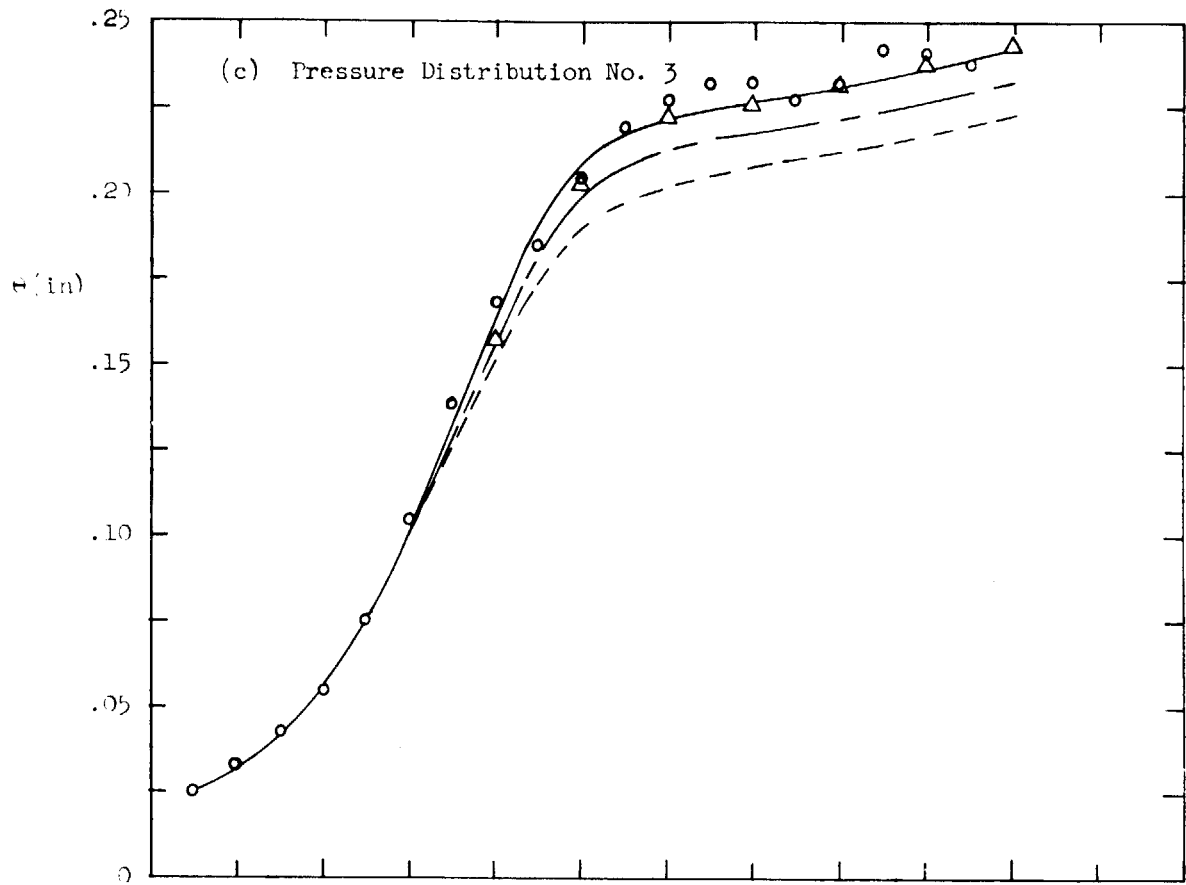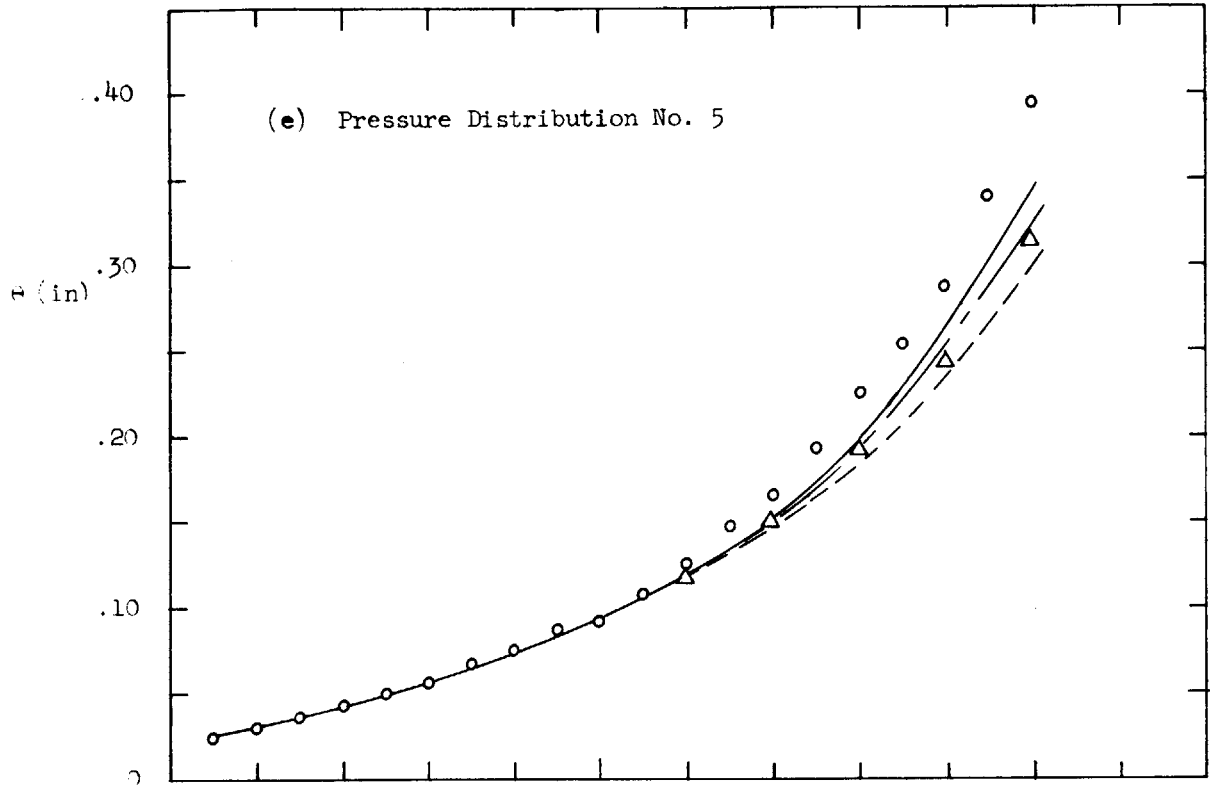
(f) Pressure Distribution No. 6
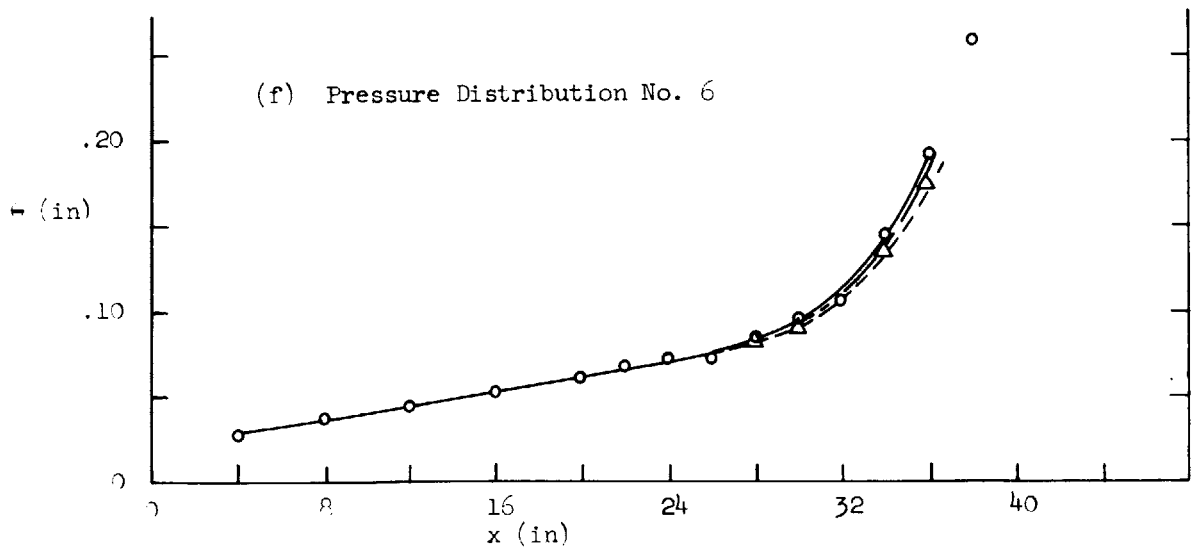
Figure 17 Continued
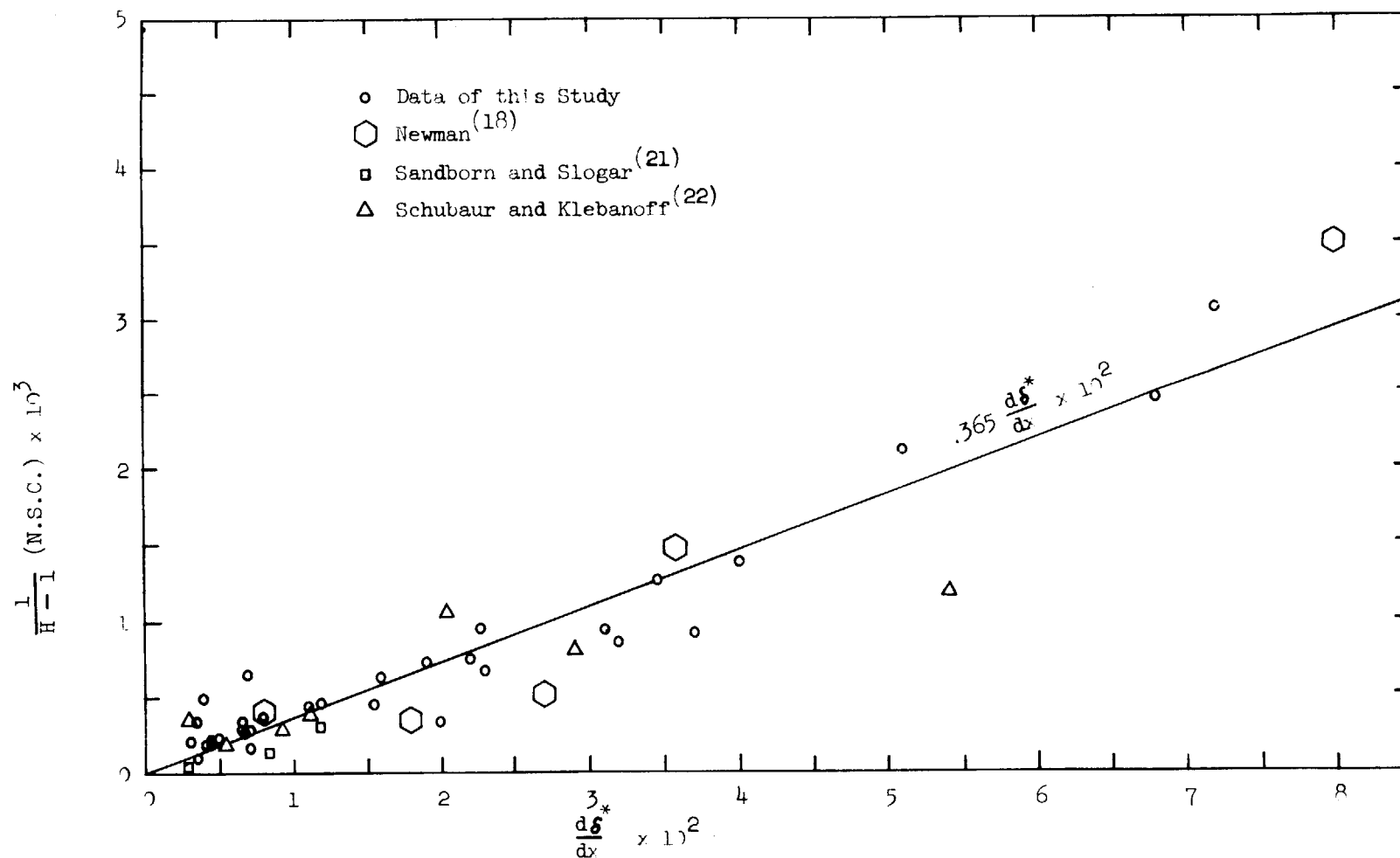
Figure 19 Impirical Correlation for Normal Stress Correction (N.S.C.) to Von Karman Momentum Integral Equation

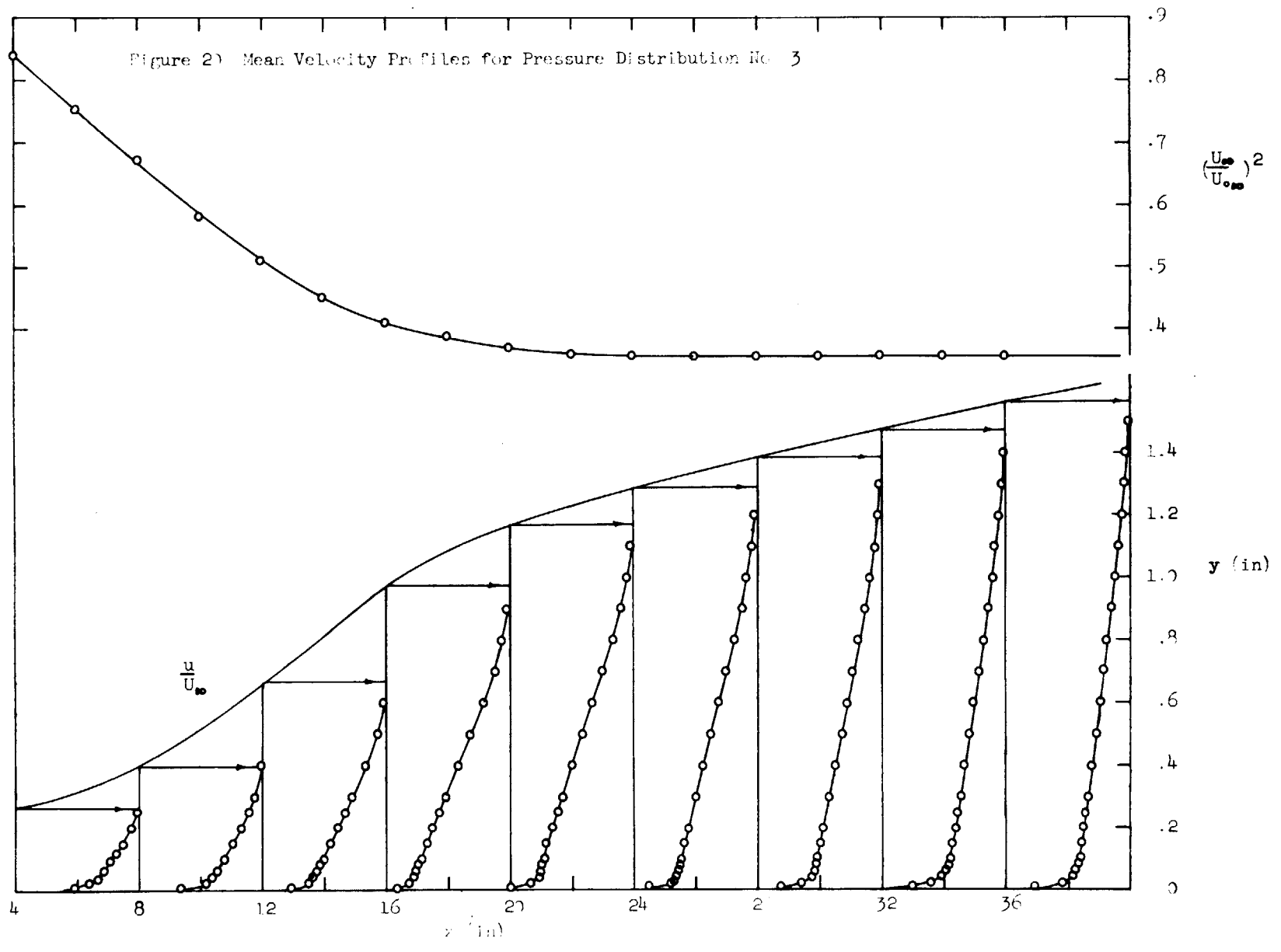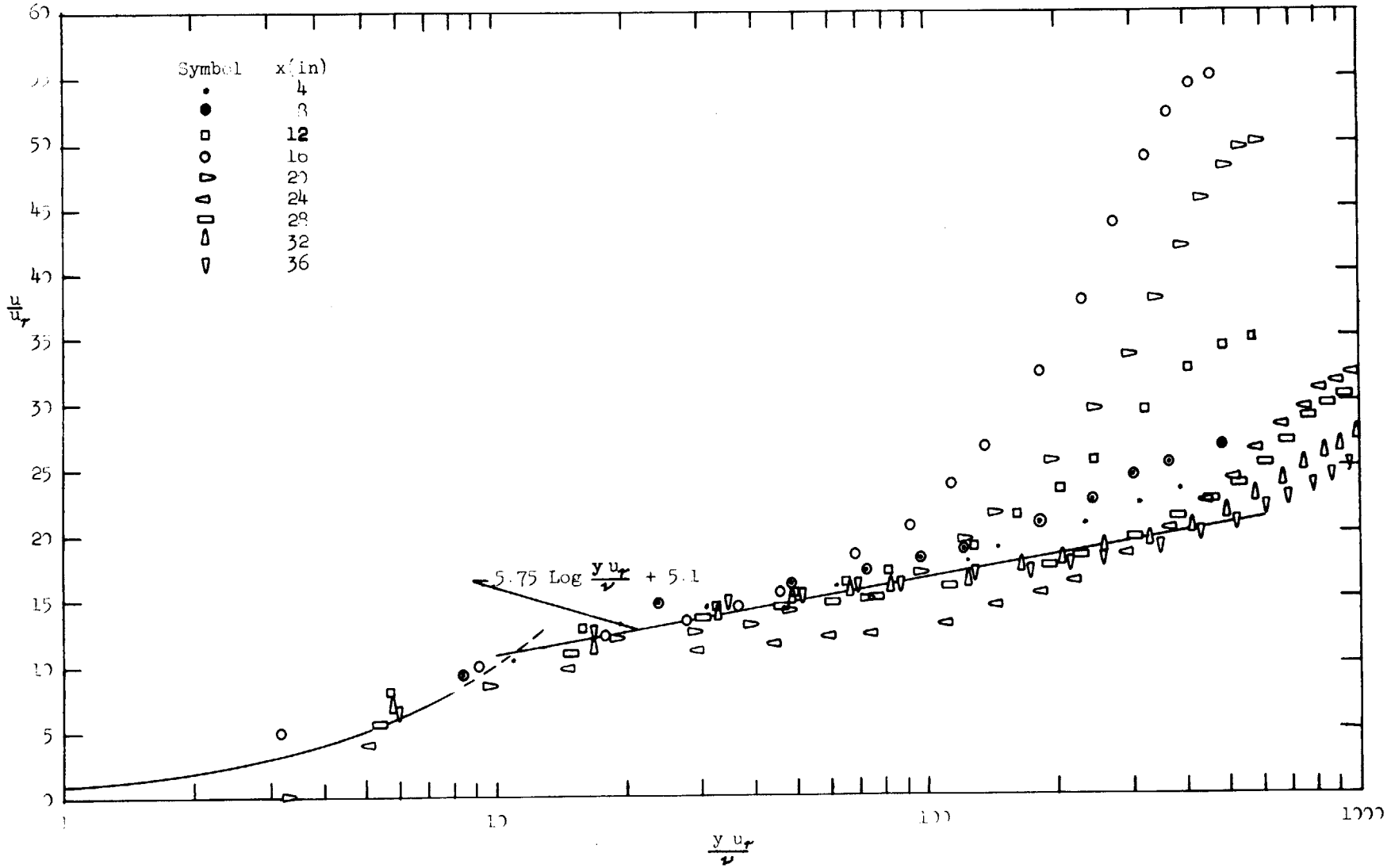Figure 20 Mean Velocity Profiles for Pressure Distribution No. 3

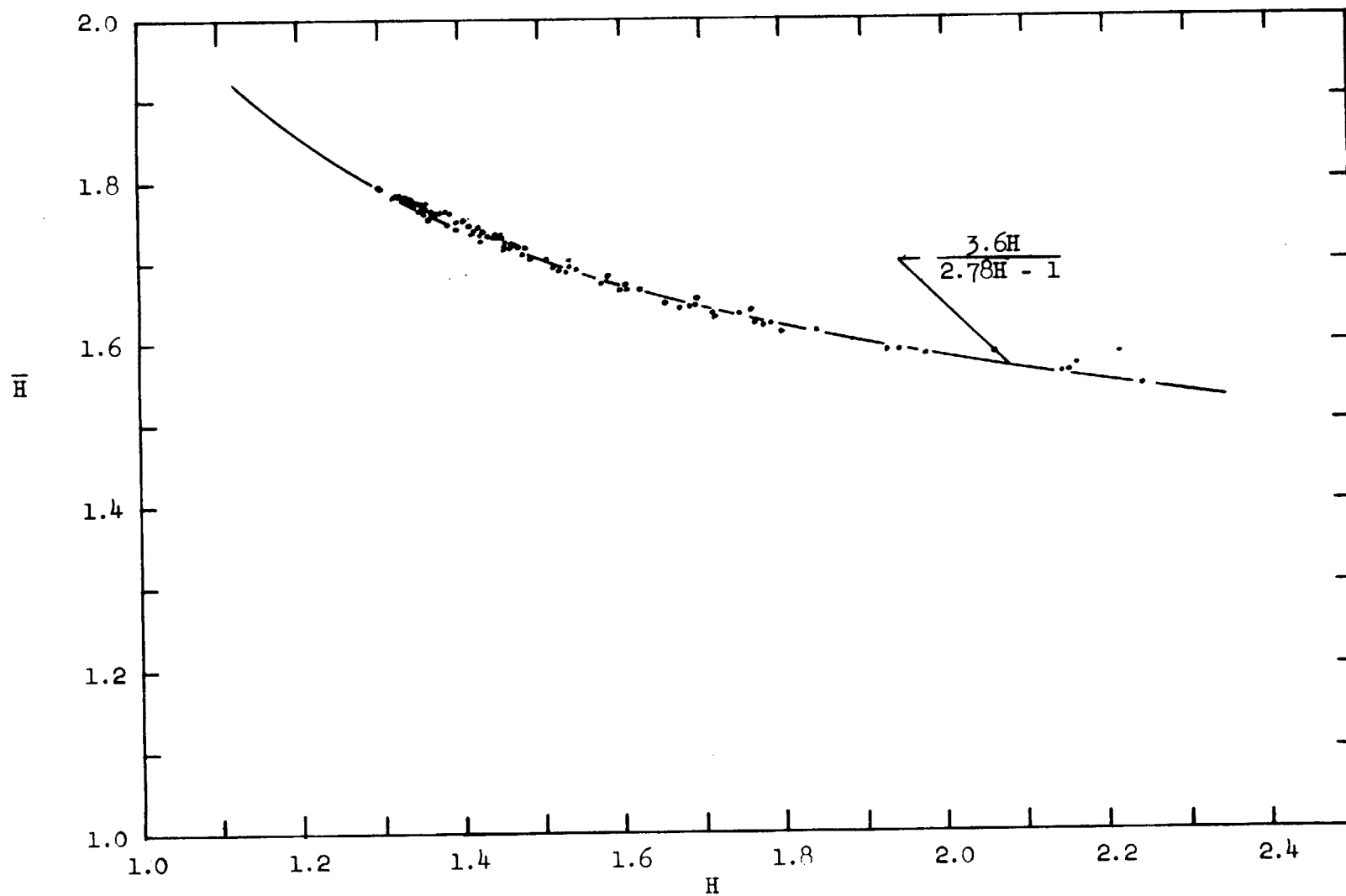Figure 21 Comparison of Velocity Profiles with Law of the Wall   Pressure Distribution No. 3

Symbol	x (in)
·	4
●	8
□	12
○	16
◁	20
◁	24
☐	28
△	32
▽	36

$5.75 \ \mathrm{Log} \ \dfrac{y \ u_\tau}{\nu} + 5.1$

$\dfrac{u}{u_\tau}$

$\dfrac{y \ u_\tau}{\nu}$

$$\frac{3.6H}{2.78H - 1}$$

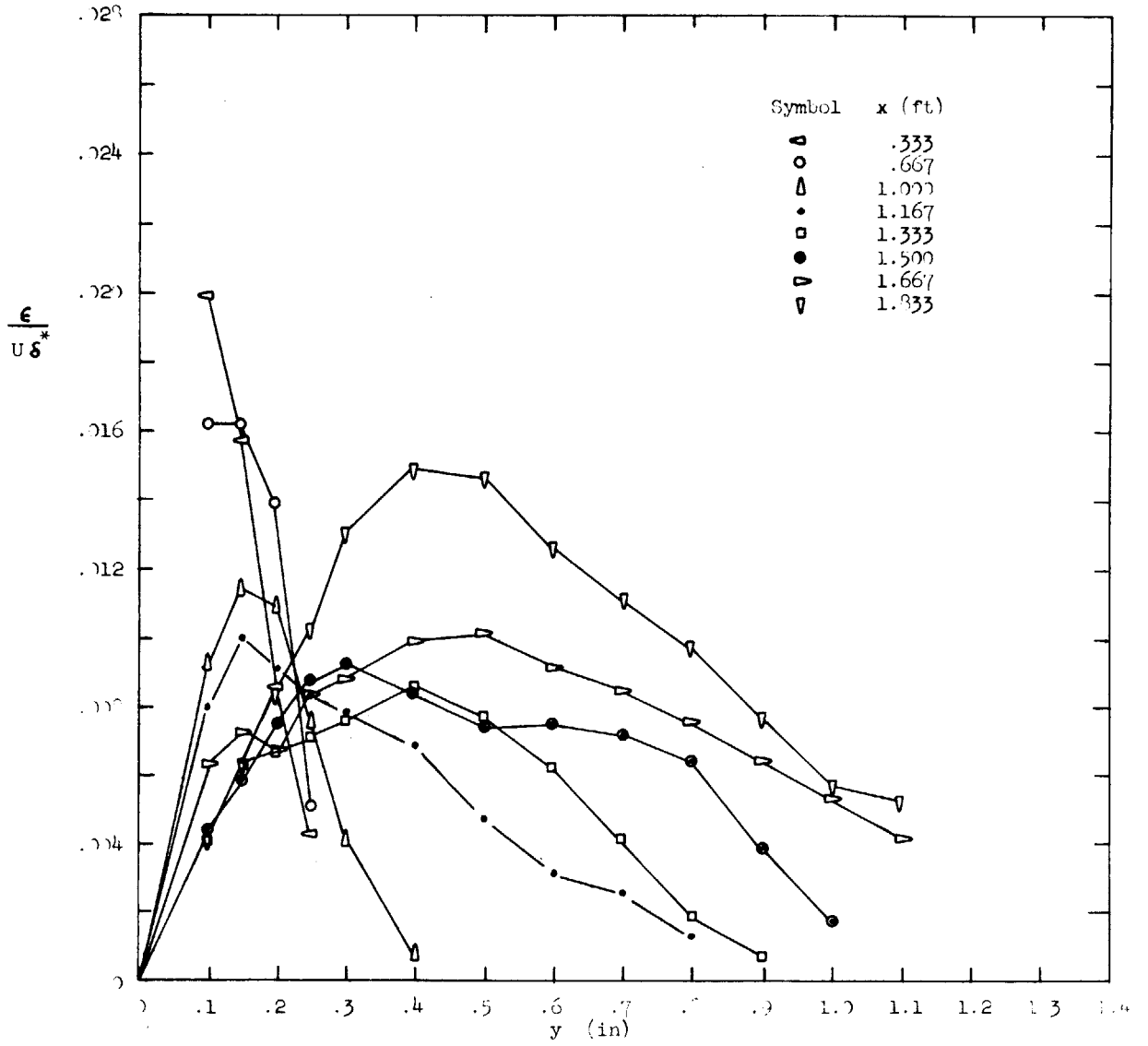Figure 22 Energy Factor $\bar{H}$ Versus Shape Factor H

• Data

Figure 23 Eddy Viscosity from Expreimental Data   Pressure Distribution No. 3
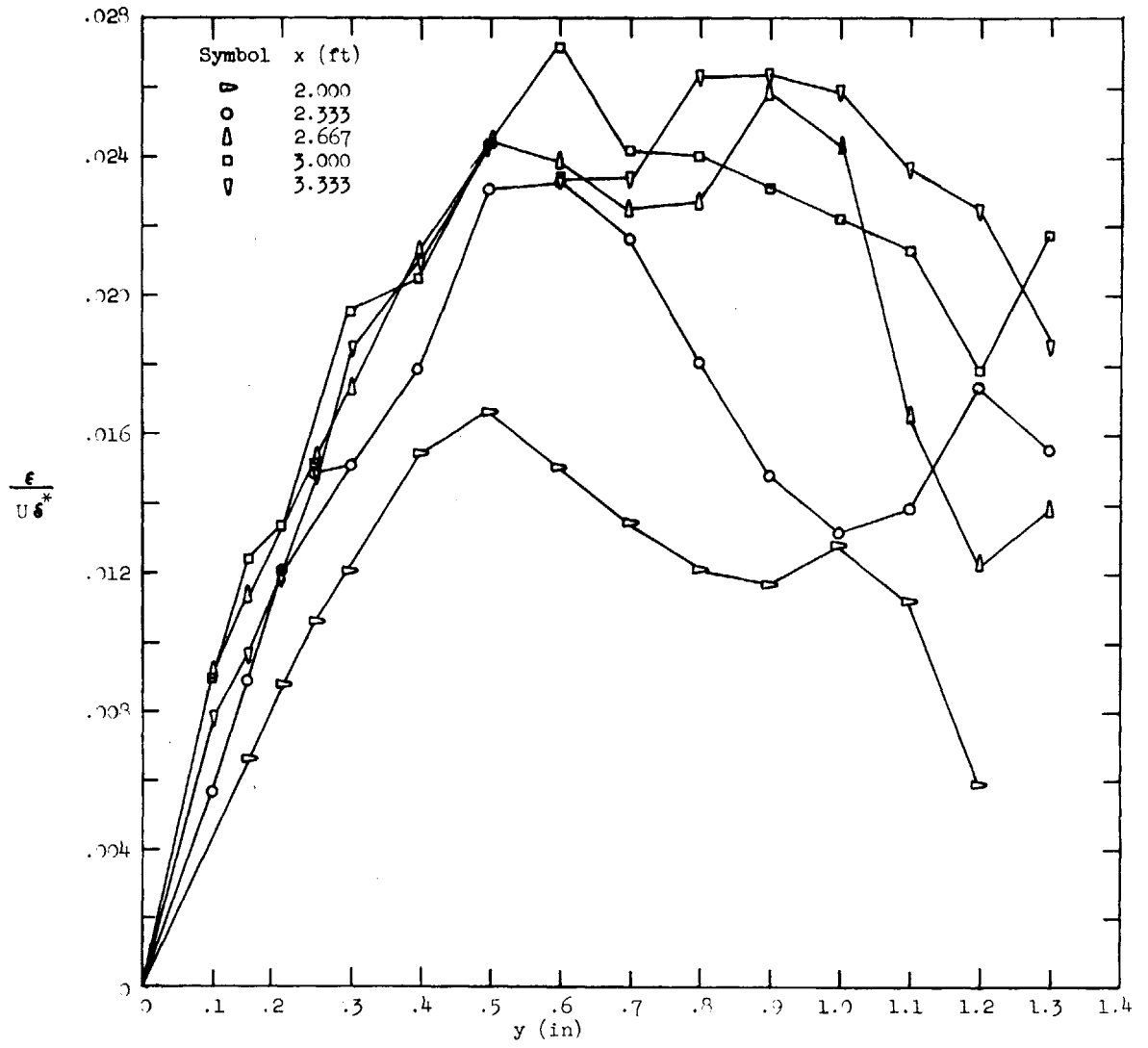
Figure 27 Eddy Viscosity from Experimental Data   Pressure Distribution No. 3
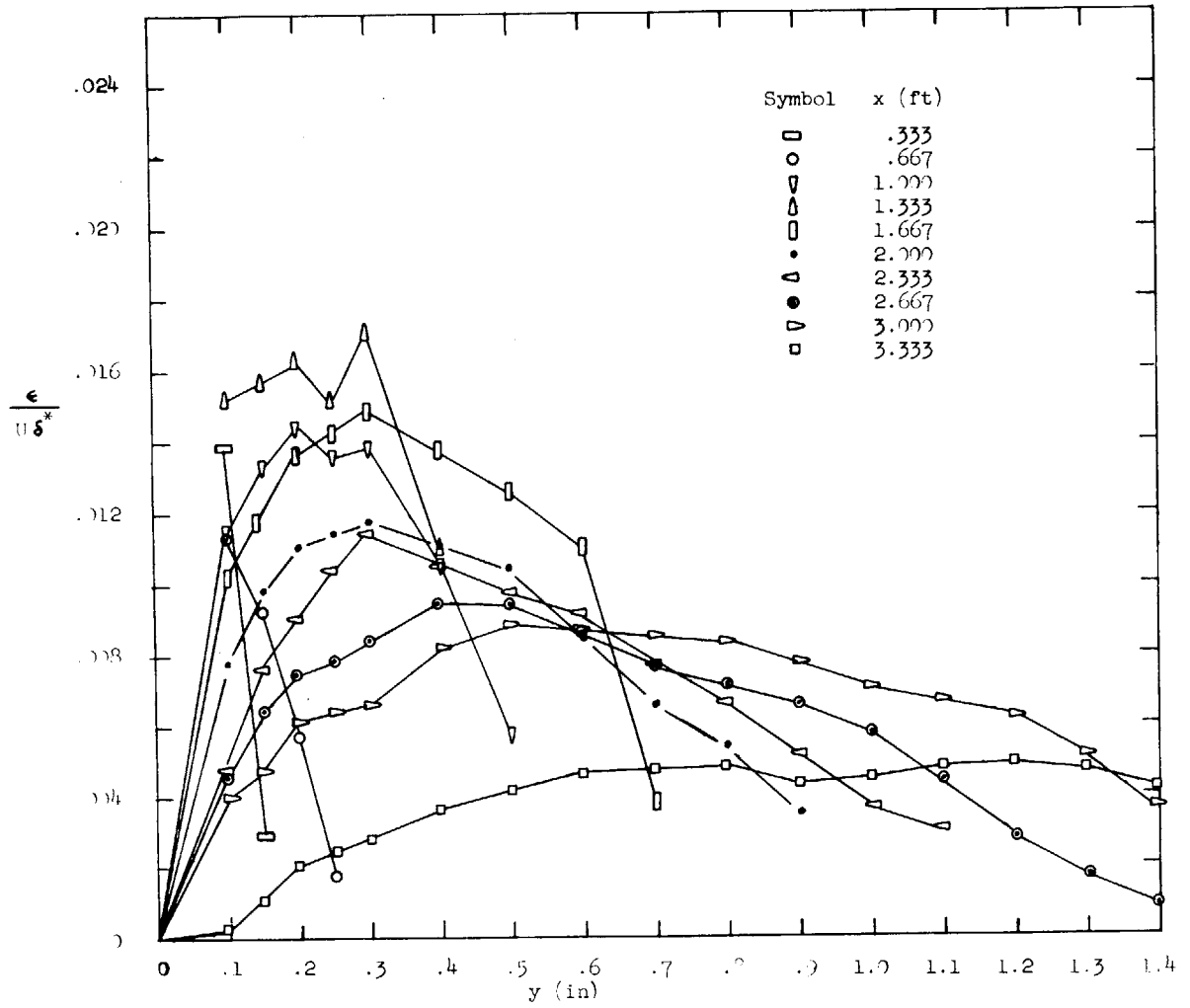
Figure 24   Eddy Viscosity from Experimental Data   Pressure Distribution No. 5
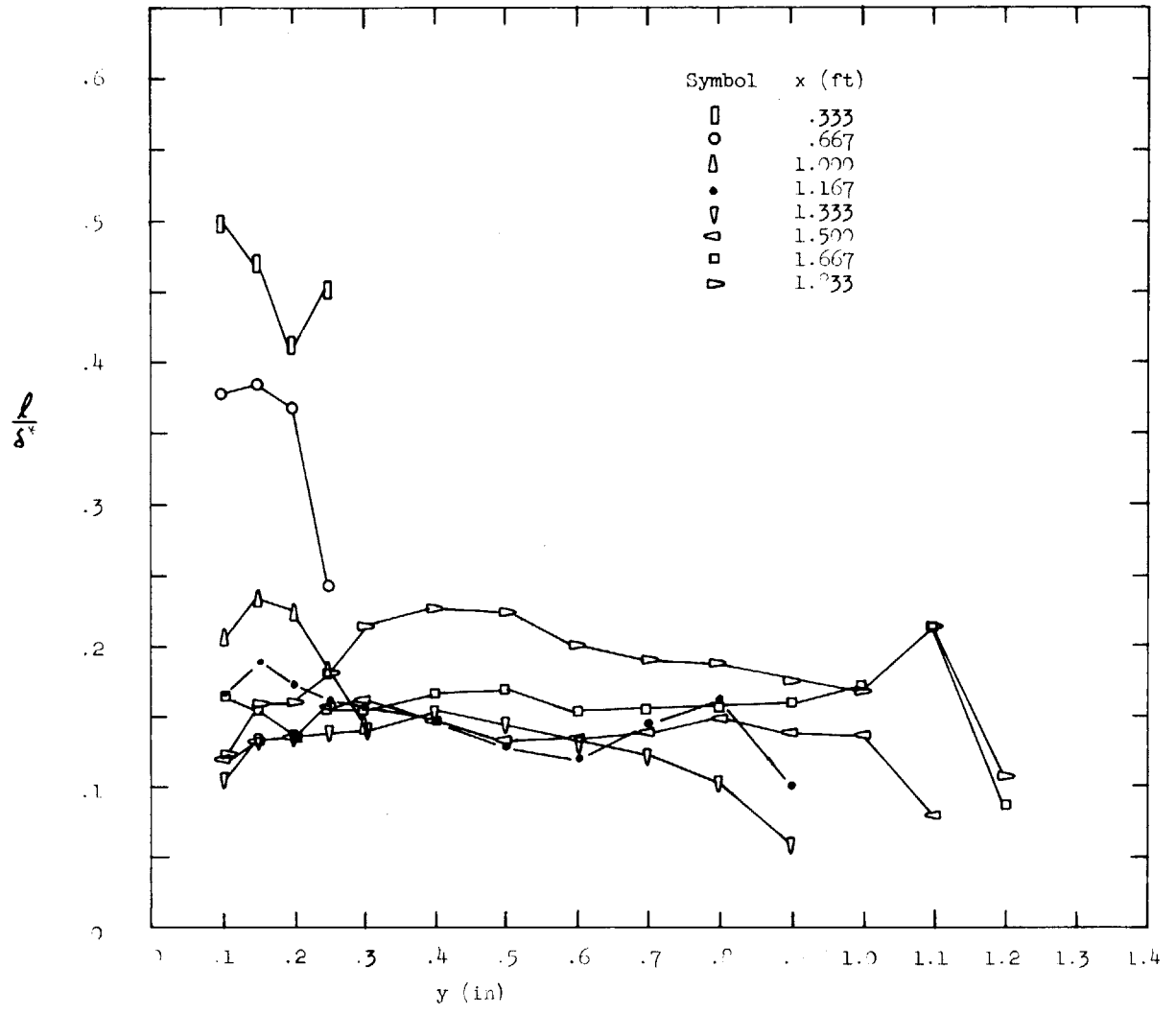
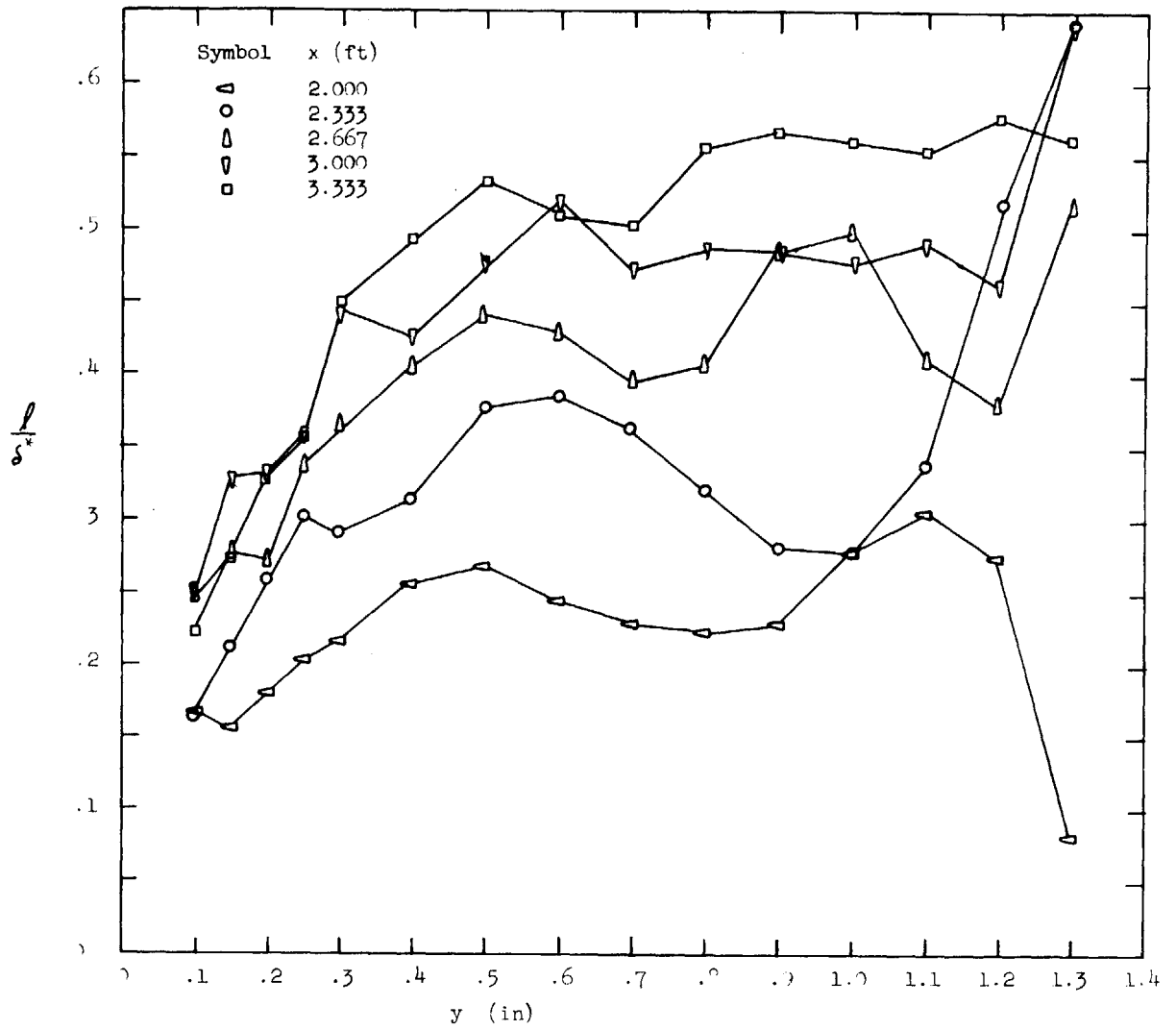Figure 25 Mixing Length from Experimental Data   Pressure Distribution No. 3

Figure 25 Mixing Length from Experimental Data   Pressure Distribution No. 3

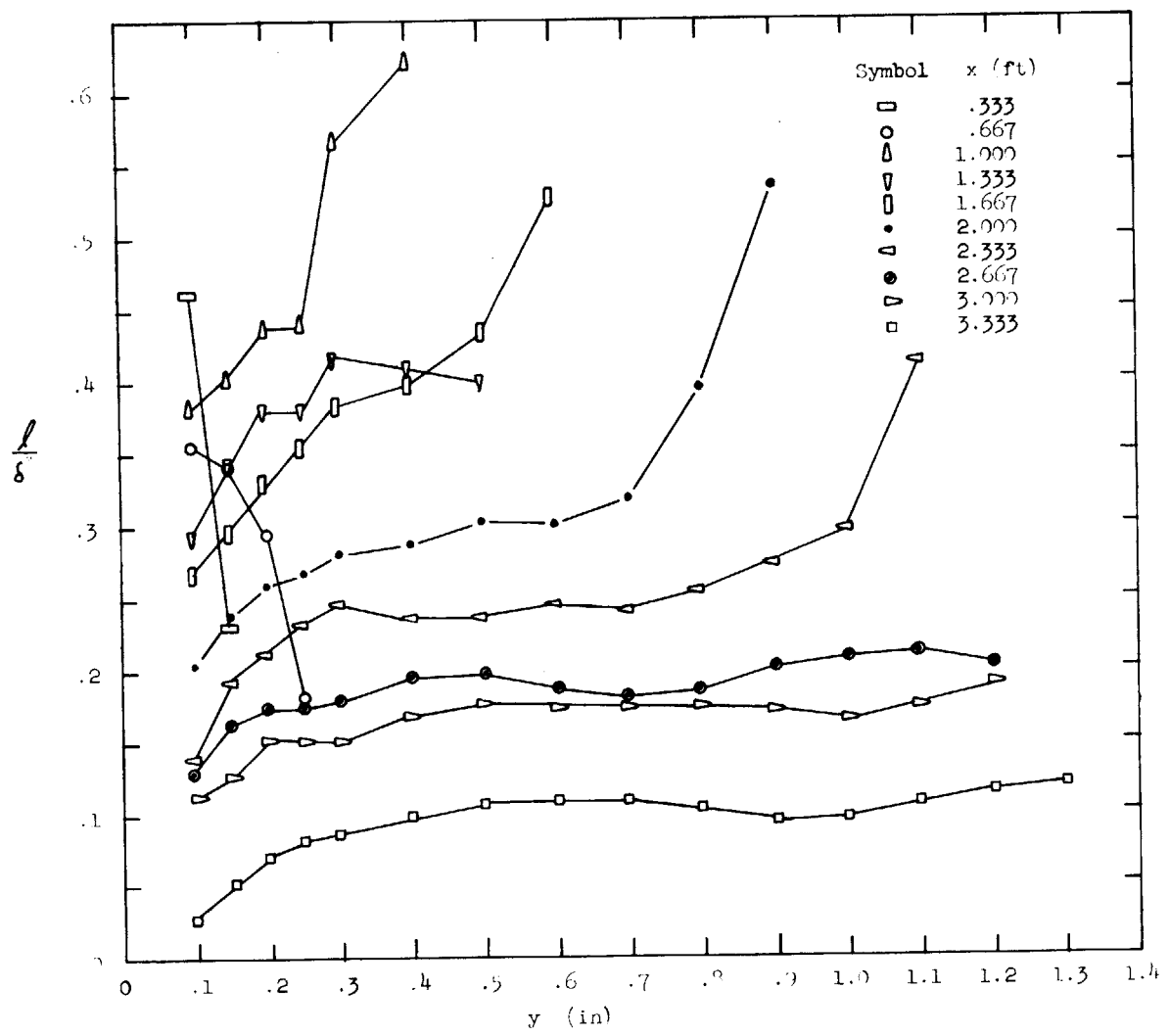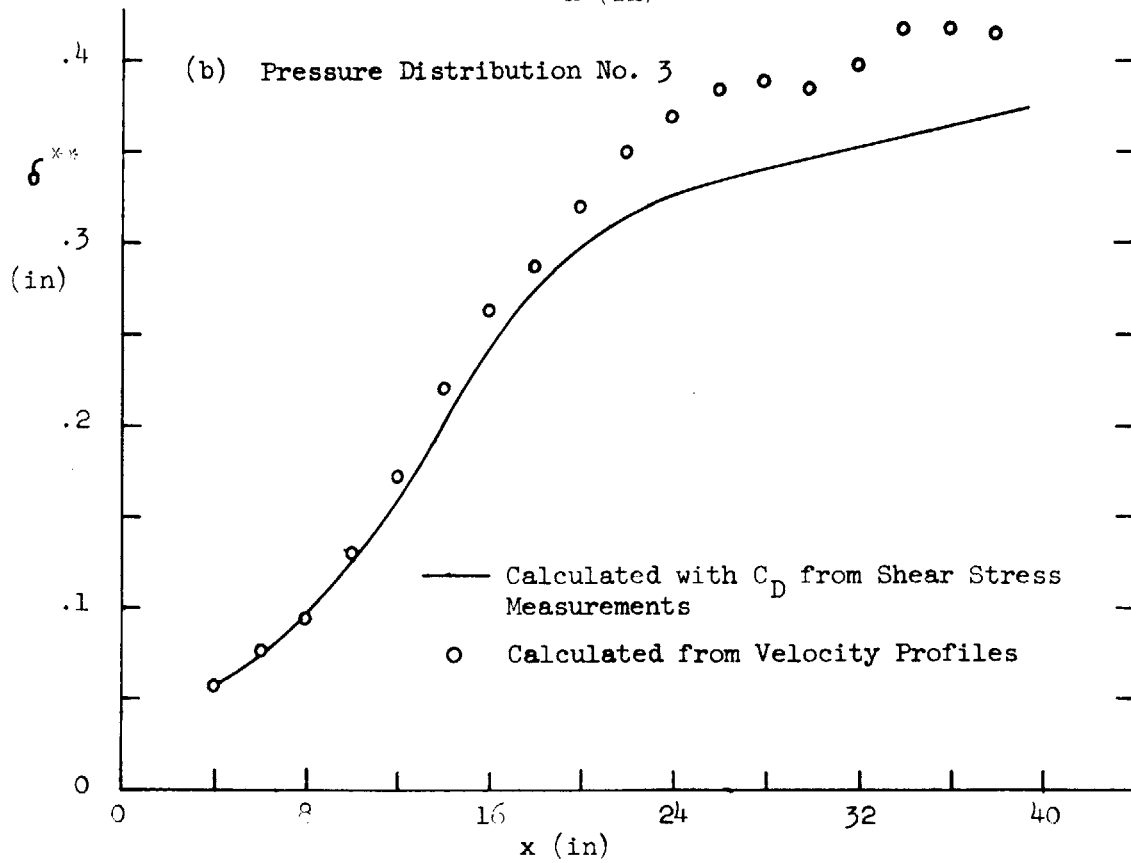Figure 26 Mixing Length from Experimental Data Pressure Distribution No. 5
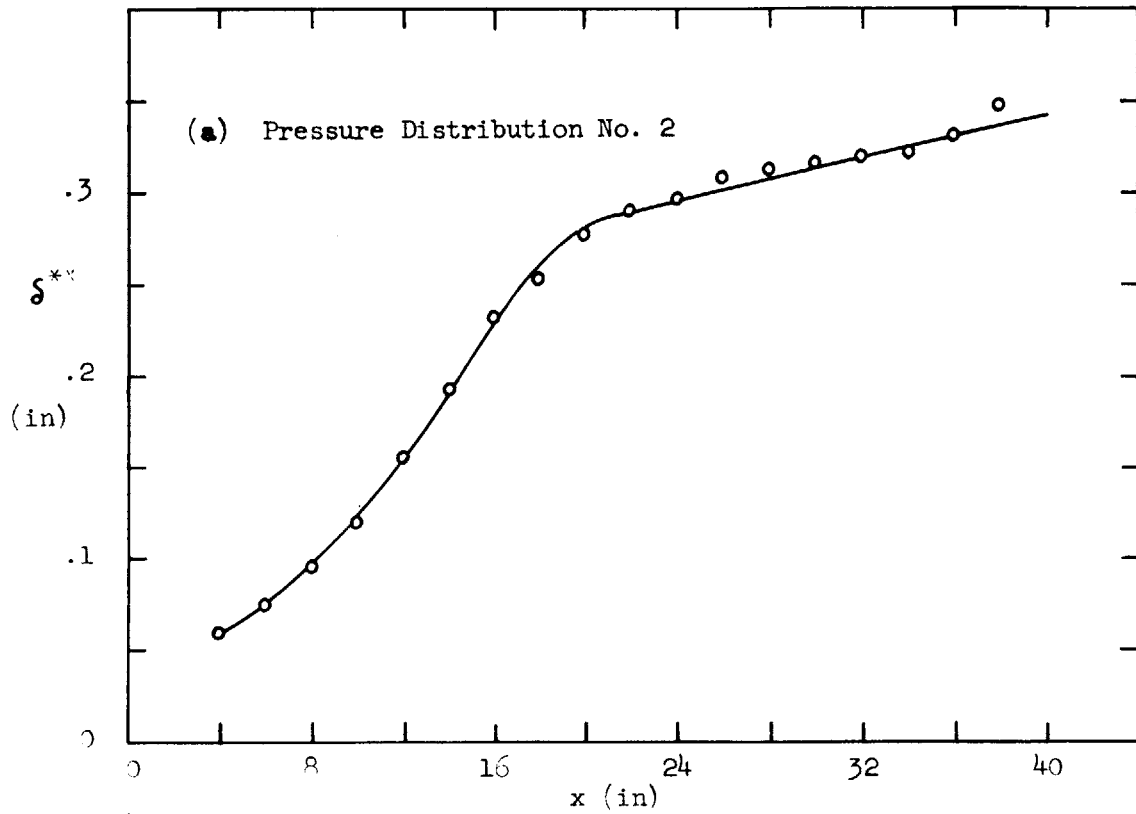
Figure 27 Comparison of Energy Thickness as Calculated from Hot-Wire and Velocity
Profile Data

(c)   Pressure Distribution No. 4

(d)   Pressure Distribution No. 5
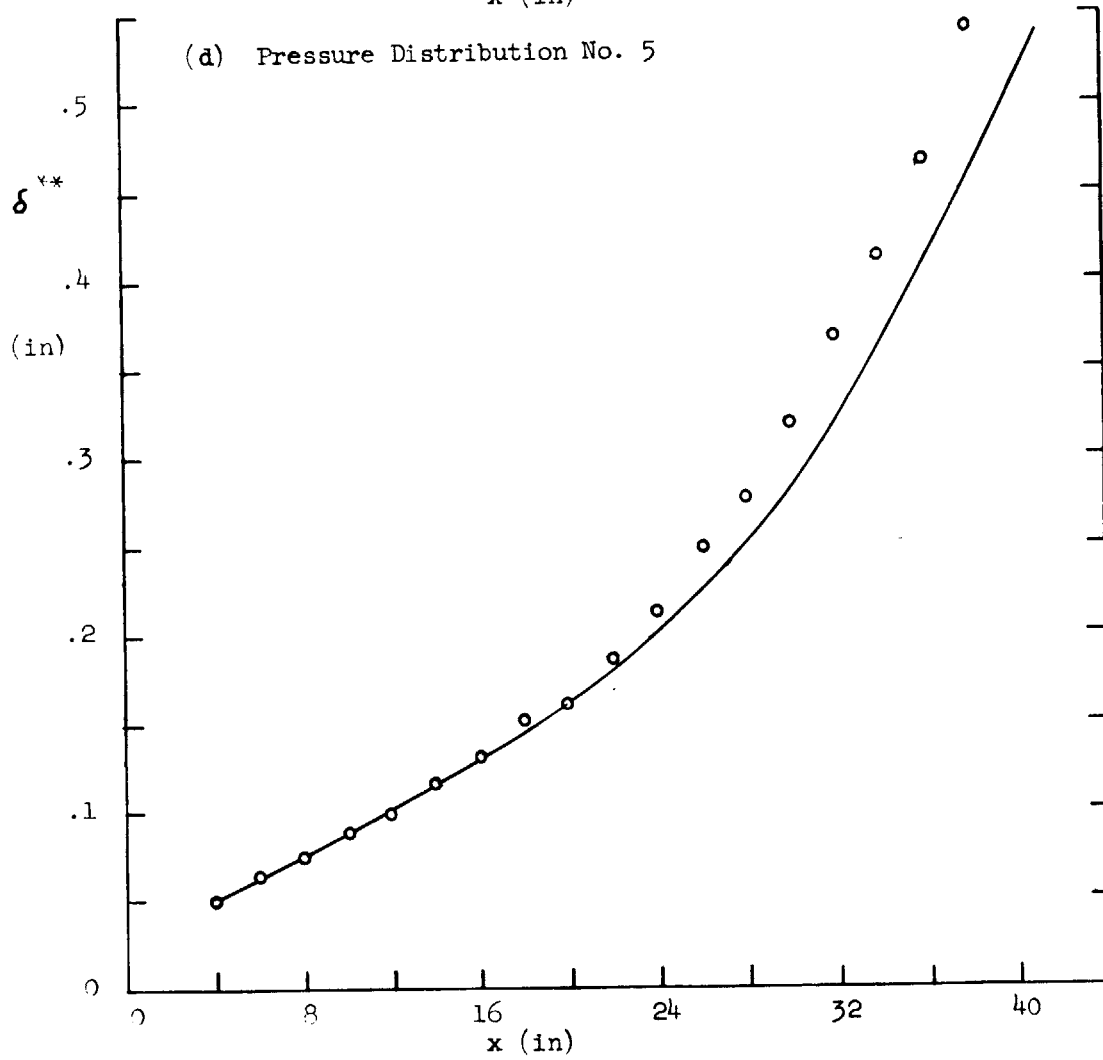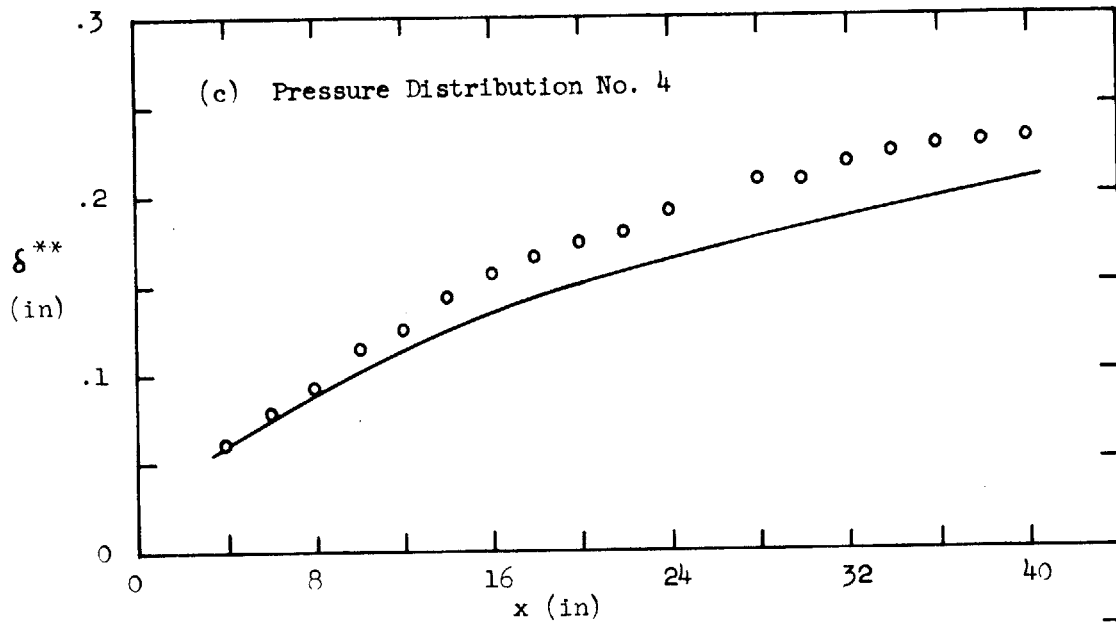
Figure 27   Continued
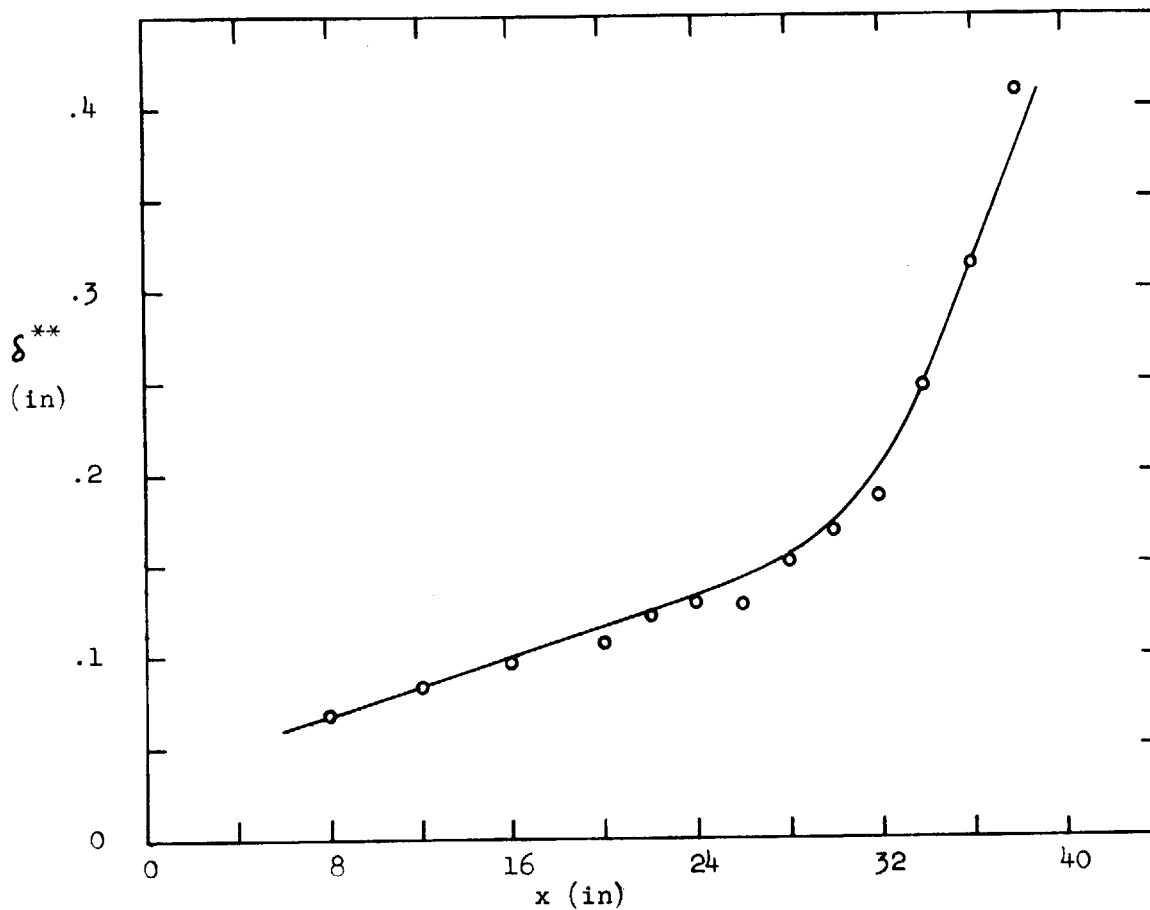
(e) Pressure Distribution No. 6

Figure 27 Continued
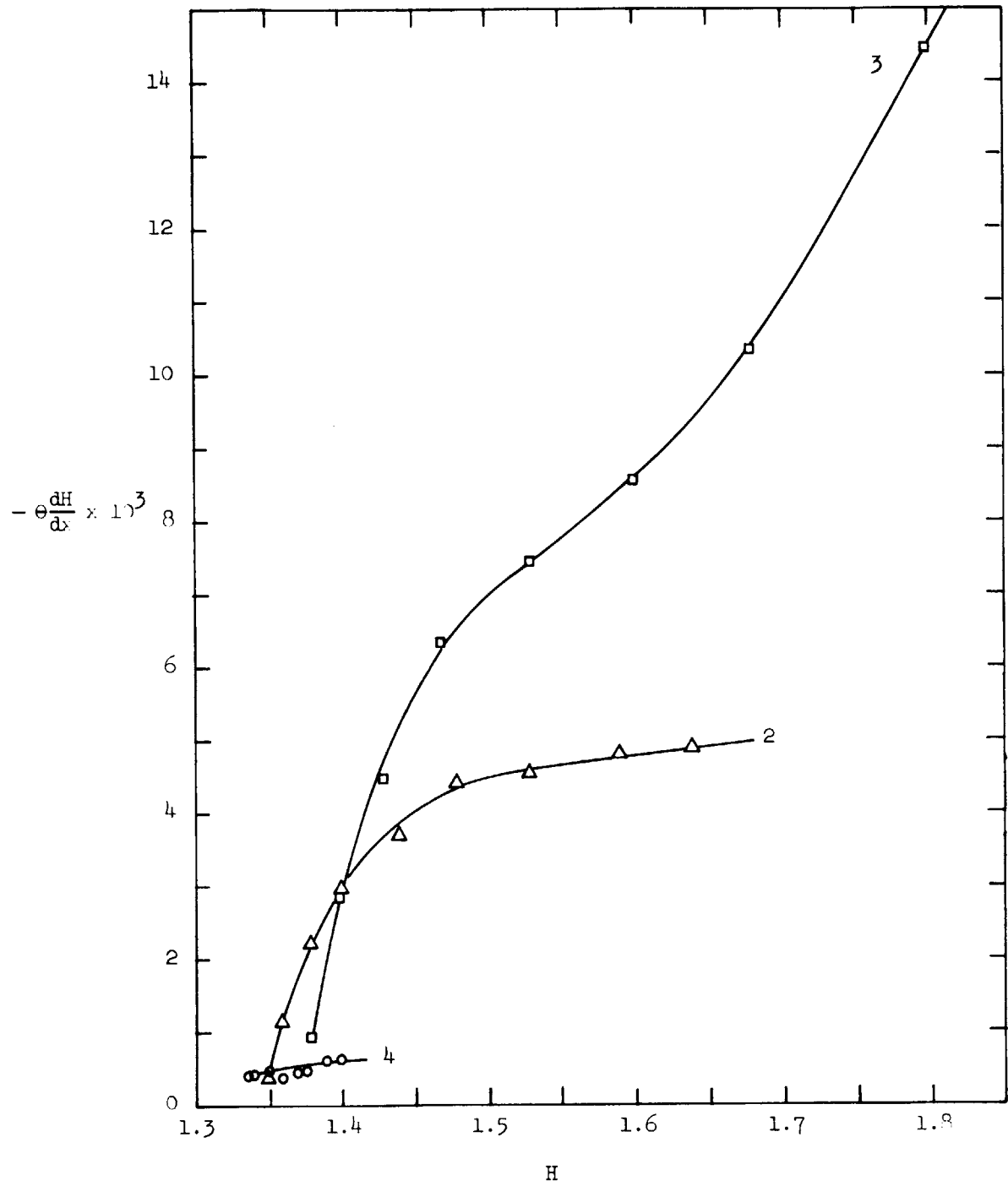
Figure 28   Shape Factor Decay Rate in Relaxing Region for Pressure
Distributions 2, 3, and 4
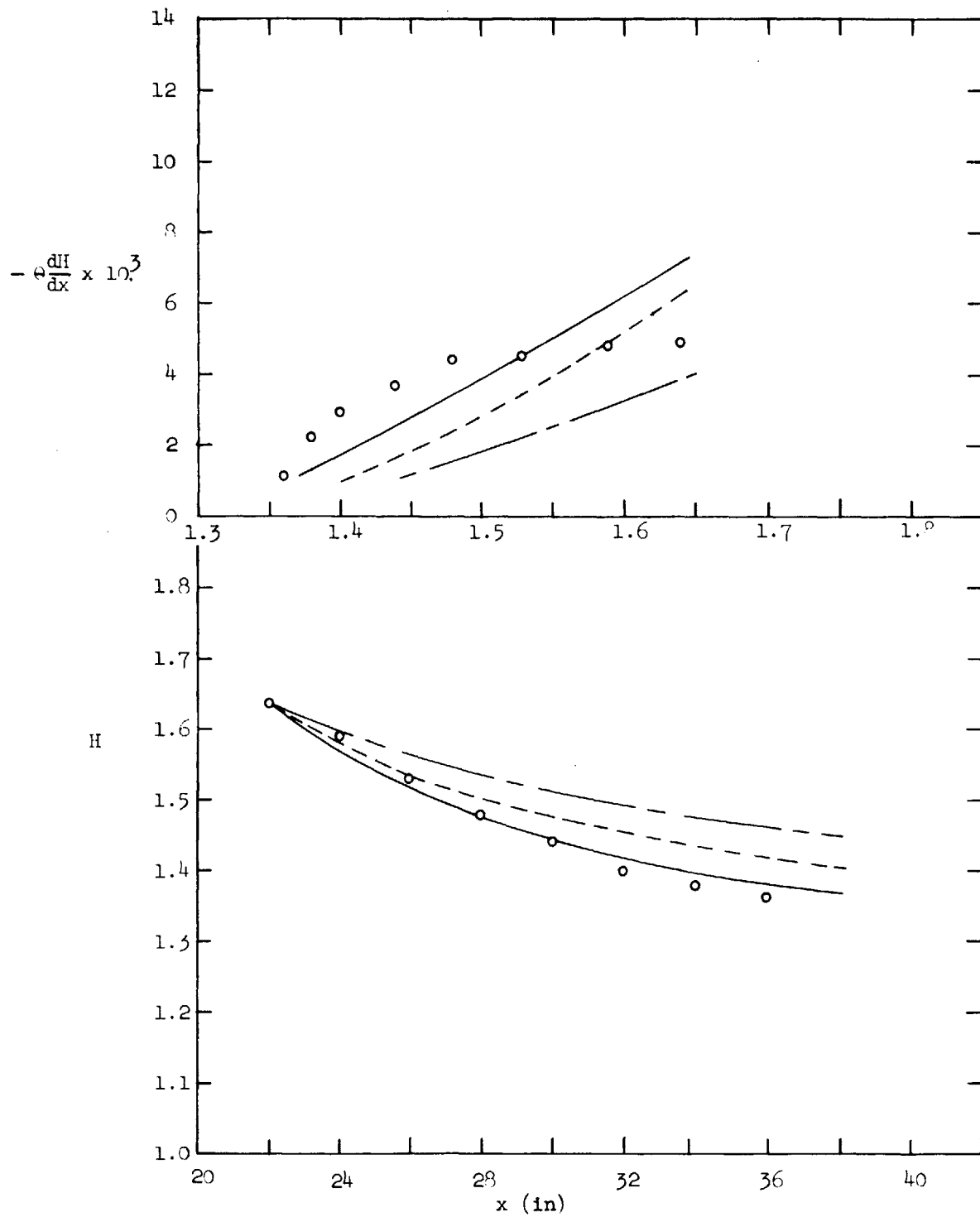
Figure 29 Comparison Between Calculated and Measured Shape Factors in Relaxing Regions

(a) Pressure Distribution No. 2   ————— Eq. (23)
                                              - - - - - Ref. (28)
                                            ——— - Ref. (29)
                                            ○   Data
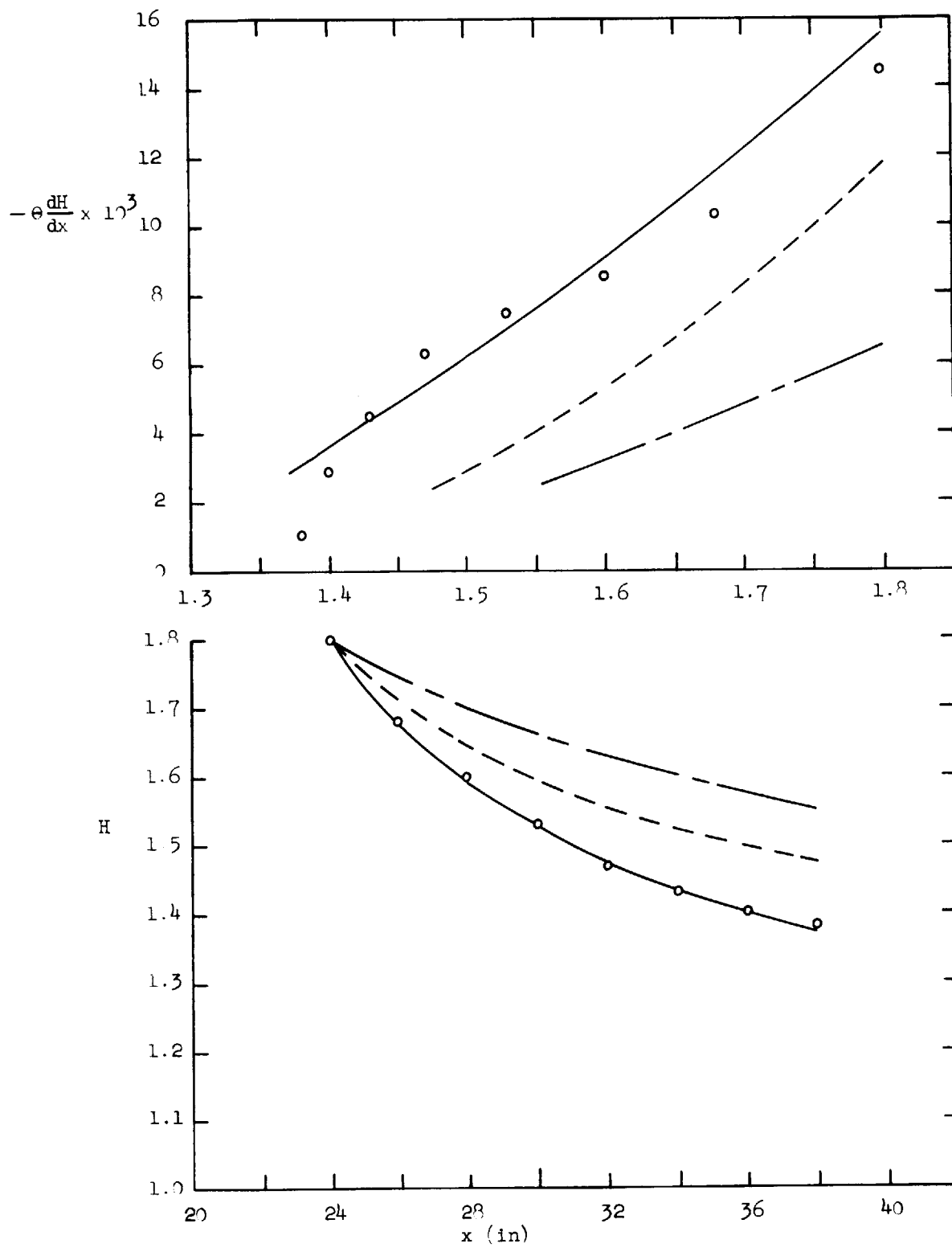
Figure 2 (b) Pressure Distribution No. 3
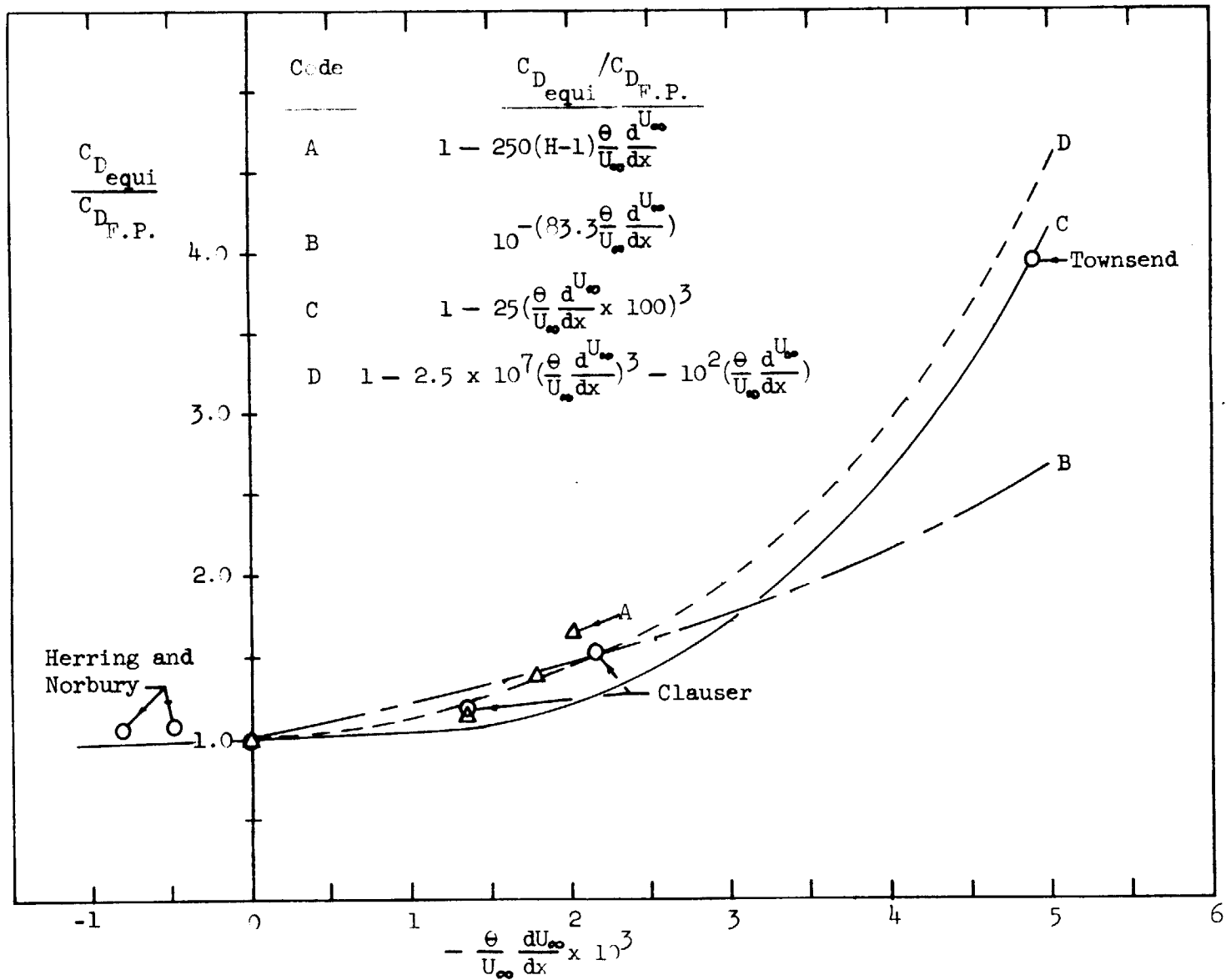
Figure 30 Equilibrium Dissipation Integrals
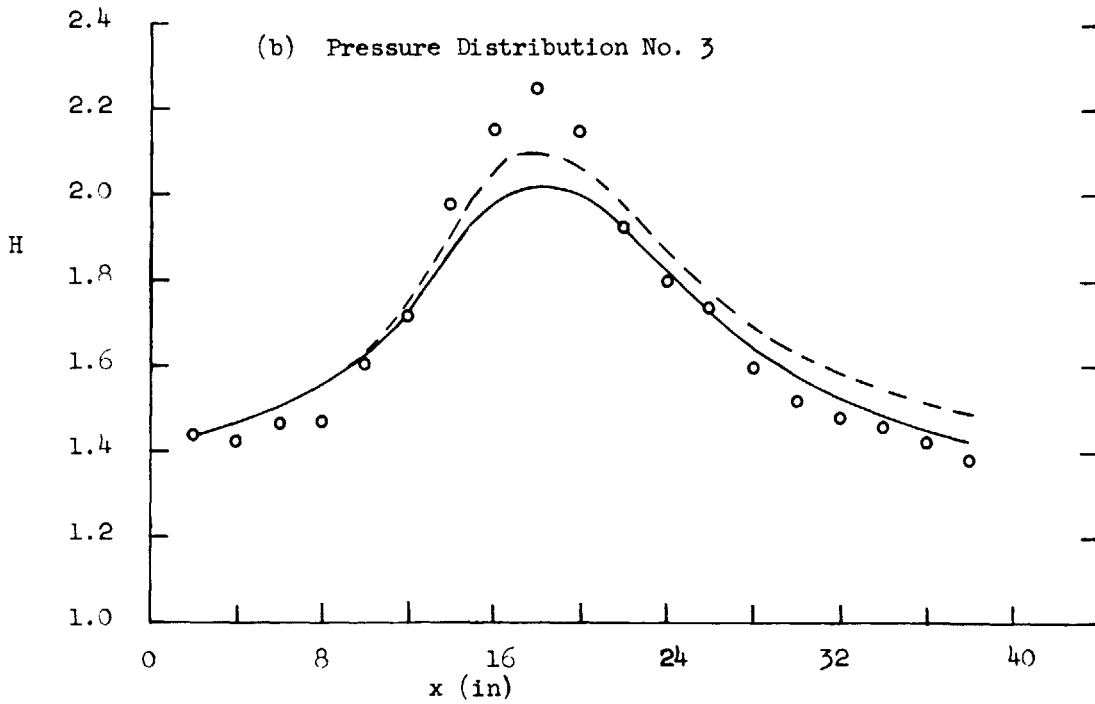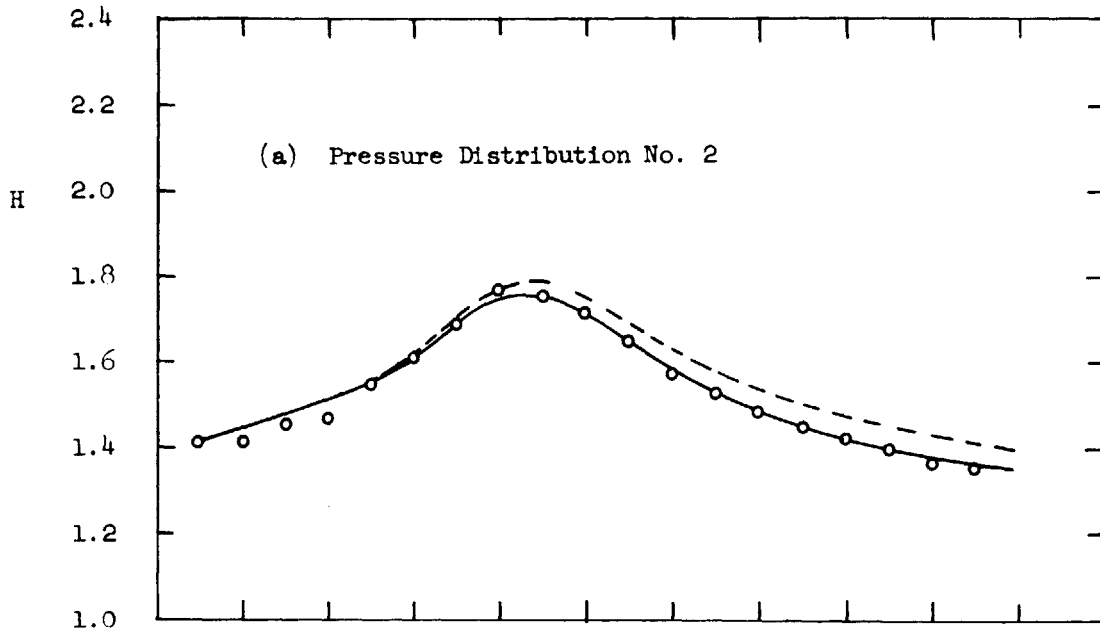
Figure 31 Comparisons Between Shape Factor Predictions and Experimental Data

—— Eq. (25)   ---- Ref. 28   O Data

(c)   Pressure Distribution No. 4

(d)   Pressure Distribution No. 5

x (in)

Figure 31 Continued

(e) Pressure Distribution No. 6

(f) Pressure Distribution No. 1 in Figure 1

Figure 31   Continued

(g) Pressure Distribution No. 2 in Figure 1

(h) Pressure Distribution No. 3 in Figure 1

Figure 31 Continued

(i) Bradshaw and Ferriss[9] Relaxing Boundary Layer
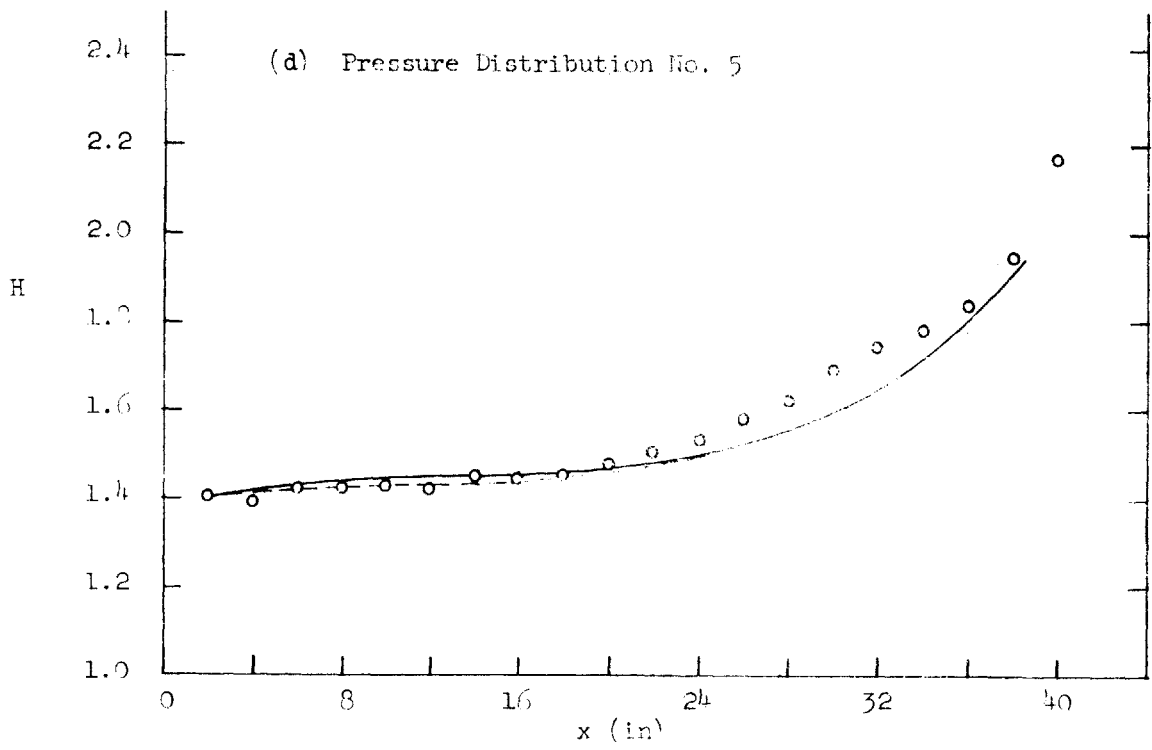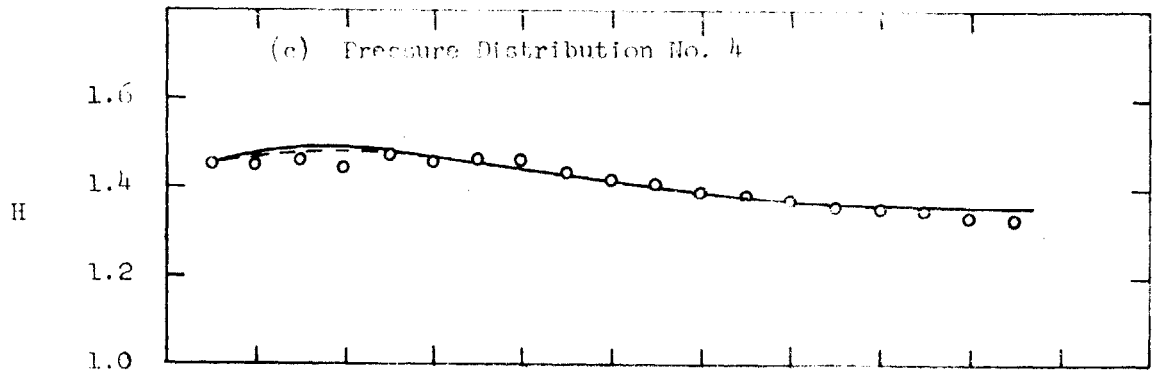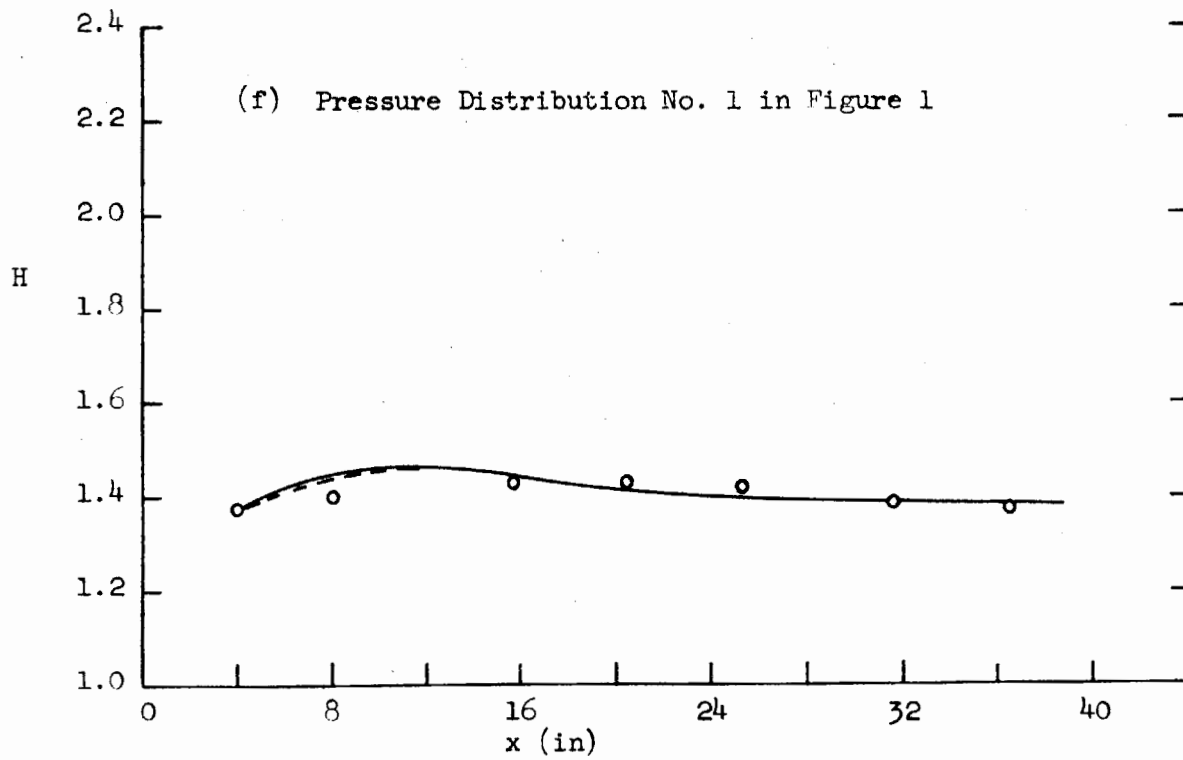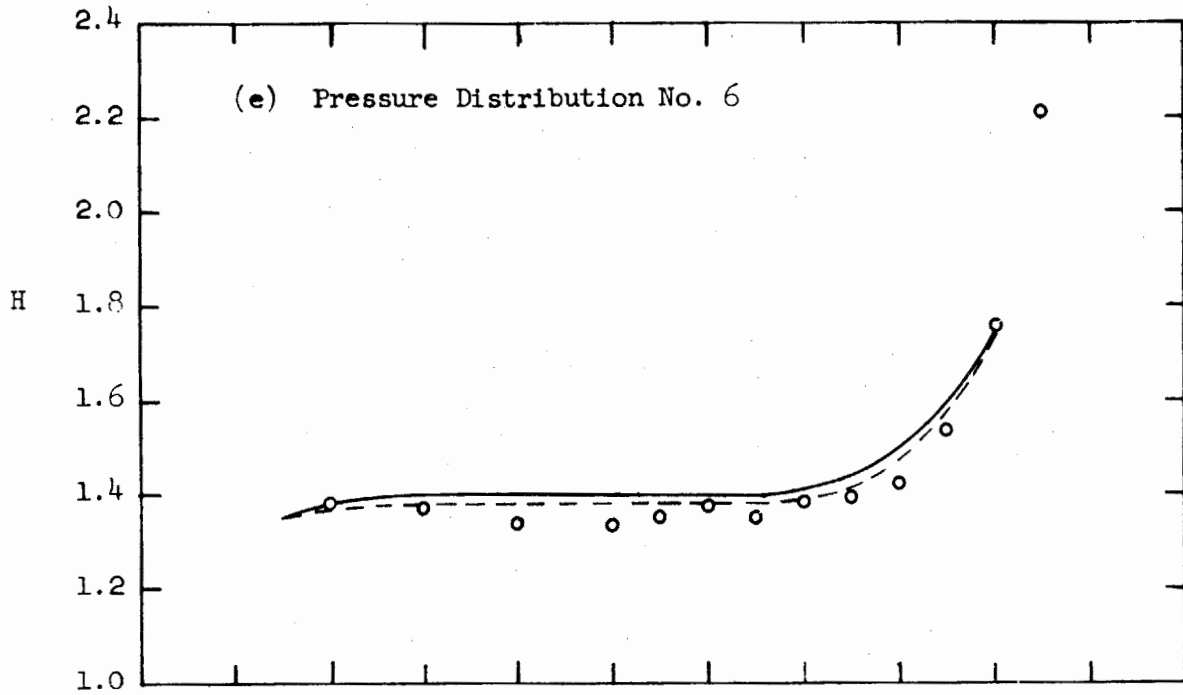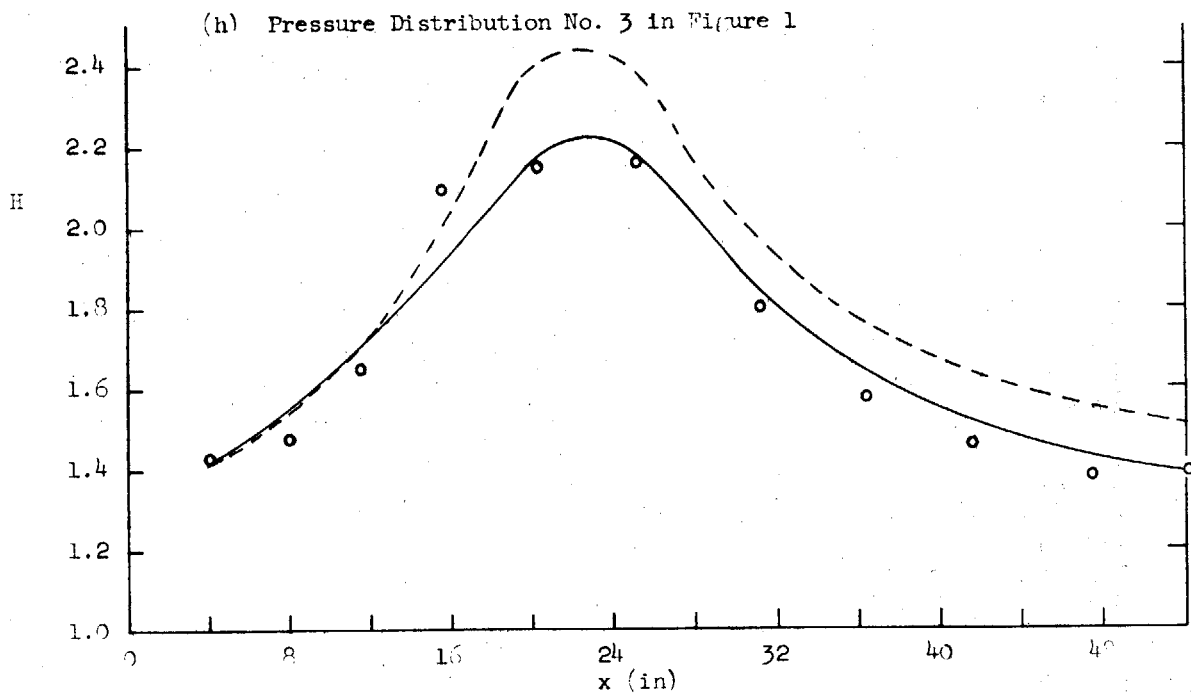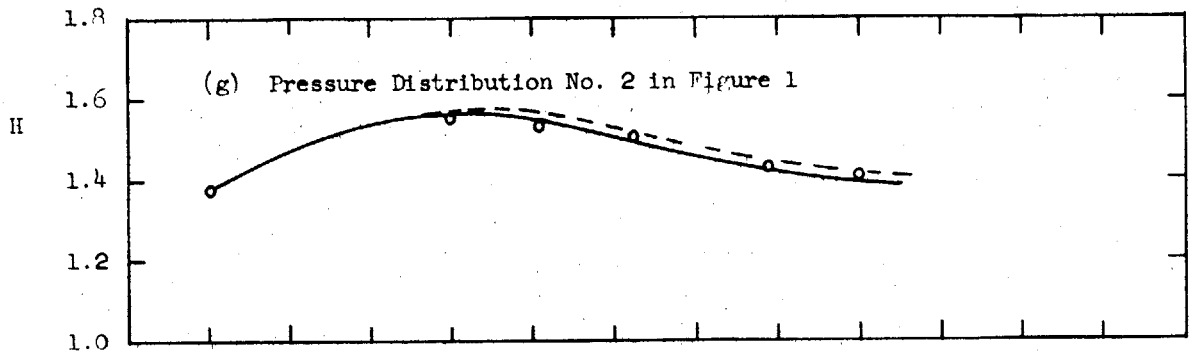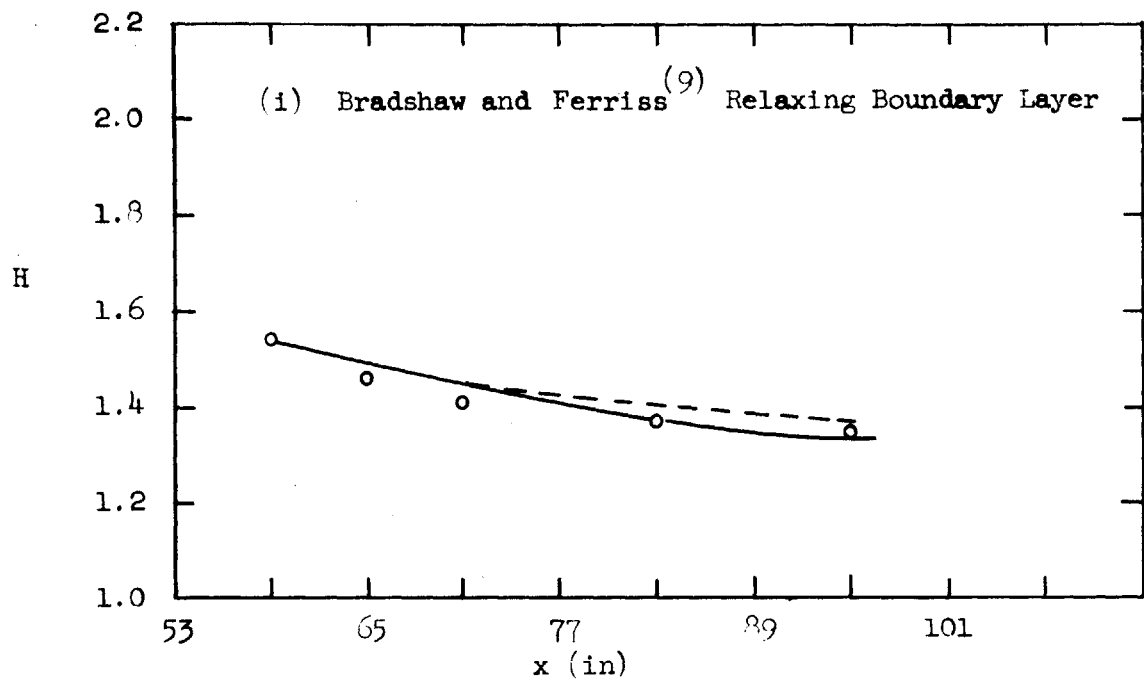
Figure 31 Continued

INITIAL DISTRIBUTION LIST

Copies	Organization
50	Commanding Officer and Director David Taylor Model Basin Washington 7, D.C. Attn: Code 513
7	Chief, Bureau of Ships Department of the Navy Washington 25, D.C. Attn: Technical Library Code 210 L (3) Code 420 (1) " 341 B (1) " 421 (1) " 345 (1)
1	Office of Naval Research Branch Office, Forrestal Research Center Princeton, N.J. Attn: Mr. J. Levy
	Office of Naval Research Department of the Navy Washington 25, D.C.
1	Attn: Head, Mechanics Branch
1	Attn: Head, Fluid Dynamics Branch
1	Attn: Head, Power Branch, Code 429
	Massachusetts Institute of Technology Cambridge 39, Mass.
1	Attn: Prof. A. Shapiro
1	Attn: Prof. E.S. Taylor
1	Attn: Prof. P.G. Hill
	The Johns Hopkins University Baltimore, Maryland
1	Attn: Prof. F. Clauser
1	Attn: Prof. L.S.G. Kovasznay
	Princeton University Princeton, N.J.
1	Attn: Prof. S.M. Bogdonoff
1	Prof. W.D. Hayes
1	Prof. S.I. Cheng
1	Prof. L. Crocco
1	Prof. H. Lam
1	Prof. L. Brush
1	Prof. W.O. Crimanale
1	Prof. D.C. Hazen
1	Engineering Library
1	Forrestal Library

Stanford University
Department of Mechanical Engineering
Stanford, California
1   Attn: Prof. S.J. Kline
1   Prof. J.P. Johnston

University of California
Berkeley, California
1   Attn: Prof. G.M. Cocos

Harvard University
Cambridge 38, Massachusetts
1   Attn: Prof. R.E. Kronauer
       Prof. H. Emmons

Dartmouth College
Hanover, New Hampshire
1   Attn: Prof. R.C. Dean, Jr.

1   Dr. H. Eichenberger
Ingersoll-Rand Co.
Research and Development
Bedminster, N.J.

Westinghouse Electric Corp.
Lester, Penna.
1   Attn: Mr. R.E. McNair
1   Mr. G. Howard

1   Dr. Howard Baum
Department R510
AVCO Research and Advanced Development
Wilmington, Mass.

1   Dr. D.C. Prince
General Electric Co.
Evendale, Ohio

1   Dr. D.M. Gibson
General Dynamics
Fort Worth, Texas

1   Dr. F.C.W. Olson
U.S. Naval Mine Defense Laboratory
Panama City, Florida

Iowa Institute of Hydraulic Research
University of Iowa
Iowa City, Iowa
1   Attn: Dr. Hunter Rouse

1   NASA
1512 H. Street, N.W.
Washington 25, D.C.

Copies	Organization
	University of Delaware Newark, Delaware
1	Attn: Prof. J. Hartnett
1	Dr. J.A. Schetz General Applied Science Lab., Inc. Westbury, L.I., New York
	University of Minnesota St. Anthony Falls Hydraulic Laboratory Minneapolis 14, Minn.
1	Attn: Director
	Aeronautical Research Associates at Princeton Princeton, N.J.
1	Attn: Dr. C. DuP. Donaldson, President
1	Dr. L. Landweber Iowa Institute of Hydraulic Research University of Iowa Iowa City, Iowa
1	Mr. Neal Tetervin Naval Ordnance Laboratory White Oak Silver Spring, Maryland
1	Dr. F.R. Hama Jet Propulsion Laboratory Pasadena, California
1	Dr. G.B. Schubauer National Hydraulic Laboratory Bureau of Standards Washington, D.C.
1	Dr. D. Coles California Institute of Technology Pasadena, California
1	Dr. J.M. Robertson University of Illinois Urbana, Illinois
1	Mr. E.M. Uram Davidson Laboratory Stevens Institute of Technology Hoboken, N.J.
1	Mr. W.B. Giles Ordnance Department General Electric Co. Pittsfield, Mass.

Copies	Organization
1	Dr. J. J. Cornish, III Department of Aerophysics Mississippi State University State College, Miss.
1	Dr. Paul Kaplan Oceanics, Inc. Technical Industrial Park Plainview, L. I., New York
2	Prof. Irving Michelson Illinois Institute of Technology Technology Center Chicago, Ill. 60616
1	Attn: Dr. T. Paul Torda
1	Prof. D. A. Nesmith Engineering Experiment Station Kansas State University Manhattan, Kansas 66504
1	Editor, Engineering Index Engineering Societies Library 29 West 39th. Street New York, N. Y. 10018
1	Editor, Applied Mechanics Reviews Southwest Research Institute 8500 Culebra Road San Antonio 6, Texas
	Office of Naval Research, Boston Branch 495 Summer Street Boston, Mass. 02010
1	Attn: Commanding Officer
1	Dr. F. B. Gardner
1	Mr. T. B. Dowd
1	Commanding Officer Office of Naval Research, New York Branch 207 West 24th. Street New York, N. Y. 10011
1	Commanding Officer Office of Naval Research, Chicago Branch 219 So. Dearborn Street Chicago 1, Ill.
1	Commanding Officer Office of Naval Research, San Francisco Branch 1076 Mission Street San Francisco 9, Calif.
1	Commanding Officer Office of Naval Research, Pasadena Branch 1030 East Green Street Pasadena 1, Calif.

Copies	Organization
1	Prof. G. L. Mellor Department of Mechanical Engineering Princeton University Princeton, N. J.
1	Mr. M. P. Tulin HYDRONAUTICS, Inc. Pindell School Road, Laurel Howard County, Maryland
1	Dr. D. L. Turcotte Graduate School of Aeronautical Engineering Cornell University Ithaca, New York
1	Mr. A. M. O. Smith Douglas Aircraft Company, Inc. Aircraft Division Long Beach, Calif.
1	Prof. G. H. Toebes School of Engineering Purdue University Lafayete, Indiana

General Electric Company
570 Lexington Avenue
New York 22, N. Y.

1	Attn: Mr. F. P. McCune, Vice Pres. Engineering Mr. C. H. Linder, Gen. Mgr. Turbine Div.

Large Steam Turbine Division
General Electric Co.
Schenectady 5, N. Y.

1	Attn: Mr. Carl Shabtach, Mgr. Engineering
1	Mr. J. E. Fowler
1	Mr. K. C. Cotton
1	Mr. J. Herzog
1	Mr. R. E. Brandon

Gas Turbine Division
General Electric Co.
Schenectady 5, N. Y.

1	Attn: Mr. C. George, Mgr. Engineering
1	Mr. R. L. Hendrickson
1	Mr. B. D. Buckland
1	Mr. G. W. Schaper

Large Steam Turbine-Generator Dept.
General Electric Co.
Schenectady 5, N. Y.

1	Attn: Mr. J. E. Downes, Mgr. Engineering
1	Mr. C. W. Elston, Gen. Manager

Copies	Organization
	Flight Propulsion Division General Electric Co. Cincinnati 15, Ohio
1	Attn: Technical Information Center, Bldg. 100
1	Mr. D. Cochran, Gen. Manager
1	Mr. J. W. McBride, Devel. Plan. Group, Bldg. 300
1	Mr. R. G. Griffin
1	Dr. S. N. Suciu, Mgr. Appl. Res. Oper., Bldg. 300
	Small Aircraft Engine Division General Electric Co. 1000 Western Avenue Lynn, Mass.
1	Attn: Mr. Edward Woll, Mgr.
	Aircraft Gas Turbine Division General Electric Co. Cincinnati 15, Ohio
1	Attn: Dr. LeR. Smith, Jr.
1	Mr. E. Perugi
	Large Jet Engine Dept. General Electric Co. Evendale, Ohio
1	Attn: Mr. D. C. Berkey
1	Mr. W. R. Cornell
1	Mr. L. Wright
1	Mr. J. E. Knott, Dir. of Engineering Aircraft Engine Operations Allison Division - General Motors Corp. Indianapolis 6, Indiana
1	Mr. E. B. Newill, General Manager Allison Division - General Motors Corp. Indianapolis 6, Indiana
	Turbine Engine Dept. Allison Division - General Motors Corp. Indianapolis 6, Indiana
1	Attn: Mr. J. N. Barney
1	Mr. B. A. Hopkins
1	Mr. C. R. Lowes
	Engineering Development Dept. General Motors Research Laboratories 12 Mile and Mound Roads Warren, Michigan
1	Attn: Dr. Gino Sovran
1	Mr. C. A. Amann
1	Librarian General Motors Technical Center Warren, Michigan

Copies	Organization
	National Science Foundation Washington 25, D. C.
1	Attn: Head, Engineering Section
1	Naval Liaison Office Massachusetts Institute of Technology Building 20E, Room 232 Cambridge, Mass. 02139
1	Library of Congress Exchange and Gift Division Washington 25, D. C.
	Dept. of Aeronautical Engineering Pennsylvania State University 233 Hammond Building University Park, Penna. 16802
1	Attn: Mr. Raphael D. Cahn
1	Mr. A. Fabula
1	Prof. J. Miller U. S. Naval Postgraduate School Monterey, Calif. 93940
1	Dr. Bruce Johnson Engineering Department U. S. Naval Academy Annapolis, Maryland

DOCUMENT CONTROL DATA - R&D

(Security classification of title, body of abstract and indexing annotation must be entered when the overall report is classified)

1. ORIGINATING ACTIVITY *(Corporate author)*	2a. REPORT SECURITY CLASSIFICATION
M. I. T. - Gas Turbine Laboratory Prof. Hal L. Moses	Unclassified
	2b. GROUP

3. REPORT TITLE

"Upstream History and Apparent Stress in Turbulent Boundary Layers"

4. DESCRIPTIVE NOTES *(Type of report and inclusive dates)*

Technical Report - October 1965 to May 1966

5. AUTHOR(S) *(Last name, first name, initial)*

Goldber, Perry

6. REPORT DATE	7a. TOTAL NO. OF PAGES	7b. NO. OF REFS
May 1966	107	37

8a. CONTRACT OR GRANT NO. Nonr 1841(91)	9a. ORIGINATOR'S REPORT NUMBER(S)
b. PROJECT NO. DTMB	Gas Turbine Laboratory Report #85
c.	9b. OTHER REPORT NO(S) *(Any other numbers that may be assigned this report)*
d.	None

10. AVAILABILITY/LIMITATION NOTICES

"Copies of this report may be obtained from the Clearing House for Federal Scientific and Technical Information, Sills Building, Springfield, Virginia 22151

11. SUPPLEMENTARY NOTES	12. SPONSORING MILITARY ACTIVITY
None	Bureau of Ships - David Taylor Model Basin

13. ABSTRACT

A comprehensive experimental and analytical study specifically desgined to investigate upsteam history and apparent stress in incompressible, two-dimensional turbulent boundary layers has been conducted. Hot-wire measurements of turbulent shear stress and longitudinal turbulence intensity, as well as velocity profile and wall shear stress measurements were made for six different pressure distributions.

It was found that the turbulent shear stress is dependent upon the upstream history of the flow and not a unieque function of the local velocity profile. A simple equation for the dissipation integral,

$$\theta \frac{dC_D}{dx} = K(C_{D_{equil}} - C_D)$$

with a constant K was found to represent the data well. This expression was used with the mean-flow energy integral equation to obtain a practical method for predicting turbulent boundary layer behavior which accounts for upstream history. The predictions made with this method for the six pressure distributions of this study and for others extracted from the literature agreed well with the experimental data.

DD FORM 1 JAN 64 **1473**

14 KEY WORDS	LINK A		LINK B		LINK C	
	ROLE	WT	ROLE	WT	ROLE	WT
Boundary Layers						
Turbulence						
Turbulent Boundary Layers						
Turbulent Shear Stress						

INSTRUCTIONS

1. ORIGINATING ACTIVITY: Enter the name and address of the contractor, subcontractor, grantee, Department of Defense activity or other organization (*corporate author*) issuing the report.

2a. REPORT SECURITY CLASSIFICATION: Enter the overall security classification of the report. Indicate whether "Restricted Data" is included. Marking is to be in accordance with appropriate security regulations.

2b. GROUP: Automatic downgrading is specified in DoD Directive 5200.10 and Armed Forces Industrial Manual. Enter the group number. Also, when applicable, show that optional markings have been used for Group 3 and Group 4 as authorized.

3. REPORT TITLE: Enter the complete report title in all capital letters. Titles in all cases should be unclassified. If a meaningful title cannot be selected without classification, show title classification in all capitals in parenthesis immediately following the title.

4. DESCRIPTIVE NOTES: If appropriate, enter the type of report, e.g., interim, progress, summary, annual, or final. Give the inclusive dates when a specific reporting period is covered.

5. AUTHOR(S): Enter the name(s) of author(s) as shown on or in the report. Enter last name, first name, middle initial. If military, show rank and branch of service. The name of the principal author is an absolute minimum requirement.

6. REPORT DATE: Enter the date of the report as day, month, year; or month, year. If more than one date appears on the report, use date of publication.

7a. TOTAL NUMBER OF PAGES: The total page count should follow normal pagination procedures, i.e., enter the number of pages containing information.

7b. NUMBER OF REFERENCES: Enter the total number of references cited in the report.

8a. CONTRACT OR GRANT NUMBER: If appropriate, enter the applicable number of the contract or grant under which the report was written.

8b, 8c, & 8d. PROJECT NUMBER: Enter the appropriate military department identification, such as project number, subproject number, system numbers, task number, etc.

9a. ORIGINATOR'S REPORT NUMBER(S): Enter the official report number by which the document will be identified and controlled by the originating activity. This number must be unique to this report.

9b. OTHER REPORT NUMBER(S): If the report has been assigned any other report numbers (*either by the originator or by the sponsor*), also enter this number(s).

10. AVAILABILITY/LIMITATION NOTICES: Enter any limitations on further dissemination of the report, other than those imposed by security classification, using standard statements such as:

(1) "Qualified requesters may obtain copies of this report from DDC."

(2) "Foreign announcement and dissemination of this report by DDC is not authorized."

(3) "U. S. Government agencies may obtain copies of this report directly from DDC. Other qualified DDC users shall request through

_____ ."

(4) "U. S. military agencies may obtain copies of this report directly from DDC. Other qualified users shall request through

_____ ."

(5) "All distribution of this report is controlled. Qualified DDC users shall request through

_____ ."

If the report has been furnished to the Office of Technical Services, Department of Commerce, for sale to the public, indicate this fact and enter the price, if known.

11. SUPPLEMENTARY NOTES: Use for additional explanatory notes.

12. SPONSORING MILITARY ACTIVITY: Enter the name of the departmental project office or laboratory sponsoring (*paying for*) the research and development. Include address.

13. ABSTRACT: Enter an abstract giving a brief and factual summary of the document indicative of the report, even though it may also appear elsewhere in the body of the technical report. If additional space is required, a continuation sheet shall be attached.

It is highly desirable that the abstract of classified reports be unclassified. Each paragraph of the abstract shall end with an indication of the military security classification of the information in the paragraph, represented as *(TS), (S), (C), or (U)*.

There is no limitation on the length of the abstract. However, the suggested length is from 150 to 225 words.

14. KEY WORDS: Key words are technically meaningful terms or short phrases that characterize a report and may be used as index entries for cataloging the report. Key words must be selected so that no security classification is required. Identifiers, such as equipment model designation, trade name, military project code name, geographic location, may be used as key words but will be followed by an indication of technical context. The assignment of links, roles, and weights is optional.

DD FORM 1473 (BACK)
1 JAN 54